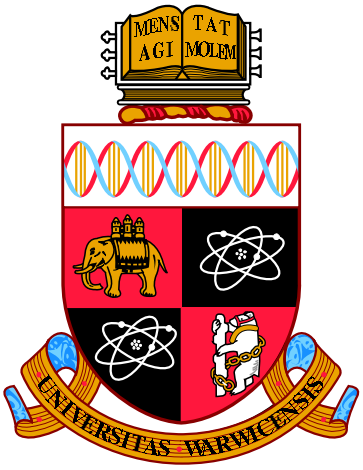

In Vivo THz Spectroscopy for Quantitative Skin Evaluation

by

Hannah Hatcher (née Lindley)

Thesis

Submitted to the University of Warwick

for the degree of

Doctor of Philosophy

Department of Physics

January 2022

Contents

List of Tables

List of Figures

Acknowledgments

In October 2017 I had a meeting with Professor Emma MacPherson to discuss the possibility of undertaking a PhD in her research group. That conversation started me on the journey taking me to where I am now and I am so grateful to the many people that have helped me along the way to get here.

I would like to begin by thanking my supervisor Professor Emma MacPherson for her help and guidance throughout the past four years. I have learnt so much being a part Emma's research group both to do with with Physics, good writing practice and work-life balance. Emma is always encouraging when it feels like no progress is being made and knows how to keep fun in the group with regular coffee breaks and castle trips.

I would like to thank the collaborators who have provided the samples that were tested in the studies reported in this work. Dr Juan Cebrian, for providing the moisturiser samples and the Corneometer and Tewameter used in Chapter 4. Professor Joseph Hardwicke, for his insight into research ethics and dermatology. Professor David Haddleton, Dr Gabit Nurumbetov and Medherant Ltd for providing the patches tested in Chapter 5. I would also like to thank everyone who has been involved in any of the studies and allowed me to measure their skin.

I would like to thank the EPSRC for the funding that I have received throughout my PhD, which has enabled me to do this research. Additionally, I would like to credit the EPSRC grant EP/S021442/1, which has supported the projects I have been involved in throughout my PhD.

I would like to thank all the members of the THz group at Warwick and in Hong Kong both past and present. From people that I have chatted and laughed

with in breaks to those who have taught me so much about doing research, thank you all so much. I would particularly like to thank Dr Qiushuo Sun for teaching me how to perform measurements in our lab, Dr Jiarui Wang for having lots of discussions with me about skin measurements and modelling and Dr Xuequan Chen and Dr Rayko Stantchev for your insight and suggestions in meetings. Finally, I would like to thank Dr Arturo Hernandez-Serrano for his help with everything, there isn't space to list all the things he has helped with throughout my PhD but I know I couldn't have done it without his support and friendship.

Finally, I would like to thank my family for their support and love throughout my studies. I would like to thank my parents for always encouraging me to take opportunities that come my way and for being patient with me when I have been busy with work. I would like to thank my brother, James, for the laughs and for helping me to take breaks when I need them. Finally, thank you to my husband Luke, thank you for reminding me of my life outside of work when I forget, thank you for having wise opinions when I don't know what to do and thank for you for reading this thesis. Thank you all so much family, I love you.

Collaborative Notes:

I would like to acknowledge the Master's students Katie Croft and Pierre Hamenya for recruiting the subjects measured in Chapter 6 and helping with the measurements of the subjects. I also acknowledge Dr Arturo Hernandez-Serrano for his help building the system used to perform the measurements in Chapters 5 and 6. Finally, Dr Xuequan Chen and Dr Qiushuo Sun for writing the first version of the code used to process THz reflection measurements that I adapted for the purposes of my research.

Declarations

I hereby declare that this thesis is my original work and contains nothing that is the result of work done in collaboration with others, except as specified in the text and the acknowledgements. This work has not been submitted in full or in part to this or any other university for the award of another degree.

The material in some chapters has been published in the following papers and conference proceedings:

Chapter 1:

H. Lindley-Hatcher, R. I. Stantchev, X. Chen, A. I. Hernandez-Serrano, J. Hardwicke, and E. Pickwell-MacPherson, "Real time THz imaging—opportunities and challenges for skin cancer detection," *Applied Physics Letters*, vol. 118, no. 23, 230501, 2021.

Chapter 3:

H. Lindley-Hatcher, A. I. Hernandez-Serrano, Q. Sun, J. Wang, J. Cebrian, L. Blasco, and E. Pickwell-MacPherson, "A Robust Protocol for In Vivo THz Skin Measurements," *J. Infrared, Millimeter, Terahertz Waves*, vol. 40, no. 9, pp. 980–989, 2019.

H. Lindley, A. I. Hernandez-Serrano, Q. Sun, J. Wang, and E. Pickwell-MacPherson, "Pressure Controlled in vivo THz Measurements of Skin: Monitoring the Effects of Moisturizers," in *International Conference on Infrared, Millimeter, and Terahertz Waves, IRMMW-THz*, 2019, vol. 2019-Sept.

Chapter 4:

H. Lindley-Hatcher, A. I. Hernandez-Serrano, J. Wang, J. Cebrian, J. Hardwicke, and E. Pickwell-MacPherson, "Evaluation of in vivo THz sensing for assessing human skin hydration," *JPhys. Photonics*, vol. 3, no. 1, 2021.

H. Lindley-Hatcher, A. I. Hernandez-Serrano, E. Hennighan, J. Cebrian, L. Blasco, and E. Pickwell-MacPherson, "Evaluating the Effects of Different Skin Products on the in vivo THz Response of Skin," in *International Conference on Infrared, Millimeter, and Terahertz Waves, IRMMW-THz*, vol. 2020-Sept.

Chapter 5:

H. Lindley-Hatcher, J. Wang, A. I. Hernandez-Serrano, D. M. Haddleton, and E. Pickwell-MacPherson, "Monitoring the Effect of Transdermal Drug Delivery Patches on the Skin using Terahertz Sensing," *Pharmaceutics*, vol. 13, no. 12, 2052, 2021.

Abstract

Terahertz (THz) light is in the range of electromagnetic waves with frequencies between 0.1 and 10 THz where 1 THz = 10^{12} Hz, this is in the region between infrared and microwave radiation. There is increasing interest in the potential biomedical applications of THz spectroscopy that take advantage of the sensitivity of THz light to the water content of biological tissues and other associated changes including the presence of cancerous tissue. The low photon energy of THz light means that it is non-ionizing, making THz light particularly attractive for *in vivo* applications.

In this thesis multiple *in vivo* studies are presented that explore the ability of THz measurements to identify changes in the hydration of the skin. Chapters 1 and 2 provide context to these studies by introducing the present state of the field and relevant theory. Chapter 3 explores the effect of variables such as pressure on the THz response of skin and introduces a protocol to reduce the effects of these variables. In Chapter 4 these approaches are applied to test the effects of three different moisturisers on the skin using THz measurements and measurements taken with two commercial devices for skin hydration assessment. In Chapter 5 the effects of different types of patches for transdermal drug delivery on the THz response of skin are investigated, including the recovery of the skin following patch removal. Chapter 6 explores the effect of skin tone and sex on the THz response of skin and the way skin responds to the application of different types of moisturisers.

Finally, Chapter 7 summarises the work performed in this thesis and identifies areas for further work in the future. In particular, the need to improve imaging speeds and develop non-contact imaging capabilities are both highlighted as important areas to focus on in future work.

Acronyms

ANOVA Analysis of Varaince

BCC Basal Cell Carcinoma

FFPE Formalin Fixed Paraffin Embedded

FSR Force Sensitive Resistor

LLL Landau Lifshitz Looyenga

MRI Magnetic Resonance Imaging

NRC Normalised Relative Change

P2P Peak-to-Peak

PET Polyethylene Terephthalate

SC Stratum Corneum

TEWL Transepidermal Water Loss

THz-TDS THz Time Domain Spectroscopy

WO Water in Oil

List of Publications

Peer Reviewed Journals:

1. **H. Lindley-Hatcher**, K. Croft, P. Hamenya, A. I. Hernandez-Serrano, J. Hardwicke and E. Pickwell-MacPherson, "Towards Robust Parameterisation of THz Properties Across Skin Types," (In Preparation).

2. X. Ding, A. I. Hernandez-Serrano, **H. Lindley-Hatcher**, R. I. Stantchev, J. Zhou and E. Pickwell-MacPherson, "Optimized Multilayer Structure for Sensitive THz Characterization of Thin-Film Glucose Solutions," *Optics Express*, vol. 30, no. 11, pp. 18079-18089, 2022.

3. **H. Lindley-Hatcher**, J. Wang, A. I. Hernandez-Serrano, J. Hardwicke, G. Nurumbetov, D. M. Haddleton, and E. Pickwell-MacPherson, "Monitoring the Effect of Transdermal Drug Delivery Patches on the Skin using Terahertz Sensing," *Pharmaceutics*, vol. 13, no. 12, 2052, 2021.

4. X. Chen, **H. Lindley-Hatcher**, R. I. Stantchev, J. Wang, K. Li, A. I. Hernandez-Serrano, Z. D. Taylor, E. Castro-Camus, and E. Pickwell-MacPherson, "Terahertz (THz) biophotonics technology: Instrumentation, techniques, and biomedical applications," *Chemical Physics Reviews*, vol. 3, no. 1, 011311, 2022.

5. **H. Lindley-Hatcher**, R. I. Stantchev, X. Chen, A. I. Hernandez-Serrano, J. Hardwicke, and E. Pickwell-MacPherson, "Real time THz imaging—opportunities and challenges for skin cancer detection," *Applied Physics Letters*, vol. 118, no. 23, 230501, 2021.

6. X. Chen, Q. Sun, J. Wang, **H. Lindley-Hatcher**, E. Pickwell-MacPherson, "Exploiting complementary terahertz ellipsometry configurations to probe the hydration and cellular structure of skin in vivo," *Advanced Photonics Research*, vol. 2, no. 1, 2000024, 2021.

7. J. Wang, **H. Lindley-Hatcher**, X. Chen, and E. Pickwell-MacPherson, "THz Sensing of Human Skin: A Review of Skin Modeling Approaches," *Sensors*, vol. 21, no. 11, 3624, 2021.

8. **H. Lindley-Hatcher**, A. I. Hernandez-Serrano, J. Wang, J. Cebrian, J. Hardwicke, and E. Pickwell-MacPherson, "Evaluation of in vivo THz sensing for assessing human skin hydration," *JPhys. Photonics*, vol. 3, no. 1, 014001, 2021.

9. J. Wang, **H. Lindley-Hatcher**, K. Lui, and E. Pickwell-MacPherson, "Evaluation of transdermal drug delivery using terahertz pulsed imaging," *Biomedical Optics Express*, vol. 11, no. 8, pp. 4484-4490, 2020.

10. **H. Lindley-Hatcher**, A. I. Hernandez-Serrano, Q. Sun, J. Wang, J. Cebrian, L. Blasco, and E. Pickwell-MacPherson, "A Robust Protocol for In Vivo THz Skin Measurements," *J. Infrared, Millimeter, Terahertz Waves*, vol. 40, no. 9, pp. 980–989, 2019.

Conference Presentations and Proceedings:

1. **H. Lindley-Hatcher**, A. I. Hernandez-Serrano, J. Wang, J. Cebrian, J. Hardwicke, and E. Pickwell-MacPherson, "Assessing Changes In Human Skin Using In Vivo Terahertz Measurements," in *International Conference on Infrared, Millimeter, and Terahertz Waves, IRMMW-THz*, vol. 2021-Sept.

2. **H. Lindley-Hatcher**, A. I. Hernandez-Serrano, and E. Pickwell-MacPherson, "Comparing Techniques for in vivo Skin Hydration Measurement," in *International THz-Bio Workshop*, 2021.

3. E. Pickwell-MacPherson, **H. Lindley-Hatcher**, Q. Sun, R. Stantchev, and A. I. Hernandez-Serrano, "Terahertz in vivo imaging for improved skin diagnosis and treatment," in *International THz-Bio Workshop*, 2021.

4. **H. Lindley-Hatcher**, A. I. Hernandez-Serrano, E. Hennighan, J. Cebrian, L. Blasco, and E. Pickwell-MacPherson, "Evaluating the Effects of Different Skin Products on the in vivo THz Response of Skin," in *International Conference on Infrared, Millimeter, and Terahertz Waves, IRMMW-THz*, vol. 2020-Sept.

5. **H. Lindley-Hatcher**, A. I. Hernandez-Serrano, Q. Sun, J. Wang, and E. Pickwell-MacPherson, "Using THz in vivo imaging to quantify changes in the skin," in *Postgraduate Women in Physics*, 2020.

6. **H. Lindley-Hatcher**, A. I. Hernandez-Serrano, Q. Sun, J. Wang, and E. Pickwell-MacPherson, "Using THz in vivo imaging to quantify changes in the skin," in *TERANET UK-THz Symposium*, 2019.

7. **H. Lindley**, A. I. Hernandez-Serrano, Q. Sun, J. Wang, and E. Pickwell-MacPherson, "Pressure Controlled in vivo THz Measurements of Skin: Monitoring the Effects of Moisturizers," in *International Conference on Infrared, Millimeter, and Terahertz Waves, IRMMW-THz*, 2019, vol. 2019-Sept.

8. X. Chen, Q. Sun, J. Wang, **H. Lindley**, K. Lui, K. Li, X. Barker, R. I. Stantchev, A. I. Hernandez-Serrano and E. Pickwell-MacPherson, "THz Instrumentation and Analysis Techniques for Biomedical Research," in *International Conference on Infrared, Millimeter, and Terahertz Waves, IRMMW-THz*, 2019, vol. 2019-Sept.

Conferences Attended:

1. 70th Lindau Nobel Laureate Meeting (Interdisciplinary), 27th June-2nd July, 2021, Virtual

2. Lindau Nobel Laureate Meeting, Online Science Day (Interdisciplinary), 28th June - 1st July, 2020, Virtual

3. UK-THz Symposium, 10th-11th December 2018, University of Warwick

Chapter 1

Introduction

1.1 Introduction to THz Spectroscopy

1.1.1 THz Light

Terahertz (10^{12} Hz) light is situated between the microwave and infrared regions of the electromagnetic spectrum as illustrated by Figure 1.1. The THz band is defined as covering the frequency range of $0.1 - 10$ THz, which equates to a wavelength range of $3\ \text{mm} - 30\ \mu\text{m}$. Research involving THz light remains a relatively new field compared to other parts of the spectrum because until 1975 there was a lack of techniques capable of generating and detecting THz frequencies, leaving what was known as the 'THz gap'.

The significant breakthrough that made THz light accessible was the development of the 'Auston Switch', which was capable of producing a broadband THz pulse [1]. Since then many approaches to detecting and producing THz light have been developed allowing a wide range of potential applications to be explored. This increase in interest in THz frequencies is reflected by the continual increase in the number of publications referring to 'Terahertz' shown in Figure 1.2. In addition to

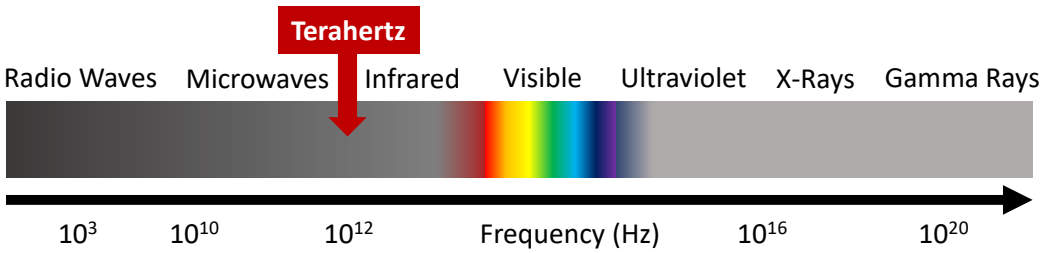

Figure 1.1: The electromagnetic spectrum showing the position of THz light.

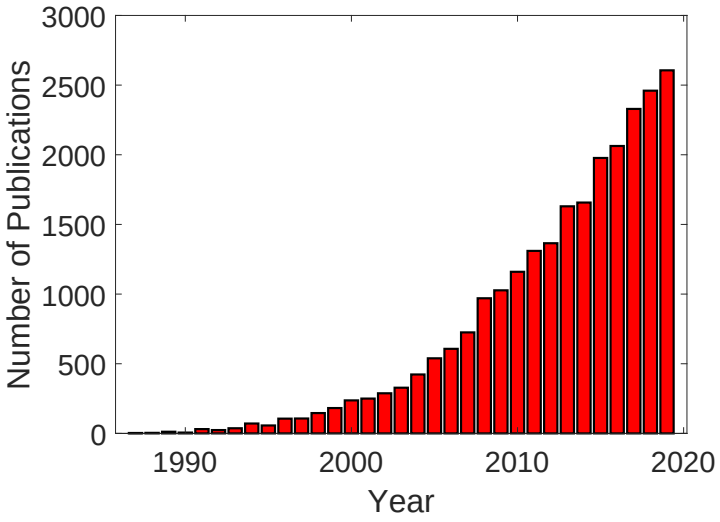

Figure 1.2: The number of publications referring to 'Terahertz' published each year up to 2019 as recorded by the web of science, search was refined by requiring the document type to be 'Article'.

exploring potential applications, research still continues to refine the mechanisms used to produce THz light to enable the development of cheaper, more compact devices, which in turn drives research into new applications.

1.1.2 THz Time Domain Spectroscopy

THz Time Domain Spectroscopy (THz-TDS) is a common technique used in studies with THz light as it is possible to measure the entire THz pulse in the time domain and the frequency information can be accessed by performing a Fourier Transform. THz-TDS was developed in 1985 [2] and it was used to study water vapour by van Exter *et al.*, using this technique they were able to observe the presence of absorption lines at THz frequencies [3]. Since these publications THz-TDS systems have been refined and are now available commercially, reducing the expertise required to operate the systems making THz spectroscopy accessible for interdisciplinary investigations.

The key components required to perform THz-TDS measurements are shown in Figure 1.3, in this figure a reflection geometry is shown, however THz-TDS can also be used for transmission measurements; a transmission geometry system differs from the one shown and this will be explained in more detail in Section 2.6.2. The key components of the systems used for the studies described in this thesis are; a femtosecond pulsed laser, a delay stage and a photoconductive emitter and

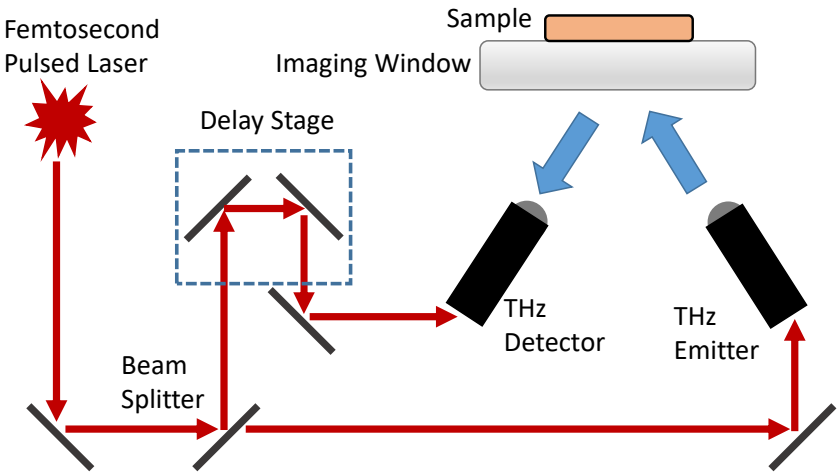

Figure 1.3: A schematic of the setup for THz Time Domain Spectroscopy in reflection geometry.

detector [4]. The femtosecond laser pulse is split in two using a beam splitter, one half of which is directed to the emitter and the other half is directed to the detector via a delay stage. The mechanisms by which the laser pulses are used in photoconductive antennas to generate and detect THz light are described in Section 1.1.3. The delay stage is made of a series of mirrors that can be mechanically moved to introduce a time delay between the arrival of the THz pulse that has been reflected from the sample and the arrival of the femtosecond laser pulse at the THz detector; this makes it possible to sample the received THz pulse across the whole of the time domain window. It should be noted that this figure shows a free space system, however, the systems used for the studies described in this thesis were fiber coupled.

1.1.3 Generating and Detecting THz Light

A common approach used to generate and detect THz light uses photoconductive antennas, the mechanisms for both producing and receiving THz pulses are remarkably similar. An ultrafast infrared pulse is used to excite carriers within a semiconductor substrate that exist for a short time before being recaptured on a picosecond timescale [5].

The mechanism for the production of THz light using a photoconductive antenna is shown in Figure 1.4, where a DC bias is applied across the antenna to accelerate the excited carriers. This movement of charges produces an electric field, E_{THz}, proportional to the rate of acceleration of this photocurrent, I_{PC}, as described

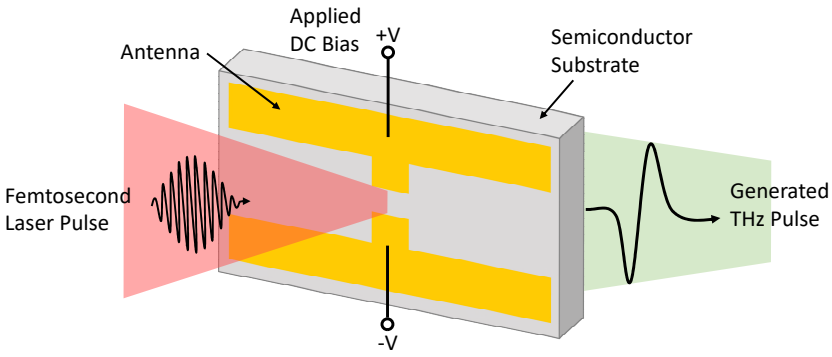

Figure 1.4: Generating THz light using a photoconductive antenna and a femtosecond laser pulse.

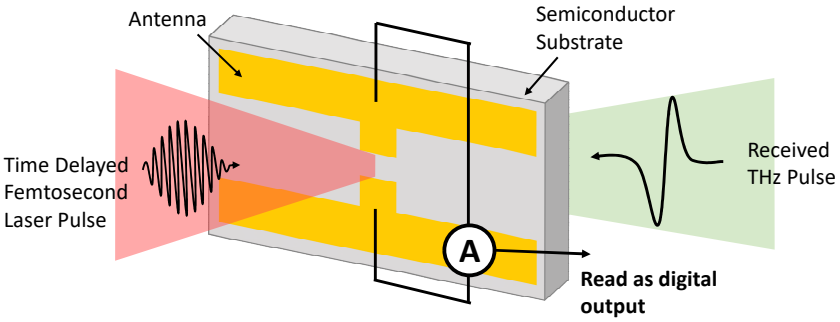

Figure 1.5: Detecting THz light using a photoconductive antenna and a delayed femtosecond laser pulse.

by Equation 1.1.

$$E_{\mathrm{THz}} \propto \frac{\mathrm{d}I_{\mathrm{PC}}(t)}{\mathrm{d}t} \tag{1.1}$$

The resulting pulse of electromagnetic radiation has a temporal width of the order of 1 ps, which is therefore a THz pulse.

The mechanism for the detection of THz pulses is shown in Figure 1.5, the key difference is that rather than applying a bias voltage across the antenna the received THz pulse is used to induce a current in the excited carriers produced by the femtosecond laser pulse. This induced current is amplified and then measured, this can be exported for further digital processing [6]. Other approaches can be used for the generation and detection of THz light, however all of the studies described in this thesis use photoconductive antennas therefore these alternative techniques will not be introduced.

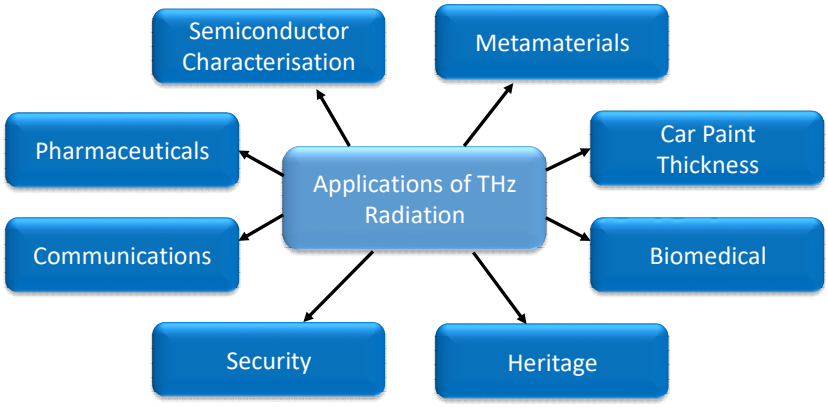

Figure 1.6: A summary of some of the potential applications for THz light.

1.1.4 Applications of THz Imaging

THz light is being utilised for a wide range of applications as it becomes cheaper and easier to produce and use [7]; a summary of some of the key areas in which potential applications for THz spectroscopy are being researched is shown in Figure 1.6. The primary focus of this thesis is potential biomedical applications, these are wide ranging and will be explained in more detail in Section 1.2 [8].

The ability of THz spectroscopy and imaging techniques to extract both time domain and frequency information from a sample opens up a range of potential applications, from identifying samples using characteristic spectra to thickness measurements using the separation between the time domain pulses. For example, in pharmaceuticals THz spectroscopy has been shown to be capable of identifying different drugs as well as differentiating between polymorphs, which can be problematic if not identified as they can cause unwanted side effects [9, 10]. Additionally, potential uses have been identified in the quality control of tablet coating thickness in pharmaceutical production [11, 12]. Similar thickness measurements have also been demonstrated to have potential in the automotive industry for checking the consistency of paint layers on cars [13]. THz measurements have also shown potential uses throughout industry for non-destructive testing to check for faults or fractures in a wide range of materials, with no known risks to the person using the THz system to perform the tests unlike X-rays [14–16].

To support studies into spectral identification using THz spectroscopy, metamaterials for THz frequencies are being developed. These are devices that are capable of enhancing the interaction of THz light with the sample, increasing the sensitivity to small spectral features and reducing the amount of sample required

for identification to occur. This is an expansive field of research and a full review is provided by Xu *et al.* [17].

Many studies have shown the potential of THz spectroscopy and imaging techniques to help investigations into a range of heritage items including historical artwork. It has been shown by various groups that THz measurements can aid in the identification of the types of paints used and in measuring the thickness of different layers of the paint [18–21]. As THz devices become cheaper and more portable to be used outside of controlled lab environments it is possible an increase in such applications will be seen.

THz imaging has also been explored as a technique for security scanning of both people and packages. It has been shown to be able to identify residues of explosives as well as hidden compartments containing weapons and weapons concealed on a person [22, 23]. Obviously the non-ionizing nature of THz light is a great advantage when considering such applications.

Increasingly the possibility of using THz light as a means of communication is being explored as the demand for higher rates of data transfer continues to grow and the frequency range used commercially draws ever closer to the THz region. This demand pushes researchers to consider how THz light can be used to transfer information and what devices such as waveguides and modulators will be required to form the infrastructure needed to facilitate such communication [24, 25].

Finally, THz imaging has been identified as a useful research tool for learning about semiconductors as non-contact measurements of the sample can be performed yielding information about the electrical properties of the sample with subpicosecond time resolution [26–28].

1.2 Biomedical Applications of THz Spectroscopy and Imaging

The low photon energy of THz light means that is non-ionizing and deemed safe for use for measuring regions on living subjects. However, the relatively new nature of the field of THz imaging and spectroscopy means that research is ongoing into the effects of THz light in biological tissues. Hough *et al.* concluded that low power THz light results in no significant modification to gene expression [29]. A full review of the cellular effects of the exposure of biological tissues to THz light has been compiled by Cherkasova *et al.* [30]. In the studies presented in this thesis photoconductive antennas were used to produce the THz light: this means that the power of the THz beam is well below the thresholds that have been identified as

having the potential to cause changes in biological tissues.

It should be noted that there have also been extensive studies exploring the potential biomedical applications of techniques that use different frequency ranges, such as microwaves. These techniques have different challenges and advantages compared to those using THz frequencies. However, a discussion of such techniques is beyond the scope of this thesis and can be found elsewhere [31, 32].

1.2.1 *Ex Vivo* THz Spectroscopy and Imaging

One approach to exploring the interactions between biological tissue and THz light is to perform *ex vivo* studies, these are tests on healthy or diseased tissues that have been extracted from the body. These studies make it possible to test theories on what types of tissue THz light can distinguish between and explore the origin of this contrast, Table 1.1 gives a summary of the wide range of *ex vivo* studies that have been performed.

There are many advantages to performing measurements *ex vivo*; as the tissue has been extracted it can be thinly sliced making it possible to choose between reflection or transmission geometries, the results can be easily repeated many times without the repeatability concerns that arise from working with a living subject that breathes, moves and changes with time; *ex vivo* studies can make it possible to ethically test the effects of inducing changes in the skin that it would not be ethical to do on a living human subject such as burning the skin; finally *ex vivo* studies can be a useful first step as proof of concept before moving onto the more time intensive task of gathering subjects for an *in vivo* study.

However, despite the advantages there are also some drawbacks of *ex vivo* measurements; due to the time constraints between extracting the sample from the subject and performing the measurements it is often necessary to find some way to preserve the sample such as by freezing or formalin fixing. It is possible that some preservation techniques could interfere with the structure of the sample. Additional considerations include the fact that the skin in no longer alive therefore it is possible that the response may not be an exact replica of the response of living tissue; to apply the approach clinically an *ex vivo* test is invasive for the patient and does not take full advantage of the non-ionizing nature of THz light, which makes it so appealing for biomedical measurements. Considering the advantages and problems with *ex vivo* imaging it can be seen that it can be very useful in testing new ideas and theories and gaining understanding of the skin, but this should be done with the goal of working towards *in vivo* tests if they are to be applied to clinical investigations.

Application	Preservation	Geometry	Species	Reference
Transdermal Drug Delivery	Fresh	Reflection	Porcine	[33]
Moisturiser Absorption	Fresh	Reflection	Porcine	[34]
Burns	Fresh	Reflection	Porcine	[35]
BCC†	Fresh	Reflection	Human	[36]
Colon Cancer	FFPE*	Reflection/ Transmission	Human	[37]
Breast Cancer	FFPE*	Reflection	Human	[38]
Breast Cancer	FFPE*	Reflection/ Transmission	Human	[39, 40]
Oral Cancers	Frozen/ Fresh	Reflection	Human	[41, 42]
Oral Cancer	FFPE*	Layered Reflection	Human	[43]
Liver Cirrhosis	Fresh/FFPE*	Reflection	Rat	[44]

Table 1.1: A summary of *ex vivo* studies performed using THz measurements to observe contrast in tissue types or understand changes in the skin. *FFPE= Formalin Fixed Paraffin Embedded, †BCC=Basal Cell Carcinoma

Ex vivo studies can be broken into two categories; those performed on fresh samples and those that use some form of preservation. When fresh samples are used for a THz study this often restricts the study to a reflection geometry as samples are rarely thin enough for the THz signal to penetrate them sufficiently for a transmission measurement due to the high water content of the tissue.

Performing studies on fresh samples can be desirable when the absorption of a substance by the skin is being measured, as preservation is likely to interfere with the response of the skin. Wang *et al.* performed an *ex vivo* study on fresh porcine (pig) skin samples to test the ability of THz imaging to quantify the penetration of drugs in a solution through the skin and assess the effects of different penetration enhancement techniques such as micro and nano needle patches [33]. Another example of an *ex vivo* study on fresh skin was performed by Ramos-Soto *et al.* who investigated the effects of common moisturiser ingredients on an excised sample of porcine skin [34]. This study took advantage of the *ex vivo* nature of the work by placing the moisturiser sample onto the skin and then measuring the underside of the sample to observe how much of the moisturiser penetrated through the skin sample.

Additionally, Taylor *et al.* used fresh porcine tissue to observe with THz imaging the effect of burning the skin and found that they were able to identify the burn even underneath ten layers of gauze [35]. Some work has been done in testing fresh cancerous tissue for THz contrast for example Woodward *et al.* demonstrated the ability to identify Basal Cell Carcinoma (BCC) from THz images [36], however much of the work on cancerous tissues to date has been performed on tissues that have been preserved.

The preservation of excised tumours is common practice in hospitals to prepare the sample for the histological analysis required to identify if all the cancer has been removed. It is likely that the samples will be Formalin Fixed Paraffin Embedded (FFPE), this removes water from the sample and protects it from deterioration. The advantage of dehydrating the sample for THz measurements is that it can enhance the penetration of the THz pulse into the sample and improve the contrast between structurally different regions of the samples. Wahaia *et al.* successfully demonstrated the ability of THz measurements taken in reflection and transmission geometries to diagnose colon cancer [37]. Fitzgerald *et al.* demonstrated that THz imaging can be used to identify areas of cancerous tissue in excised breast samples from cancer patients, and the area of these regions was found to have moderate correlation with the results obtained when the samples underwent routine histological tests [38]. Bowman *et al.* also found contrast between different types of breast

tissue [39] and went on to use thin samples of breast cancer removed in surgery to compare the efficacy of reflection and transmission geometries [40].

An alternative approach to preserving samples is to freeze the tissue, this removes the liquid water from the sample so the THz signal is still able to penetrate further into the sample. Sim *et al.* performed a series of reflection measurements on a variety of excised oral cancers from a human subject at 20°C and −20°C [41, 42]. It was found that freezing the sample enhances the contrast between the cancerous and healthy tissue and makes it possible to identify cancerous regions below the sample surface by studying the time domain pulse for additional reflections. They also confirm that freezing the sample does not appear to disturb the structure of the sample observed in the THz image. Fan *et al.* proposed gelatin embedding as a way to keep the properties of the sample stable for at least 35 hours without changing the water distribution within the sample, this is a good option in cases where the origin of contrast between healthy and diseased tissue is thought to be the water concentration [45].

Sun *et al.* proposed a novel geometry for imaging thin samples in reflection and found that it is possible to enhance the contrast between healthy and cancerous regions of a paraffin embedded colon cancer sample [43]. By assembling a sandwich structure of a quartz prism and a quartz window around the thin tissue sample and imaging in reflection, it is possible to increase the contrast to five times that observed in a transmission measurement with results that agree well with the histological findings.

While some questions still remain about the origin of the contrast between healthy and diseased tissues in THz images, performing *ex vivo* studies can be a useful way to explore this as more controlled changes can be induced in an excised sample than in a living subject. For example, Sy *et al.* tested cirrhotic liver samples from rats when freshly excised and following formalin fixing [44]. They found that the fixing process slightly reduces the contrast between healthy and cirrhotic tissue but does not remove it. This indicates that while water content is a source of contrast it is not necessarily the only source and that structural changes in the tissue also affect the THz response.

1.2.2 *In Vivo* THz Spectroscopy and Imaging

Due to the non-ionizing nature of THz light it is desirable to find applications that can fully take advantage of this and perform clinical investigations *in vivo*. Depending on the region needing to be imaged it may be possible to perform studies non-invasively with no surgery required to remove the sample and take it away for

Application	**Species**	**Reference**
Burns	Rat	[46–48]
Burns	Pig	[49]
Burn Treatment	Human	[50]
Silicone Gel	Human	[51]
Flap Viability	Rat	[52]
Diabetic Foot	Human	[53]
Nevi Classification	Human	[54]
BCC	Human	[55]
Glucose Measurement	Mouse	[56]
Corneal Hydration	Rabbit	[57, 58]
Brain Glioma	Mouse	[59]

Table 1.2: A summary of *in vivo* THz measurements performed to investigate various potential applications.

analysis. This reduces associated risks from surgery and decreases the time between the investigation and getting the results to the patient. However, THz light is strongly absorbed by water, this means that the penetration into living tissue is very limited, so there are few regions that can be imaged non-invasively using THz light. Primarily the applications considered for *in vivo* measurements involve regions that can be accessed without passing through other tissues for example the skin and the eye. For these applications a reflection geometry is required as the samples are too thick for the radiation to penetrate for a transmission setup to be utilised. A summary of recent studies testing the efficacy of *in vivo* THz measurements for various applications is shown in Table 1.2.

The advantage of performing *in vivo* skin studies is that it is possible to study the response of living skin to certain treatments or observe the recovery of the skin from certain stimuli. However, *in vivo* measurements can be harder to perform as there are many more variables that need to be controlled throughout the measurements. For example with a living subject it is much harder to keep constant contact with the region to be imaged as the subject may move around. Also, human subjects interact with a variety of stimuli before entering the lab for the study, including weather conditions, food, drink, washing and skin treatments.

In order to perform repeatable *in vivo* measurements it is necessary to consider the effect all these variables could have on the measurement and develop a protocol to control these as much as possible. If THz imaging is to be adopted as a clinical imaging modality it is essential that a suitable approach can be adopted to isolate the desired feature of the skin from all the other variables. These considerations have been developed further through the research described in this thesis and will be discussed in detail in Chapter 3.

When the tissue to be studied is on the surface of the skin it is easier to perform non-invasive THz measurements as there are fewer limitations caused by the small penetration depth. For example, Tewari *et al.* compared the THz response of burned rat skin to optical images of the same regions [46]. The key factor when considering studies like this is to ensure that the two images can be aligned for comparison; in this study they used reflective markers that can be seen with both THz and optical images to aid alignment. This study integrates the THz and optical measurements to produce a combined image to yield more information about the severity of the burn. Additionally, Bajwa *et al.* performed an *in vivo* study on rat burns, comparing the THz results with Magnetic Resonance Imaging (MRI) to confirm that THz imaging can identify the presence of burns and strong correlation was found between the results of the two techniques [47].

Arbab *et al.* also explore the application of THz measurements for the classification of burns [48]. This study used THz-TDS to measure the spectral response of a single region of a burn. They used nine rats in their study, five of which were inflicted with a second degree burn and four with a third degree burn, regions left uninjured were also marked on each rat to act as a control region. Both regions were measured on each rat immediately following the burn and 72 hours following the burn. The results were compared to histology results obtained following the excision of the burned area at the end of the study. Using these results with a defined spectral parameter for skin classification, they were able to demonstrate the ability of THz spectroscopy to identify healthy and burned skin.

This group then expanded upon the study by performing measurements on porcine skin, as this is thought to be a better model for human skin [49]. Three pigs were measured and on each pig three regions were burned for increasing durations to increase the severity and depth of the burn. The results of the THz measurements were compared to the current gold standard for burn depth assessment: vimentin immunohistochemistry. They found that there was good correlation between the burn depth and the spectral parameter, suggesting that THz measurements could be an effective way to quickly assess the severity and depth of a burn. It is hoped

that this work could be used to develop THz spectroscopy into a technique that can predict healing outcomes and identify which treatment option would be most effective.

Fan *et al.* demonstrated that it is possible to use THz imaging to observe the healing process of scars on human subjects [50]. By comparing the THz images of the scarred tissue and surrounding healthy tissue to visible images of the same regions it was possible to confirm the contrast in the THz images and the links to the structural changes in the skin. It was also possible to continue to observe changes in the refractive index and absorption coefficient at THz frequencies up to six months post injury, even when the visible changes within the region were minimal.

Wang *et al.* used *in vivo* measurements on human forearms to observe the effects of silicone gel sheeting on the skin, a common treatment for severe burns [51]. This study could not be performed *ex vivo* as the primary effect arises from the accumulation of water within the upper layers of the skin caused by the occlusive effect of the sheet. Even after the sheet has been removed an increase in the water content can be observed in the skin for up to 80 minutes following treatment.

THz imaging has also been explored as a possible approach for assessing whether skin grafts will be successful, Bajwa *et al.* performed an *in vivo* study measuring the change in water content of partially and fully excised skin samples [52]. The results from the THz images were compared with those from visible images and histological analysis. The THz imaging results showed a significant difference between the study groups 24 hours after the procedure, while the visible image did not yield a significant difference until 72 hours after the procedure. This means that THz imaging could yield earlier results about the viability of skin flaps for surgery and verifies the ability of THz imaging to diagnose the water content of skin.

One of the largest scale tests of the potential of THz imaging to solve a clinical need is the study by Hernandez-Cardoso *et al.* demonstrating the success of THz imaging in diagnosing diabetic foot syndrome [53]. As diabetic foot syndrome is linked to extreme dehydration the high sensitivity of THz imaging to water content can be applied to not only diagnose patients with the disease but also classify the severity of the case. An additional advantage of studying diabetic foot syndrome is that the present clinical approach to diagnosis is to check for patient sensitivity in the region, which can be very subjective. This study involved 33 healthy control subjects and 38 subjects with diabetes, and was able to find significant differences in the THz responses of the two groups.

Zaytsev *et al.* performed *in vivo* measurements of healthy skin, dysplastic nevi (precancerous moles) and non-dysplastic nevi (regular moles) on four pa-

tients [54]. It was found that there was significant contrast in the extracted dielectric constant between the different tissue types from 0.3−1 THz. In the study by Wallace *et al.* it was demonstrated that it is possible to observe contrast in THz images between healthy tissue and BCCs [55]. In this study 18 BCCs were imaged *ex vivo* and five were imaged *in vivo*. Similar levels of contrast were observed *in vivo* and *ex vivo* suggesting that THz imaging could be a quick and safe technique to diagnose skin cancers. Additionally, the tumour margins identified from the THz images agreed with the histology results.

Another application for which it is hoped that THz measurements could provide a non-invasive *in vivo* solution is blood glucose evaluation. At present people with diabetes are often required to prick their finger to extract blood to test their blood glucose levels, which can be painful and inconvenient. Chen *et al.* demonstrated the potential sensitivity of THz *in vivo* measurements to blood glucose in mice [56]. A key difference for this study is that the measurements were performed using a transmission geometry using the thin capillaries in the mouse's ear, an approach which is not yet replicable in humans.

Taylor *et al.* demonstrated the successful application of THz imaging for assessing corneal water content on rabbits. Using a contact reflection geometry it was possible to observe changes in the water content caused by the death of the rabbit, this shows that it could be possible to use THz imaging to diagnose corneal diseases [57]. In a further study by the same group, a non-contact imaging system was used to image human corneas *in vivo* [58]. This demonstrates the progression of the field from the proof of concept to further development into a clinical tool that can be used non-invasively on humans.

One final example of an *in vivo* THz study involved the diagnosis of brain gliomas in mice [59]. However, this procedure was invasive and involved drilling into the skull and the subject was euthanised straight after the measurement, so it is a proof of concept rather than a clinical option. Despite this the study was successful in demonstrating correlation between the MRI results and those from THz imaging.

1.3 Thesis Overview

This thesis presents a series of studies into the potential of THz imaging and spectroscopic techniques for observing changes in the skin. In Chapter 2 the theory used in the remainder of the thesis is outlined, including the approaches used to process the measured data and the various modelling techniques that have been used in this and other studies to extract the water content of the skin using THz

measurements. These approaches were then put into practice in Chapter 3 where the effects of pressure and occlusion on the THz response of skin were investigated and a protocol was developed and tested in order to make it possible to control and account for the effects of these variables on the measured changes in the skin. Chapter 4 contains a study performed involving 20 human volunteers comparing the results of THz measurements of the skin with two other techniques for skin hydration assessment, which are commonly used in the skin care industry, the three measurement techniques were used following the application of three different types of skin moisturisers, which are expected to increase the hydration of the skin. In Chapter 5 a study is presented on the application of THz measurements of the skin to assess the effect of patches for transdermal drug delivery on the skin in order to investigate how this could affect the rate of drug delivery through the skin barrier, as this is largely dependent on the hydration levels of the skin. The final study that was performed involved 34 subjects and explored how variables such as skin tone and sex can affect the THz response of the skin and how the skin responds to the application of different types of moisturisers, this is presented in Chapter 6. Finally, Chapter 7 is a summary of the work in this thesis and identifies potential areas in which this research could be built upon and areas for further work.

Chapter 2

Theory and Systems

2.1 Introduction

Whilst the experimental considerations for *in vivo* THz measurements are a primary focus of the subsequent work, it is vital that the theory and processing techniques used to extract parameters such as the refractive index are explained. Section 2.2 begins with a general overview of how waves propagate through materials and respond to interfaces. Section 2.3 explains how optical parameters are extracted for transmission measurements for both bulk and thin film samples. In Section 2.4, the processing techniques employed for the data obtained using a reflection geometry are explained. Processing data obtained using a reflection geometry is particularly vital for the *in vivo* studies described in this thesis, this section only considers bulk samples as these were the only type of reflection measurements performed for this work. The various approaches used to model the skin in order to link the observed changes in the THz reflectivity to physical changes in the skin are introduced in Section 2.5. Finally, Section 2.6 outlines the experimental setups used to perform measurements using reflection and transmission geometries for the studies described in subsequent chapters.

2.2 Wave Propagation in Media

2.2.1 Wave Equations

The behaviour of electric and magnetic fields is described by Maxwell's equations in Equations 2.1-2.4, this form of the equations is for a homogeneous, isotropic medium in the absence of charges or currents, where $\boldsymbol{E}$ and $\boldsymbol{B}$ are the electric and magnetic

fields respectively and ϵ and μ are the permittivity and permeability of the medium.

$$\boldsymbol{\nabla} \cdot \boldsymbol{E} = 0 \tag{2.1}$$

$$\boldsymbol{\nabla} \times \boldsymbol{E} = -\frac{\partial \boldsymbol{B}}{\partial t} \tag{2.2}$$

$$\boldsymbol{\nabla} \cdot \boldsymbol{B} = 0 \tag{2.3}$$

$$\boldsymbol{\nabla} \times \boldsymbol{B} = \mu\epsilon\frac{\partial \boldsymbol{E}}{\partial t} \tag{2.4}$$

From these equations it is possible to derive the wave equation to describe the propagation of electric fields in a medium by taking the curl of Equation 2.2 and applying the vector identity stated in Equation 2.5.

$$\boldsymbol{\nabla} \times (\boldsymbol{\nabla} \times \boldsymbol{A}) = \boldsymbol{\nabla}(\boldsymbol{\nabla} \cdot \boldsymbol{A}) - \boldsymbol{\nabla}^2\boldsymbol{A} \tag{2.5}$$

The wave equation for an electric field propagating in the medium is given by Equation 2.6.

$$\nabla^2\boldsymbol{E} = \mu\epsilon\frac{\partial^2 \boldsymbol{E}}{\partial t^2} \tag{2.6}$$

From this it is possible to deduce the speed of propagation in the medium: $v = \frac{1}{\sqrt{\epsilon\mu}}$. In the case where the wave is travelling through a vacuum $v = c$, the value for the speed of light can be obtained in terms of two vacuum constants; the permittivity of free space $\epsilon_0 = 8.85 \times 10^{-12}$ Fm^{-1} and the permeability of free space $\mu_0 = 4\pi \times 10^{-7}$ NA^{-2}: $c = \frac{1}{\sqrt{\epsilon_0\mu_0}} = vn$. Here the refractive index n is introduced as a property of the given medium representing the ratio between the speed of light in a vacuum c and the propagation speed in the medium v. A solution to the wave equation is given by Equation 2.7, for a wave travelling in the x direction where t is time, E_0 is the amplitude of the wave, ω is the angular frequency given in terms of the frequency f by $\omega = 2\pi f$ and k is the wavenumber given by $k = \frac{\tilde{n}w}{c}$.

$$E(x,t) = E_0 e^{i(\omega t - kx)} \tag{2.7}$$

Here the refractive index is a complex variable defined by: $\tilde{n} = n - i\kappa$, where n is the real part of the refractive index and κ is the extinction coefficient. From here on the term 'refractive index' will be used to refer to the real part of the refractive index n, and $\tilde{n}$ will be referred to explicitly as the complex refractive index. The minus sign used in the definition of $\tilde{n}$ arises from the form of the wave given in Equation 2.7 and ensures that a positive κ corresponds to the loss of the signal in the medium. Both the complex refractive index and complex permittivity, $\boldsymbol{\epsilon_r}$,

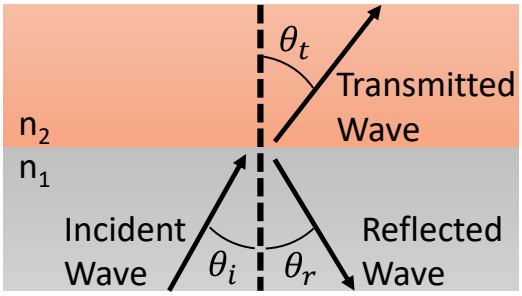

Figure 2.1: The behaviour of an incident wave travelling in a medium with refractive index n_1 upon encountering an interface with a medium with refractive index n_2, showing the reflected and transmitted waves and the corresponding angles of their trajectories.

are parameters that will be useful in characterising properties of media, they are related to one another by Equation 2.8, where ϵ_r' and ϵ_r'' are the real and imaginary components of the complex permittivity.

$$\boldsymbol{\epsilon_r} = \epsilon_r' - i\epsilon_r'' = \tilde{n}^2 = (n^2 - \kappa^2) - i2n\kappa \tag{2.8}$$

Returning to the wave defined in Equation 2.7, some of these definitions can be applied to rewrite this equation in order to obtain Equation 2.9.

$$E(x,t) = E_0 e^{-\frac{\alpha x}{2}} e^{i(\omega t - \frac{\omega n x}{c})} \tag{2.9}$$

Here the absorption coefficient α is introduced, defined by $\alpha = \frac{2\omega\kappa}{c}$, which determines how the magnitude of E will decrease with distance as the wave travels through a medium. It can be observed from this result that n will change the phase of the wave as it propagates through the medium.

2.2.2 Reflection and Transmission at Interfaces

Having considered how the motion of waves through media can be described, the behaviour of waves at interfaces between two media with different optical properties must now be considered. The change in angle when a wave is refracted at an interface is described by Snell's law in Equation 2.10, where n_1 and n_2 are the refractive indices of the two layers and θ_i and θ_t are angles of the incident and transmitted waves as demonstrated in Figure 2.1.

$$n_1 \sin\theta_i = n_2 \sin\theta_t \tag{2.10}$$

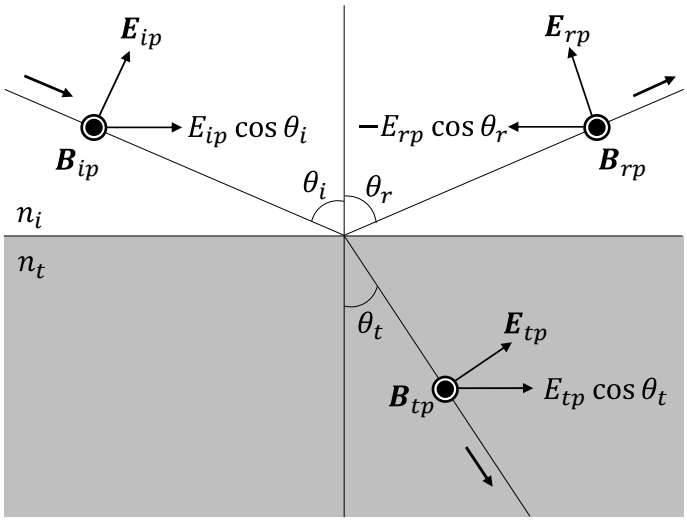

Figure 2.2: The behaviour of p-polarised light upon reflection and transmission at an interface.

The figure shows that in addition to being transmitted at an interface some of the light is also reflected at an angle $\theta_r = \theta_i$. The proportion of light reflected depends on the properties of the two layers, the incident angle and the polarisation state (s or p) of the incident radiation. When the electric fields of the incident and reflected light oscillate in the incident plane this is known as p-polarised light. The behaviour of $\boldsymbol{E}$ and $\boldsymbol{B}$ fields for p- and s-polarised states upon reflection and transmission can be seen in Figures 2.2 and 2.3 respectively.

It is possible to derive the reflection and transmission coefficients of an interface, which define the ratio of the electric fields reflected or transmitted at the interface relative to the incident wave. These coefficients are different for s- and p-polarised light and can be derived using the boundary condition that requires $\boldsymbol{E}$ and $\boldsymbol{B}$ components parallel to the interface to be continuous at the interface.

In order to derive the properties of the interface for p-polarised light, the expressions in Equations 2.11 and 2.12 are extracted using the boundary condition and components of the fields shown in Figure 2.2.

$$E_{ip}\cos\theta_i - E_{rp}\cos\theta_r = E_{tp}\cos\theta_t \tag{2.11}$$

$$B_{ip} + B_{rp} = B_{tp} \tag{2.12}$$

Using $E = \frac{c}{\tilde{n}}B$ it is possible to rewrite Equation 2.12 in terms of E, as shown in

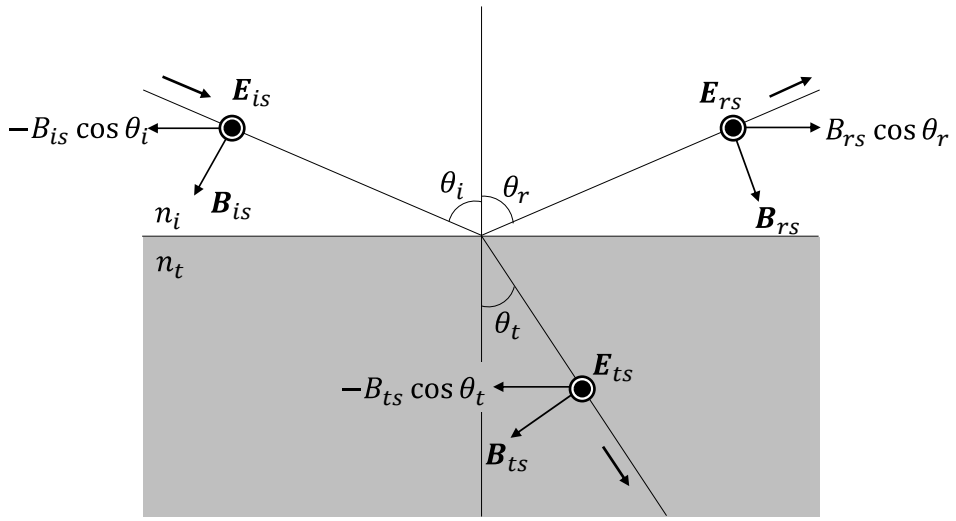

Figure 2.3: The behaviour of s-polarised light upon reflection and transmission at an interface.

Equation 2.13.

$$\tilde{n}_i E_{ip} + \tilde{n}_i E_{rp} = \tilde{n}_t E_{tp} \tag{2.13}$$

By combining Equations 2.11 and 2.13 it is possible to obtain the reflection coefficient, r_p, and transmission coefficient, t_p, for p-polarised light, as stated by Equations 2.14 and 2.15.

$$\frac{E_{rp}}{E_{ip}} = r_p = \frac{\tilde{n}_t \cos\theta_i - \tilde{n}_i \cos\theta_t}{\tilde{n}_t \cos\theta_i + \tilde{n}_i \cos\theta_t} \tag{2.14}$$

$$\frac{E_{tp}}{E_{ip}} = t_p = \frac{2\tilde{n}_i \cos\theta_i}{\tilde{n}_t \cos\theta_i + \tilde{n}_i \cos\theta_t} \tag{2.15}$$

Moving to Figure 2.3 and the boundary conditions at the interface, it is possible to derive the expressions for the Fresnel coefficients for s-polarised light, the expressions obtained from the application of the boundary condition are given by Equations 2.16 and 2.17.

$$-B_{is}\cos\theta_i + B_{rs}\cos\theta_r = -B_{ts}\cos\theta_t \tag{2.16}$$

$$E_{is} + E_{rs} = E_{ts} \tag{2.17}$$

As before the B field terms in Equation 2.16 can be replaced with E terms, in order to obtain Equation 2.18.

$$-\tilde{n}_i E_{is}\cos\theta_i + \tilde{n}_i E_{rs}\cos\theta_r = -\tilde{n}_t E_{ts}\cos\theta_t \tag{2.18}$$

Combining Equations 2.17 and 2.18 it is possible obtain the Fresnel reflection coefficient, r_s, and transmission coefficient, t_s, for the interface for s-polarised light, as stated by Equations 2.19 and 2.20 respectively.

$$\frac{E_{rs}}{E_{is}} = r_s = \frac{\tilde{n}_i \cos\theta_i - \tilde{n}_t \cos\theta_t}{\tilde{n}_i \cos\theta_i + \tilde{n}_t \cos\theta_t} \tag{2.19}$$

$$\frac{E_{ts}}{E_{is}} = t_s = \frac{2\tilde{n}_i \cos\theta_i}{\tilde{n}_i \cos\theta_i + \tilde{n}_t \cos\theta_t} \tag{2.20}$$

Note that while the derived reflection and transmission coefficients have a dependence on θ_t, it is possible to rewrite them in terms of θ_i alone using Snell's law introduced in Equation 2.10, an example of this is shown by Equation 2.21.

$$r_s = \frac{\tilde{n}_i \cos\theta_i - \sqrt{\tilde{n}_t^2 - \tilde{n}_i^2 \sin\theta_i}}{\tilde{n}_i \cos\theta_i + \sqrt{\tilde{n}_t^2 - \tilde{n}_i^2 \sin\theta_i}} \tag{2.21}$$

2.3 Processing THz Transmission Measurements

The geometries and experimental setups used to perform transmission measurements in the studies in this thesis are described in more detail in Section 2.6.2. In this thesis the primary use of transmission measurements is to characterise liquid samples before they are applied to the skin. To measure liquids in transmission a liquid cell is used, where the liquid to be measured is sandwiched between two pieces of quartz. A spacer is placed between the quartz pieces to control the thickness of the sample. For samples such as water that are highly absorbing at THz frequencies a very small spacer must be used (around 0.1mm) to allow enough of the THz signal to penetrate the liquid cell so as to be able to obtain a sufficient signal to noise ratio to characterise the sample. These calculations assume that the THz pulse enters the sample at normal incidence.

2.3.1 Bulk Samples

If the liquid sample being measured is sufficiently thick (greater than the wavelength of THz light) any etalon effects from reflections within the cell are separated enough that they can be easily removed from the measured pulse, so when deriving equations to describe the propagation of the THz light through the system only transmission terms need to be considered. This experimental configuration cannot be used for highly absorbing materials such as water as the sample would be too thick in this setup for any THz light to be transmitted, in this case thin films should be measured,

these results can be processed using the techniques described in Section 2.3.2.

To study a sample sandwiched between two layers, the transmission of the THz light at each interface and the propagation of the pulse through each of the layers must be considered. By doing this a theoretical sample to reference ratio, E_s/E_r, can be obtained in terms of the Fresnel transmission coefficients, t_{ij}, as shown in Equation 2.22. Where $P_i = e^{-ik_0 d_i \tilde{n}_i}$ describes the propagation of the pulse through the ith layer, d_i is the thickness of the ith component of the liquid cell system, k_0 is the propagation constant where $k_0 = 2\pi f/c$. In this equation the reference is a measurement of the sandwich structure without the sample, meaning that there is an air gap in the middle with the same thickness as the sample.

$$\frac{E_s}{E_r} = \frac{t_{01}P_1t_{12}P_2t_{23}P_3t_{30}}{t_{01}P_1t_{10}P_0t_{03}P_3t_{30}} \tag{2.22}$$

$$= \frac{t_{12}t_{23}P_2}{t_{10}t_{03}P_0} \tag{2.23}$$

By replacing the transmission and propagation terms in Equation 2.23 with their full definitions in terms of the complex refractive index, it is possible to equate this theoretical ratio to the optical properties of the sample to give a problem that can be solved analytically.

2.3.2 Thin Film Samples

When measuring a thin material using a transmission geometry, reflections within the sample cell must be accounted for as the signal can be reflected between the two windows and arrive in a short enough time after the initial pulse that they cannot be separated from the first pulse. In order to process results measured using thin film samples the equation for the theoretical sample to reference ratio must be adapted to include the pulses that have been internally reflected within the sample before being transmitted through the structure.

Equations 2.24−2.28 show the derivation of the expressions for the sample and reference pulses in terms of the Fresnel coefficients and P_i. Equation 2.24 is the expression representing each of the terms for pulses reflecting, transmitting and propagating through the liquid cell system. The first term represents the propagation of the pulse straight through the cell as occurs in the bulk, the second term involves a reflection between the two quartz windows before arriving at the detector and subsequent terms correspond to an increasing number of reflections between the windows. Etalon effects within the quartz windows can be ignored in this case as

it is assumed that they are thick enough that any pulses that have been reflected would arrive significantly later. This series of terms can be written in the form of a power series as shown in Equation 2.26, making it possible to rewrite the equation using the summation identity: $\sum_{n=0}^{\infty} x^n = \frac{1}{1-x}$, giving the result shown in Equation 2.27 [60]. Note that the sign change in Equation 2.27 comes from the reordering of the indices in the r_{21} term.

The equivalent expression for the reference is shown in Equation 2.28, the only difference being that the index of 2 has been replaced with 0 as the reference is air, which will be the same as the medium before and after the liquid cell. This can be edited accordingly if an alternative measurement is used as a reference.

$$E_s = (t_{01}t_{12}t_{23}t_{30}P_1P_2P_3 + t_{01}t_{12}r_{23}r_{21}t_{23}t_{30}P_1P_2^3P_3 + ...) \tag{2.24}$$

$$= t_{01}t_{12}t_{23}t_{30}P_1P_2P_3(1 + P_2^2r_{23}r_{21} + P_2^4r_{23}^2r_{21}^2 + ...) \tag{2.25}$$

$$= t_{01}t_{12}t_{23}t_{30}P_1P_2P_3\sum_{n=0}^{\infty}(P_2^2r_{23}r_{21})^n \tag{2.26}$$

$$= t_{01}t_{12}t_{23}t_{30}P_1P_2P_3\frac{1}{1 + r_{12}r_{23}P_2^2} \tag{2.27}$$

$$E_r = t_{01}t_{10}t_{03}t_{30}P_1P_0P_3\frac{1}{1 + r_{03}r_{10}P_0^2} \tag{2.28}$$

By dividing Equation 2.27 by Equation 2.28 the theoretical sample to reference ratio can be calculated, as shown in equation Equation 2.29. This is useful for extracting the optical properties of the sample as this ratio can be found from the measured response of the system, which can then be compared to the theoretical value.

$$\frac{E_s}{E_r} = \frac{t_{12}t_{23}P_2}{t_{10}t_{03}P_0}\frac{(1 + r_{10}r_{03}P_0^2)}{(1 + r_{12}r_{23}P_2^2)} \tag{2.29}$$

The code used to perform this calculation in this thesis uses the numerical approach described by Chen *et al.* [61].

2.4 Processing THz Reflection Measurements

To study biological samples *in vivo* a reflection geometry is often used as the attenuation of light at THz frequencies is too high for the signal to penetrate bulk samples. As with the transmission geometry, a bulk sample is considered to be one with a width much larger than the wavelength of the THz light used to perform the measurements, meaning that internal reflections within the sample can be neglected and do not interfere with the measured sample response. Therefore, at 1 THz a

thin film is classified as a material with a thickness less than 0.3 mm. In all of the studies presented in this thesis the volar forearm is considered to be a bulk material as the separate structures of the Stratum Corneum (SC) and epidermis are neglected, therefore thin film reflection measurements will not be discussed here. However, some models account for these distinct structural layers within the skin and for the internal reflections within these layers; such models will be discussed further in Section 2.5.3. The experimental setup uses a reflection geometry system in which a quartz imaging window is used to ensure consistent alignment of the THz beam relative to the arm and flatten the region to be imaged, as curvature can make it harder to align the system. Additionally, the reflection from the lower surface of the quartz window should be identical for all sample and reference measurements if there is no variation in the incident THz pulse. So this first reflection can be used to calibrate the measurements to account for any fluctuations in the incident THz pulse between measurements. Whilst the use of the quartz imaging window is helpful, the effects of the window on the measured signal must be removed for the properties of the sample to be isolated.

2.4.1 Baseline Subtraction Techniques

Figure 2.4 shows the schematics for the measurements of the sample, reference and baseline: E_{sam}, E_{ref} and E_{base}, which must be acquired in order to complete the data processing techniques required to extract the properties of the sample. When the sample is measured whilst in contact with the quartz window as shown in Figure 2.4 a) there are two reflected pulses measured, one from the lower surface of the quartz window and one from the upper surface of the quartz window, which is in contact with the sample. Additionally, an air reference measurement is acquired when there is no sample in contact with the window, this is illustrated by Figure 2.4 b). As the first reflection from the lower surface of the quartz is present in both E_{sam} and E_{ref} it is necessary to take a third measurement of the first reflection alone so that it can be removed from the sample and reference measurements. To do this a second piece of quartz is placed on top of the quartz imaging window as shown in Figure 2.4 c) to prevent the second reflection, this measurement of E_{base} makes it possible to fully characterise the first reflection including the ongoing ringing effect caused by the presence of water vapor in the air, which can persist into the second reflection [62]. The optics must remain in the same configuration relative to the imaging window for the reference and baseline measurements corresponding to each sample measurement.

The sample, reference and baseline pulses are indicated on a schematic of the

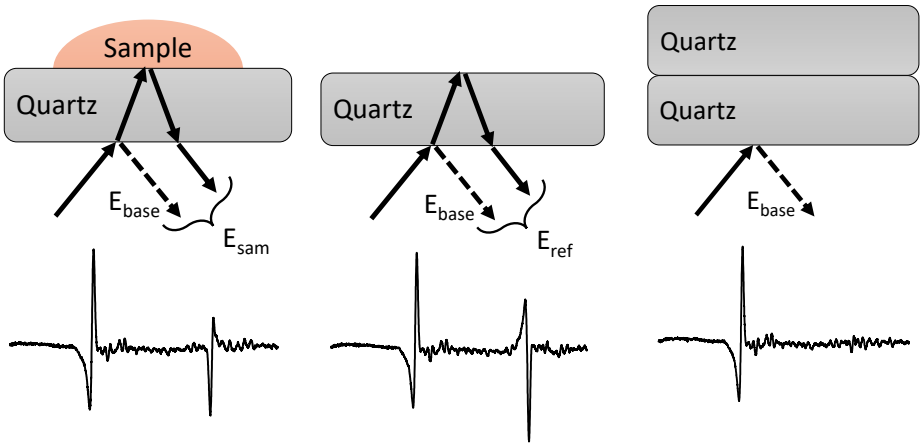

(a) Sample (b) Reference (c) Baseline

Figure 2.4: The measurements taken to study a bulk sample in reflection geometry using a quartz window, including examples of the measured THz pulses.

system used to perform reflection measurements in Figure 2.5. These measurements of the sample, reference and baseline pulses in the time domain can then be used to calculate the measured sample to reference ratio M_{meas}, as shown in Equation 2.30.

$$M_{meas} = \frac{FFT(E_{\text{sam}}(t) - E_{\text{base}}(t))}{FFT(E_{\text{ref}}(t) - E_{\text{base}}(t))}, \tag{2.30}$$

This ratio is useful for interpreting the results and extracting the optical properties of the sample. For example a processed time domain signal is defined in Equation 2.31, which uses the measured sample to reference ratio M_{meas} with a double Gaussian filter to remove low and high frequency noise from the measurement.

$$\text{Processed Signal} = iFFT[FFT(\text{filter}) \times M_{meas}] \tag{2.31}$$

This processed signal is commonly used and referred to throughout this thesis, in particular the amplitude of the signal is used to quantify changes in the THz response of the skin. The links between the amplitude of this signal and the water content of the skin will be explored further using various modelling approaches in Section 2.5.4.

2.4.2 Calculating the Optical Properties of Samples

From the measured responses of the sample and reference acquired it is possible to extract the optical properties of the sample. In this section the sample is assumed

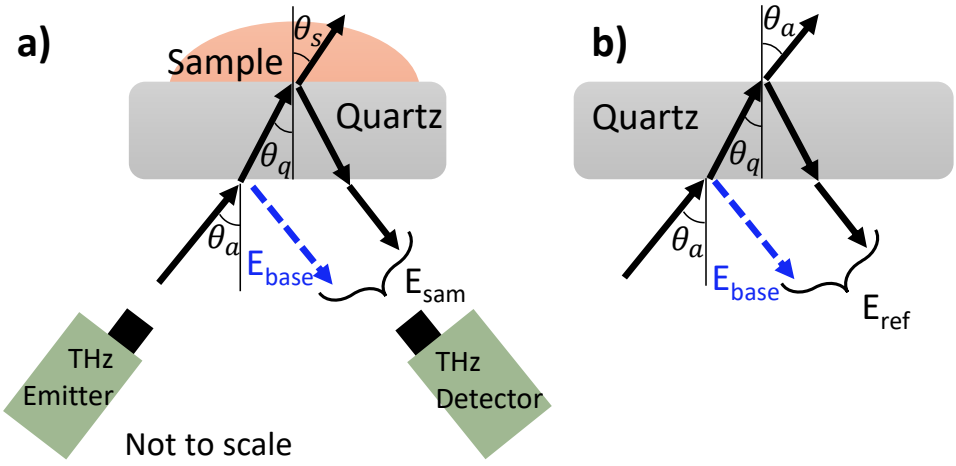

Figure 2.5: A schematic for THz reflection measurements a) acquiring the sample measurement and b) acquiring the air reference. The baseline reflection from the lower surface of the quartz is shown by the dashed blue lines in both figures. a) includes the locations of the THz probes.

to be comprised of a single homogeneous layer, this is an oversimplification of the structure of the skin but it gives a problem that can be quickly solved analytically. More complex theoretical models of the skin will be introduced in Section 2.5.

The theoretical sample to reference ratio, M_{theo}, can be written in terms of the Fresnel coefficients for the quartz-sample and quartz-air interfaces r_{qs} and r_{qa} respectively, which are a function of the complex refractive index of the sample. Using Snell's law to reduce the number of unknown variables, M_{theo} can be equated to the measured ratio M_{meas} using Equations 2.32 and 2.33.

$$M_{theo} = \frac{r_{qs}}{r_{qa}} = \frac{\tilde{n}_q \cos\theta_q - \tilde{n}_s \cos\theta_s}{\tilde{n}_q \cos\theta_q + \tilde{n}_s \cos\theta_s} \times \frac{\tilde{n}_q \cos\theta_q + \tilde{n}_a \cos\theta_a}{\tilde{n}_q \cos\theta_q - \tilde{n}_a \cos\theta_a} = M_{meas} \tag{2.32}$$

$$n_a \sin\theta_a = n_q \sin\theta_q = n_s \sin\theta_s \tag{2.33}$$

Where n_q, n_a and n_s are the refractive indices of the quartz, air and sample respectively and θ_q, θ_a and θ_s are the angles of the THz light within the quartz window, air and sample respectively, as shown in Figure 2.5.

Using Equations 2.32 and 2.33 an expression can be found for the properties of the sample in terms of known variables including M_{meas}, which can be input into this equation following the measurement. For clarity X is used to denote $\tilde{n}_s \cos\theta_s$, it is therefore possible to find $\tilde{n}_s$ in terms of known properties of the system and the

measured sample to reference ratio, as shown in Equations 2.34−2.36 [63].

$$X = \tilde{n}_s \cos\theta_s \tag{2.34}$$

$$= \frac{\tilde{n}_q^2 \cos^2\theta_q(1 - M_{meas}) + \tilde{n}_a\tilde{n}_q \cos\theta_a \cos\theta_q(1 + M_{meas})}{\tilde{n}_q \cos\theta_q(1 + M_{meas}) + \tilde{n}_a \cos\theta_a(1 - M_{meas})} \tag{2.35}$$

$$\tilde{n}_s = \sqrt{X^2 + \tilde{n}_q^2 \sin^2\theta_q} \tag{2.36}$$

From $\tilde{n}_s$ it is possible to extract various optical properties of the samples using the definitions stated in Section 2.2.1, as shown in Equations 2.37-2.39.

$$n_s = Re(\tilde{n}_s) \tag{2.37}$$

$$\kappa_s = -Im(\tilde{n}_s) \tag{2.38}$$

$$\alpha_s = \frac{4\pi f \kappa_s}{c} \tag{2.39}$$

These equations are for s-polarised light, a similar process can be performed for p-polarisation however the mathematics are slightly more complicated meaning that a numerical approach is often preferable. Owing to the speed and ease of calculating the optical properties from measurements using s-polarised THz light, all of the studies described in this thesis were performed using s-polarisation. Additionally, using s-polarised THz light makes it possible to compare the trends in the refractive index of the skin with those observed in previous THz studies of the skin, which commonly used s-polarisation.

2.5 Approaches to Skin Modelling

In addition to using the measured THz response of skin to calculate the optical properties such as the refractive index and the absorption coefficient, modelling techniques can also be used to learn more about changes in the skin, particularly its hydration. As the complexity of the model used increases so do the time taken to perform such calculations and the number of unknown parameters, leading to a greater number of potential solutions. Many of the models presented in this section have only been used for untreated skin and have not yet been adapted to include the effects of moisturisers or other skin treatments on the THz response of the skin. Therefore, the application of such approaches throughout this thesis are limited, however they are important to understand how the measured changes in the THz response are linked to changes in the hydration and structural properties of the skin. There is still much more work to be done in this area in order to enhance the

information that can be gained about the skin using THz measurements. In this section only a brief introduction is given to some of the key models that are most relevant for this thesis, a more complete summary can be found in reference [64].

2.5.1 Double Debye Model

One of the first models used to describe the interaction of THz light with biological tissues was the Double Debye model. This has previously been used to describe the permittivity of liquid water, due to the high water content of biological tissues the Double Debye model can also be used to describe the THz response of human skin. The complex permittivity of biological tissues $\boldsymbol{\epsilon}_r$ according to the Double Debye model is given by Equation 2.40.

$$\boldsymbol{\epsilon}_r(\omega) = \epsilon_\infty + \frac{\epsilon_s - \epsilon_2}{1 + i\omega\tau_1} + \frac{\epsilon_2 - \epsilon_\infty}{1 + i\omega\tau_2} \tag{2.40}$$

Where ϵ_∞ is the limiting permittivity at high frequencies, ϵ_s is the static permittivity, ϵ_2 is the intermediate permittivity limit. τ_1 and τ_2 are relaxation constants corresponding to the slow and fast relaxation processes occurring when the hydrogen bonds between water molecules break and reorientate and move to a new tetrahedral site. This set of five parameters are known as the Double Debye parameters and can be used to describe the complex permittivity of biological samples.

Pickwell *et al.* successfully used the Double Debye model with finite difference time domain techniques to simulate the THz response of the skin [65, 66]. Truong *et al.* showed that extracting the Double Debye parameters from THz measurements of the skin makes it possible to distinguish between healthy and cancerous skin [67, 68]. The Double Debye model has been investigated as an approach that can be used to help classify healthy and diseased tissue and give a quantitative comparison between different types of tissues. A summary of the Double Debye parameters that have been extracted for different tissues is presented by Zaytsev *et al.* [69].

Despite the successes of the Double Debye model there are some concerns about its suitability for describing dry skin regions as it only describes the water component of the skin. More complex models use the Double Debye model alongside other components that account for the contribution of dry skin to the dielectric properties of biological tissues.

2.5.2 Effective Medium Theory

Effective medium theories make it possible to combine the dielectric properties of the individual components of a sample in order to obtain the dielectric properties of the mixture as a function of the fractional contents of each of the components in the mixture. This makes effective medium theories useful tools for describing the dielctric properties of biological tissues in terms of a water component and a biological background component, which represents dry skin. The dielectric properties of water can be described using the Double Debye model introduced in Section 2.5.1 and the biological background can be modelled using measurements of dehydrated skin such as those obtained by He *et al.* [70]. The choice of biological background model used in a study can lead to variation in the results obtained by different groups.

The Landau Lifshitz Looyenga (LLL) model considers the shape of the biological background components to be arbitrary and is commonly used to extract the hydration of a tissue from the measured THz response of the sample such as in the study on diabetic feet performed by Hernandez-Cardoso *et al.* [53]. The LLL model describes the effective permittivity of a biological sample $\boldsymbol{\epsilon}_{eff}$ in terms of the permittivity of water $\boldsymbol{\epsilon}_w$ and dehydrated skin $\boldsymbol{\epsilon}_s$ and the fractional content of water and dehydrated skin in the sample η_w and η_s respectively, as shown in Equation 2.41.

$$\sqrt[3]{\boldsymbol{\epsilon}_{eff}} = \eta_w \sqrt[3]{\boldsymbol{\epsilon}_w} + \eta_s \sqrt[3]{\boldsymbol{\epsilon}_s} \tag{2.41}$$

The Bruggeman model shown in Equation 2.42, is a commonly used alternative to the LLL model and works on the assumption that the dehydrated skin components are spherical inside the water component.

$$\eta_w \frac{\boldsymbol{\epsilon}_w - \boldsymbol{\epsilon}_{eff}}{\boldsymbol{\epsilon}_w + 2\boldsymbol{\epsilon}_{eff}} + \eta_s \frac{\boldsymbol{\epsilon}_s - \boldsymbol{\epsilon}_{eff}}{\boldsymbol{\epsilon}_s + 2\boldsymbol{\epsilon}_{eff}} = 0 \tag{2.42}$$

Both the LLL and Bruggeman models can be expanded to include additional components in the mixture if required by adding more terms; however, this does increase the number of unknown parameters leading to a higher number of degrees of freedom when fitting the theoretical THz response to the measured response.

These models alongside others can be used to express the theoretical permittivity of a biological sample as a function of the fractional water content. Therefore, a fitting function can be used to find the optimum water content value that gives a theoretical permittivity that matches the measured value most closely. The choice of which optical parameter is used for this fitting varies between groups with values such as the refractive index and reflectivity of the sample being popular choices in

recent studies.

A complete description of the effective medium theories that can be applied to the modelling of the dielectric response of biological tissues at THz frequencies and an evaluation of the suitability of each model for such investigations can be found in the review article by Hernandez-Cardoso *et al.* [71]. Effective medium theories are not used to analyse the data obtained in the studies described in this thesis because these studies involved the application of moisturiser samples. These treatments lead to structural changes in the skin such as the swelling of the SC and the presence of the moisturiser within the skin, which must be accounted for using an additional component in the effective medium theory.

2.5.3 Layered Models of the Skin

Up until this point only models for biological tissues that make the assumption that the sample is a single homongeneous layer have been considered. However, the skin is comprised of several layers, from the perspective of modelling the interaction of THz light with the skin three key layers are considered [72, 73]: the SC, the epidermis and the dermis, within these layers there are variations in the fractional water content. The SC is the outermost layer of the epidermis, the hydration and thickness of this layer vary across the body; on the volar forearm, the region measured in this thesis, the average SC thickness is $\sim$20 μm [74]. The properties of the SC are different from those of the rest of the epidermis, meaning that THz light is reflected at the interface between the SC and the rest of the epidermis. Therefore, the SC and the epidermis are considered to be distinct layers of the skin when performing THz measurements. The thicknesses of the epidermis and dermis layers are $\sim$60 μm and $\sim$1 mm respectively [75, 76]. Given that the absorption coefficient of water at 0.6 THz is $\sim$160 cm^{-1}, the penetration depth of the THz light is $\sim$60 μm; therefore, many THz measurements of the skin consider only the reflection from the surface of the skin; however, some models extend this to consider reflections at the SC-epidermis interface.

The simplest way to develop a model that more closely resembles the physical structure of the skin is to use a two layer model to represent the SC and epidermis layers. The dermis layer can often be ignored for dielectric models at THz frequencies as this is deep enough into the skin that the THz light is unlikely to penetrate to this layer. A two layer model is simple enough to be described using Fresnel coefficients as was done for the single layer model in Section 2.4.2. This model is summarised in Figure 2.6 where each reflection from the layered structure is expressed in terms of the Fresnel coefficients at each interface and a propagation term $P_s = exp(-i\beta)$,

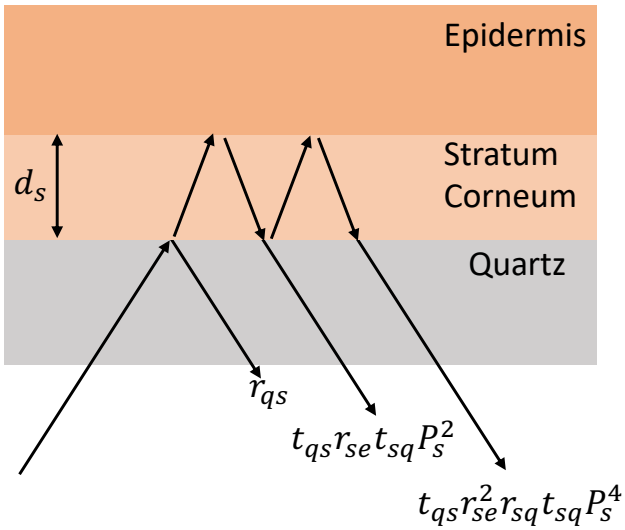

Figure 2.6: The model for a two layer structure of the skin in contact with a quartz imaging window, including the expressions for each reflection in terms of the Fresnel coefficients for each interface.

where β is defined in Equation 2.43 and d_s is the thickness of the SC. By adding these reflection terms together the reflection coefficient for the three layer quartz-SC-epidermis structure, r_{qse}, is obtained in Equation 2.44. Note that multiple reflections within the quartz and epidermis layers can be neglected due to the thickness of these layers.

$$\beta = \frac{2\pi d_s \tilde{n}_s \cos\theta_s}{\lambda} \tag{2.43}$$

$$r_{qse} = \frac{r_{qs} + r_{se} \times exp(-i2\beta)}{1 + r_{qs}r_{se} \times exp(-i2\beta)} \tag{2.44}$$

This expression for the reflection from the sample can be used in the same way as the result from the single layer model to calculate a theoretical sample to reference ratio, which can be used to fit to the measured response of the sample to extract the unknown parameters. Wang *et al.* used this model with the LLL effective medium theory to extract the percentage water content of the SC and epidermis layers of the skin, following the treatment of the skin with silicone gel sheeting [51].

In addition to the two layer model of the skin, more complex models have also been used, such as the stratified medium model proposed by Bennett *et al.* [73], which models the water gradients in the layers of the skin. This model expresses the

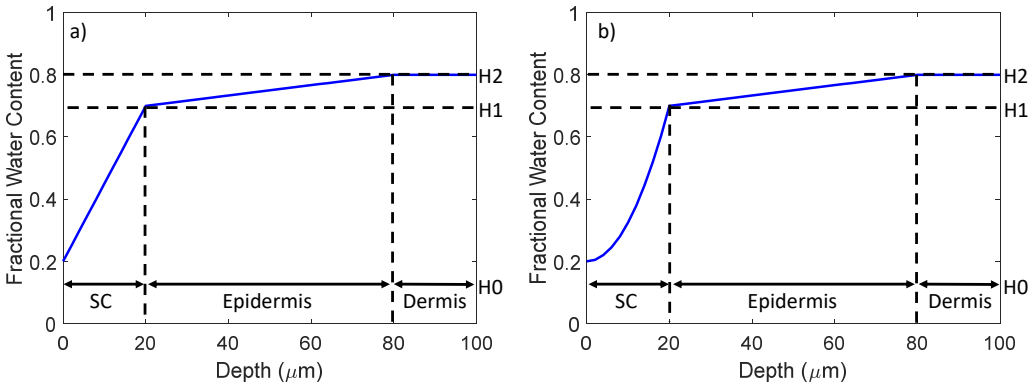

Figure 2.7: Models for the hydration of the skin as a function of depth, with a) linear and b) parabolic water distributions in the Stratum Corneum.

permittivity of the skin as a function of six unknown parameters: H_0, H_1 and H_2, which are fractional water contents at the surfaces of the SC, epidermis and dermis, and the depth of each of these layers, these are all marked in Figure 2.7. These parameters are then extrapolated to construct a model for the hydration of the skin as a function of the depth. There have been two types of model that have been used for this purpose, the first of which was proposed by Bennett *et al.* and has a linear water distribution in the SC [73], Sun *et al.* then extended this by changing this distribution to have a parabolic form [72], this is thought to be more representative of the true hydration distribution in this layer. Both of these models are displayed in Figure 2.7.

Using these models, the hydration of the skin can be expressed fully using six parameters and can be used with effective medium theories to write the optical properties of the skin as a function of skin hydration. The stratified media model, which is described fully in reference [73], extracts the theoretical surface reflectivity of this multilayered structure and uses it with the measured THz response of the sample to extract the unknown sample properties.

2.5.4 Understanding the Observed Changes in the THz Response of Skin

From the Fresnel equations introduced in Section 2.2.2 it can be seen that the proportion of THz light reflected at an interface is linked to the differences in the properties of the two interfaces. When considering the interface of a quartz window ($n_{\text{quartz}} = 2.1$) in contact with skin ($n_{\text{skin}}(0.5\text{ THz}) \sim 1.7$), when the water content of the skin increases ($n_{\text{water}}(0.5\text{ THz}) \sim 2.3$) it is expected that the properties of the

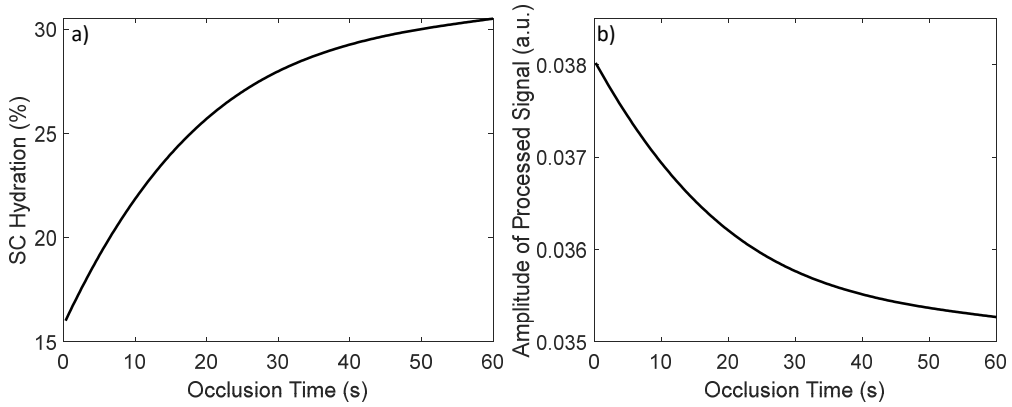

Figure 2.8: The results of simulating the THz response of skin as the water content increases where a) shows the Stratum Corneum hydration input into the model and b) shows the amplitude of the theoretical processed THz signal.

skin will be closer to those of quartz; therefore, the amplitude of the reflected signal will decrease. This approach offers an intuitive explanation for how changes in the reflected THz signal are linked to changes in the hydration of the skin; however, this is an oversimplification as it fails to account for reflections from the SC-epidermis interface.

Throughout this thesis a parameter that is often used to quantitatively represent the changes in the THz response of the skin following different treatments is the peak-to-peak amplitude of the processed signal defined in Equation 2.31. This approach has been used in multiple previous studies in this field and when the imaging window is made of quartz a decrease in the amplitude of the signal is associated with an increase in water content [77]. This can be verified experimentally by observing the decrease in the amplitude of the processed signal throughout occlusion, a process that is known to increase the water content of the skin, which will be explained in more detail in Chapter 3.

It is also possible to verify this by simulating the THz response of the skin using some of the models introduced above. A model of the skin was created using the two layer model introduced in Equation 2.44 in which the Fresnel reflection coefficient for the quartz-SC-epidermis structure is obtained. To calculate this reflection coefficient the complex refractive indices of the SC and epidermis are calculated using the LLL effective medium theory to convert from fractional water content of each layer to the optical properties. Using the Fresnel coefficients a theoretical sample to reference ratio can be calculated that can be input into Equation 2.31 to obtain a theoretical processed THz signal for the two layer skin model.

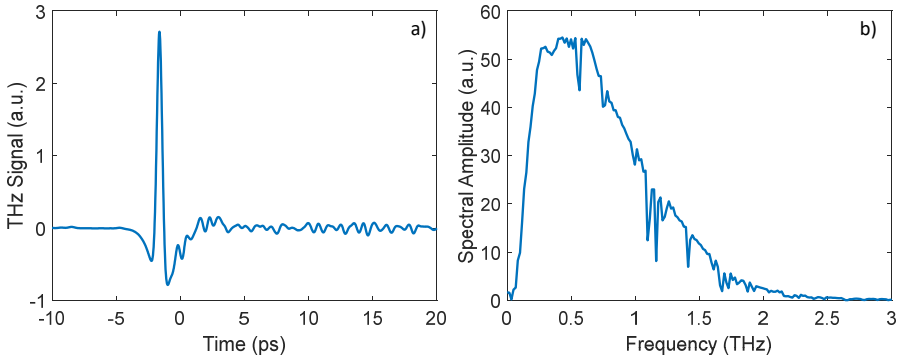

Figure 2.9: An example of a THz pulse in the a) time and b) frequency domains produced using a THz-TDS system.

To test the effect of changing the SC hydration on the amplitude of the processed THz signal, a varying SC hydration was input of the form shown in Figure 2.8 a) to model the changes in the hydration observed when the skin is occluded, while the hydration of the epidermis and thickness of the SC are kept constant. The amplitude of the theoretical THz signal output by the model is shown in Figure 2.8 b), this confirms the prediction that a decrease in the amplitude is linked to an increase in the hydration of the SC.

2.6 Experimental Setup

Finally, this section describes the two THz-TDS systems used to perform the measurements outlined in this thesis. An example of a THz pulse in the time domain and its spectrum in the frequency domain is shown in Figure 2.9. The shape of the pulse and the bandwidth of the spectrum will vary depending on the THz-TDS system used to perform the measurement and the experimental configuration.

2.6.1 Reflection Measurements

Two commercial fiber coupled systems were used to perform the reflection measurements of the skin described in this thesis, one supplied by Teraview Ltd (Cambridge, UK) and one by Menlo Systems GmbH (Planegg, Germany). Both are THz-TDS systems and follow the general design described in Section 1.1.2. In both systems the THz pulse is focussed on the upper surface of the quartz imaging window.

The TeraPulse 4000 spectrometer produced by TeraView mounts the THz emitter and detector on a large gantry frame at 30 degrees incident to the imaging window as shown in Figure 2.10, these can be raster scanned to cover the area of the

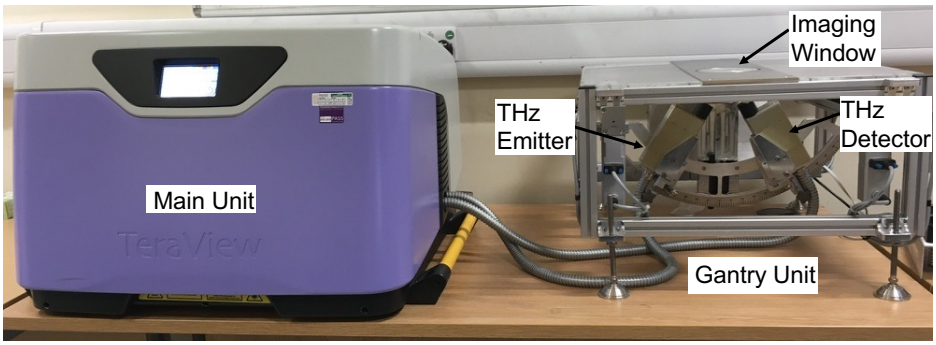

Figure 2.10: The TeraPulse 4000 spectrometer used to perform measurements, showing the main unit and the gantry system used for reflection geometry measurements.

imaging window if required. However, acquiring images in this way can take a long time and for measurements of the skin where the response of the skin is changing throughout the measurement, this approach can lead to too much variation caused by the difference in time between the start and end point of the measurement. Therefore, in the studies described in this thesis only point scan measurements of the skin were acquired, the reasons for this are explained further in Section 3.2.1. The THz emitter and detector can be rotated to acquire measurements with s- and p-polarised THz light, however all measurements in these studies were performed with s-polarised THz light. This system is capable of producing pulses with a usable bandwidth in the range from 0.06 to 4 THz. In this thesis results in the frequency range from 0.2 to 0.8 THz are used, as higher frequencies are more sensitive to the effects of scattering from the roughness of the surface of the skin. The rate of pulse acquisition can be varied depending on the measurements being performed, in the studies described in this thesis the commonly used settings are 15 or 30 Hz, and automatic averaging settings can also be used.

The other system used to perform reflection measurements is a fiber-coupled TeraSmart THz spectrometer from Menlo systems GmbH (Planegg, Germany). This system is able to deliver broadband electromagnetic pulses with a usable bandwidth ranging from 0.1 to 5 THz. The THz emitter and detector were mounted on optical rails at an angle of 30 degrees to the quartz imaging window as shown in Figure 2.11. The presence of the pressure sensors shown either side of the imaging window will be explained in Chapter 3. The system is capable of acquiring THz pulses at a rate of 4 Hz. This system is much more compact than the TeraView system, this means that during measurements a smaller region of skin is in contact with the metal surrounding the imaging window.

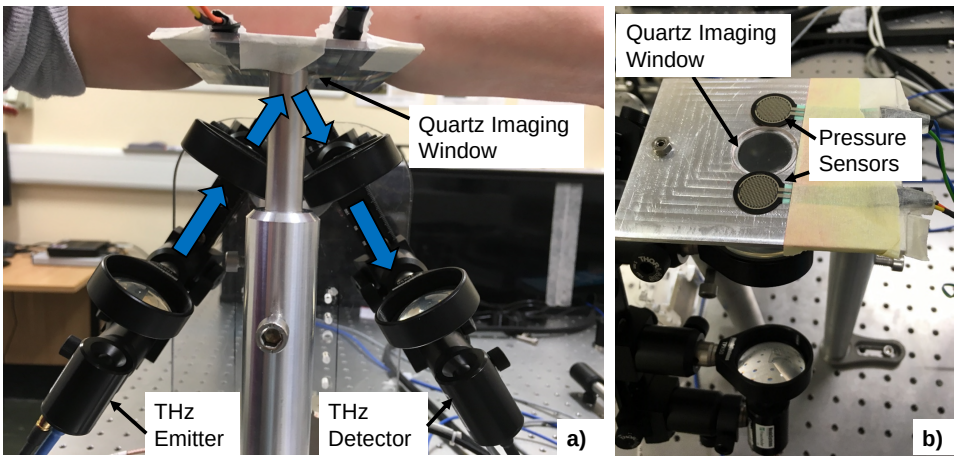

Figure 2.11: The Menlo system used to perform reflection measurements of the skin pictured a) from the side showing the emitter and detector and b) from above showing the quartz imaging window.

2.6.2 Transmission Measurements

Transmission measurements of the samples were performed inside the main unit of the TeraView system. During THz measurements with this setup the unit was purged with Nitrogen gas to remove the effect of water vapour from the measured signals, which can lead to characteristic absorption peaks in the frequency domain signal. This system has a sample holder into which a sample such as the liquid cell shown in Figure 2.12 can be slid and measured with THz light, which passes through the sample at normal incidence. The liquid cell is used to hold samples such as skin products so that the properties of these samples can be measured prior to sample application. In this liquid cell the sample is sandwiched between two quartz windows using a spacer of known thickness to control the thickness of the sample.

2.7 Summary

This chapter introduced the fundamental theory required to understand and interpret the THz measurements of the skin performed in this thesis. The equations that will be used to extract the optical properties of samples measured with reflection and transmission geometries were derived and the relevant processing techniques were introduced. Additionally, several of the models that have been used in previous studies to link the measured THz properties of biological tissues to the water content of the samples were described. Finally, the experimental systems that were used to perform the studies described in this thesis were introduced.

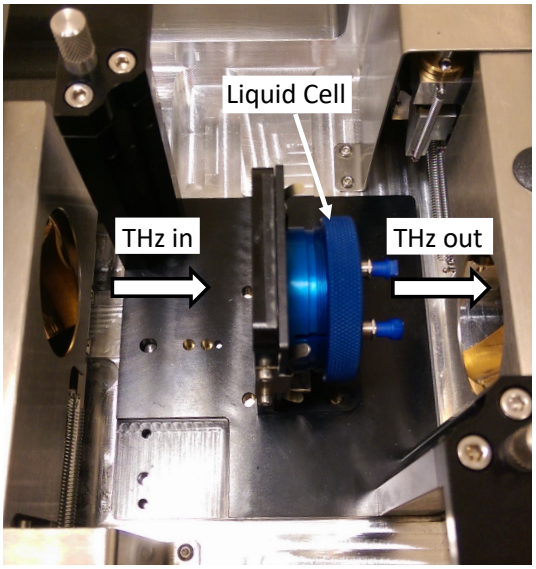

Figure 2.12: Transmission unit of the TeraView system set up to measure a sample in the liquid cell.

Chapter 3

Controlling Variables in THz Measurements of the Skin

3.1 Introduction

This chapter presents a summary of the variables that can impact the results of THz measurements of the skin including occlusion by the imaging window, the applied pressure of the skin on the imaging window and environmental factors. These variables must be carefully controlled in order to ensure that *in vivo* THz measurements are repeatable. This is done using two approaches, firstly a robust protocol is developed to reduce the effect of occlusion and pressure on the measured THz response of the skin. Secondly, a processing technique is used to account for the effects of natural variation of the skin and environmental factors on the changes measured in the skin following treatment with moisturisers. These approaches are tested using measurements of the skin of a single subject following the application of a commercially available moisturiser, this is repeated three times to investigate the repeatability of the results of THz measurements of the skin.

3.2 Variables Affecting the THz Response of Skin

3.2.1 Occlusion

To date the majority of *in vivo* studies performed using THz measurements involve contact between the skin and an imaging window, using a setup similar to the ones introduced in Section 2.6.1. The use of an imaging window is important for ensuring consistent alignment of the system as THz reflection measurements are very sensitive to the effects of misalignment. An imaging window makes it easier for the subject

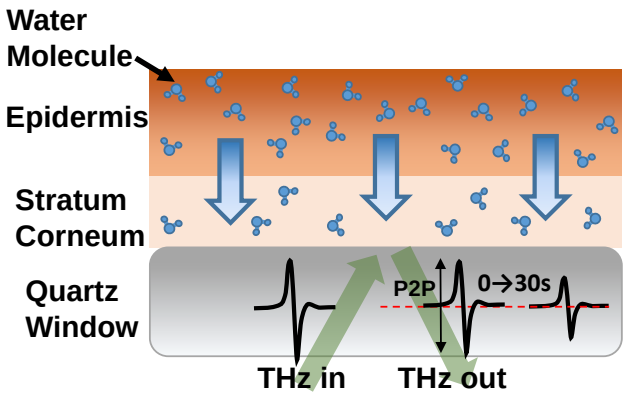

Figure 3.1: The occlusive effect of the imaging window on the skin causing water to build up in the Stratum Corneum, leading to a decrease in the amplitude of the THz signal reflected from the quartz-skin interface.

to keep the region being measured in the same position throughout the duration of the measurement. Additionally, using an imaging window leads to two THz pulses being reflected from the air-quartz-skin measurement as described in Section 2.4.1, the first reflection from the underside of the quartz imaging window can be used to calibrate the signal and account for variations in the incident THz pulse between and during measurements. Whilst the use of an imaging window is important for *in vivo* THz measurements of the skin, contact with the imaging window can affect the properties of the skin leading to changes in the measured THz response.

Changes in the THz response of skin during contact with a quartz imaging window were first observed by Cole *et al.* [78], they identified that the changes were due to the movement of water in the SC. Sun *et al.* performed an extensive study on the effect of occlusion of the skin by a quartz imaging window on the amplitude of the reflected THz pulse [77]. They observed a decrease in the amplitude of the measured THz pulse with increasing occlusion time and found that the refractive index increased by $10-15\%$ following 20 minutes of occlusion. Both of these observations correspond to an increase in the water content as explained in Section 2.5.4. In their study Sun *et al.* rule out the influence of temperature, movement of the imaging window and the accumulation of insensible perspiration as possible explanations for this observation, as any change in the THz amplitude caused by these factors would be too small to account for the changes observed. The effect of occlusion on the THz response of skin can therefore be attributed to the sensitivity of THz measurements of the skin to the build up of water in the SC, as the normal loss of water through the surface of the skin is prevented by the imaging window, as shown in Figure 3.1.

These changes due to occlusion were found to be problematic when raster

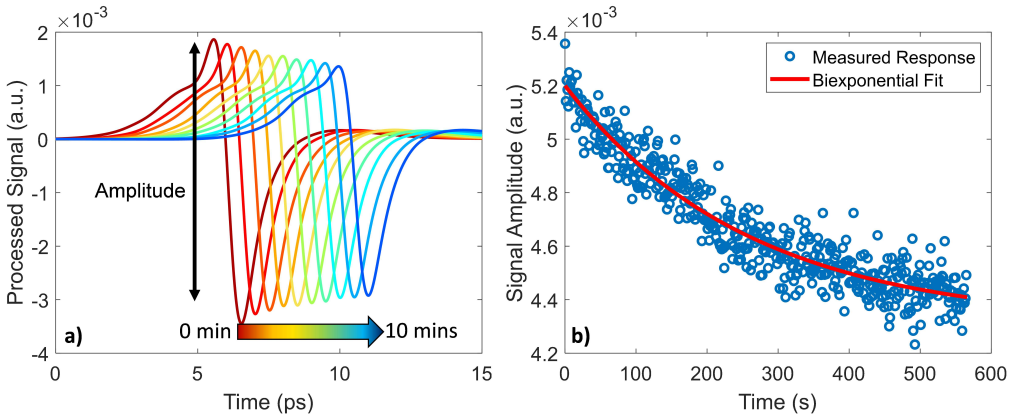

Figure 3.2: a) Processed THz signals obtained at one minute intervals when measuring skin for ten minutes under occlusion, the waveforms have been horizontally shifted for clarity. b) The amplitude of the processed waveform plotted against occlusion time and fitted with a biexponential function shown in red.

scanned images were being acquired of the surface of the skin due to the relatively slow imaging speeds achievable with present approaches, as the first point of the skin to be imaged had been in contact with the imaging window for far less time than the final point to be measured. This difference in occlusion time across the image led to a gradient in the reflected amplitude across the image due to the build up of water in the skin during the measurement.

Sun *et al.* proposed that a biexponential fit could be used to describe the change in the reflected THz amplitude during occlusion as described in Equation 3.1, where t is the occlusion time, β_1 and β_2 are constant coefficients, τ_1 and τ_2 are time constants and $C_{(x,y)}$ is a variable to account for spatial variation across the surface of the skin when an image is acquired [77].

$$\text{fitted signal} = \beta_1 \exp(-t/\tau_1) + \beta_2 \exp(-t/\tau_2) + C_{(x,y)} \tag{3.1}$$

It was demonstrated that this model could be used to compensate for the effects of occlusion on the measured THz response of skin when acquiring an image.

An example of the effect of occlusion on THz measurements of the skin is shown in Figure 3.2. For these measurements the skin was in contact with the imaging window for ten minutes, the processed THz waveforms are shown in Figure 3.2 a) and are plotted at one minute intervals where the colour gradient marks increasing occlusion time as shown by the coloured arrow. These pulses have been horizontally shifted for clarity. Figure 3.2 b) shows the change in the amplitude of the signal during the ten minute measurement and the red line shows the biexponential fit to

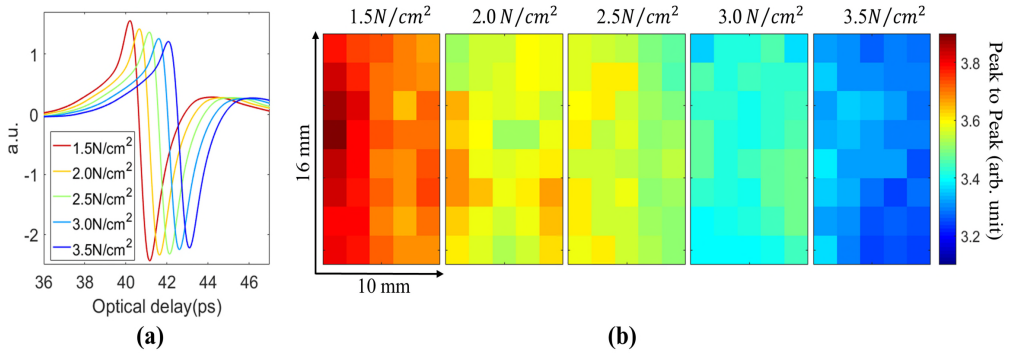

Figure 3.3: a) Processed THz pulse of a single point under different pressures, b) images of the skin showing the amplitude of the processed THz pulse under different pressures. Used with permission from [79].

the data.

3.2.2 Pressure

In addition to the occlusion of the skin by the imaging window throughout the measurement, the pressure of the contact between the skin and the imaging window can also influence the results of THz measurements of the skin. Wang *et al.* investigated this by using a Force Sensitive Resistor (FSR) to record the applied pressure throughout the duration of the THz measurements [79]. By modelling the skin using a stratified media model with effective medium theories as described in Section 2.5.3, they were able to quantify the changes in the hydration and thickness of the SC and epidermis layers of the skin under different applied pressures.

In the study performed by Wang *et al.* five subjects were asked to apply five different pressures ranging from $1.5-3.5$ Ncm^{-2} in different THz measurements of their skin and each pressure was repeated three times. Some of the results of this study are shown in Figure 3.3, where a decrease in the amplitude of the processed THz signal can be seen as the applied pressure increases, this trend was verified using images of the regions in addition to point scan measurements in order to confirm that this observation was not due to spatial inhomogeneities on the surface of the skin. The measurements found that the refractive index of the skin increased as applied pressure increased, while no change was observed in the absorption coefficient. It is likely that this disparity between the changes observed in the refractive index and the absorption coefficient can be attributed to the use of the single layer model of the skin to extract the optical properties of the skin, which neglects the structurally distinct layers of the SC and the epidermis. Using modelling of the skin

to extract the changes in the physical properties of the skin under different pressures, it was observed that increasing pressure decreased the thickness of the SC and increased the SC hydration. Additionally, it was observed that the refractive index of the biological background component of the skin model increased as the pressure increased. These observations suggest that the measured changes in the THz response of skin as the applied pressure is increased are linked to increasing biological density and water concentration in the upper layers of the skin as the skin is compressed. This study identifies that it is important that pressure is carefully controlled in THz measurements of the skin in which the skin is in contact with an imaging window.

3.2.3 External Factors

Previous studies have found that properties of the skin such as hydration and barrier function vary depending on a host of external factors that are hard to control including changes in temperature and humidity [80, 81], diet [82] and the time of the day [83]. Unlike the effect of pressure these factors are hard to quantify and control for each subject between the measurements. However, it is important that an approach is used that reduces the effects of these variables on the measured changes in the THz response of skin so that the results can be repeatable and do not depend on other factors such as weather.

3.3 Methods

3.3.1 Experimental Setup

The measurements performed for this study were done using the TeraView system described in Section 2.6 using a reflection geometry as shown in Figure 3.4. FSRs were positioned either side of the quartz imaging window. The THz emitter was positioned so that the incident THz beam arrived at 30° to the quartz imaging window. The average spot size of the THz beam was ∼1 mm. The system was used to acquire measurements of 30 THz pulses a second, with every five pulses acquired being averaged to form a single recorded THz pulse. Therefore, the measurement of the 200 pulses acquired in this study took 33 seconds.

3.3.2 Circuit Design

An electronic circuit capable of converting the measured mechanical pressure into voltage was constructed, as shown in Figure 3.5. An arduino microcontroller board

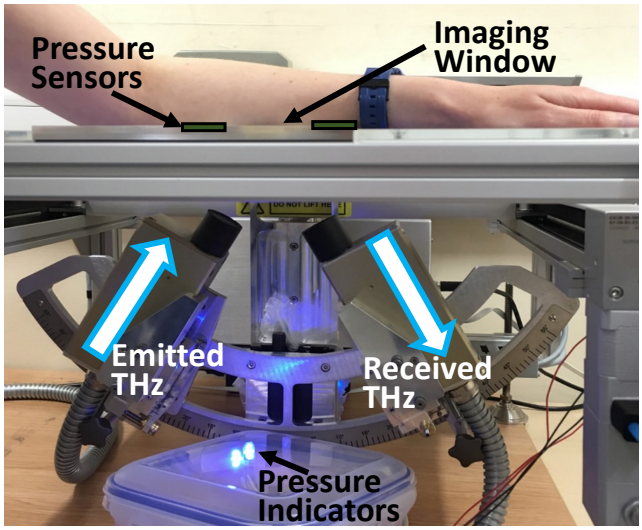

Figure 3.4: a) The experimental setup used to take *in vivo* measurements of the skin with THz light in a reflection geometry, combined with pressure sensors and indicator lights to improve repeatability of the measurements.

was used to process the measured voltage into a pressure value and turn on the appropriate indicator light. FSRs are connected in a voltage divider circuit as shown in Figure 3.5, as suggested by the manufacturer [84]. As the resistance of the FSRs is a function of applied pressure, the output voltages V_1 and V_2 vary with the applied pressure and are input back into the microcontroller. The two input voltages correspond to the two FSRs either side of the imaging window. The measured responses from the FSRs are used to provide a real time visual output by changing the colour of two LEDs to help the subject change the applied pressure throughout the measurement as required. Additionally, a binary signal is sent to the TeraView system, which is recorded simultaneously with the THz pulse, that can be used to help process the data and reject measurements that were recorded at the incorrect pressure.

The right hand side of Figure 3.5 shows a flow chart of how the arduino microcontroller is programmed to use the measured voltages from the FSRs to control the LED indicators and the digital output. If the pressure applied to the FSR is below the programmed low-pressure limit the light will be blue, if the pressure is above the high-pressure limit the light will be red and finally if the pressure is within these two limits the light will be pink. The low-pressure limit chosen for this study was 0.6 Ncm^{-2}, as this is the lowest value of pressure detectable by the FSRs, and a lower pressure is easier to maintain for a long period of time. The high-pressure limit chosen was 1.1 Ncm^{-2}, as this allows for some variation in pressure that is

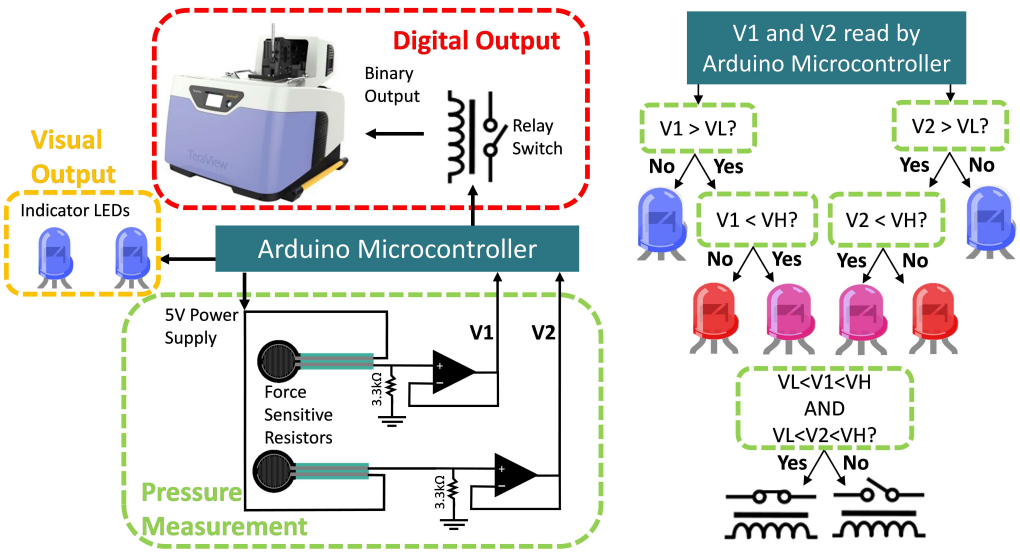

Figure 3.5: Diagram of the circuit used to integrate a pressure sensor with the TeraPulse 4000 and a flow chart describing the code used by the Arduino microcontroller to implement this. V_1 and V_2 are the output voltages from the responses of the two FSRs and V_L and V_H are the lower and higher threshold voltages for the pressure sensor. When the voltage is between V_L and V_H a pink light is shown to the subject and a binary signal is recorded alongside the THz response to aid processing.

below the sensitivity of the THz system. It is simple to change the desired pressure range by uploading new code to the arduino board, depending on the region of skin being measured, the requirements of the experiment and the experience of the subject with using the pressure sensor. If the subject is inexperienced it is beneficial to use a wider pressure range as otherwise extra errors are introduced as they try to apply the desired pressure; with more experienced volunteers the desired pressure range can be tighter as this will be achievable without moving, this will significantly reduce the uncertainty introduced by pressure. As part of the protocol for *in vivo* THz measurements of the skin, subjects should have the opportunity to practice applying the desired pressure, in order to reduce errors induced by the subject moving their arm to apply the correct pressure.

Furthermore, the circuit also provides a digital output to the THz system using a relay switch controlled by the arduino board. When both pressures read by the arduino microcontroller board are within the specified range of values, the board applies a voltage across the switch, closing the circuit and triggering a binary signal that is received by the THz system while it is recording the THz signal. After this, the THz signal is saved in an h5 file together with a binary mark indicating whether

the measurement was recorded when the pressure read by the sensors was in the specified range. This procedure makes it possible to select only the THz signals recorded in the pre-defined pressure range. The use of the pressure sensor output when processing the THz signals will be discussed further in Section 3.3.5.

3.3.3 Protocol For Skin Measurements

A protocol for *in vivo* skin studies has been designed to allow a more rigorous comparison between measurements taken at different times and from different subjects. The outline of this protocol is displayed in the table in Figure 3.6. Before the measurements can be performed, the subject must acclimatise to the controlled temperature and humidity of the room where the measurements will be taken, with the area to be imaged exposed e.g. sleeves rolled up. During this adjustment time the subject is given the opportunity to train to use the pressure sensor system as shown in Figure 3.6 a) and b), to practice applying the correct pressure consistently. The subject is also asked that their arm not be removed from the imaging window at any point during the measurement as this will introduce uncertainty into the occlusion process of the skin.

Additionally, the acclimatisation time is used to mark the region to be imaged with a 5 by 5 cm square on the volar forearm halfway between the elbow and the wrist, as shown in Figure 3.6 c). This region was chosen for study as it can be easily placed on the imaging system, also it has few hairs, which would interfere with the contact of the skin with the imaging window, and has minimal environmental exposure, for example to UV radiation. The marking of the region makes it possible for the same location to be measured repeatedly and helps ensure that the area that the moisturiser product was applied is the area that is imaged. All the experiments were performed with the informed consent of the volunteers.

The imaging parameters that are used result in a 33 second measurement consisting of 200 waveforms, this yields measurements at small enough time intervals for dynamic changes in the skin, such as those caused by occlusion, to be observed. The measurement is started before the skin is in contact with the imaging window, then the subject is asked to place their arm on the window. Using this approach it is possible to observe in the recorded THz pulses and pressure response, the point at which the arm first contacted the imaging window, making it possible to know exactly how long the skin had been occluded for. Otherwise the unknown duration of occlusion has the potential to induce uncertainty and variation between measurements at different time points and of different subjects.

To allow the skin to recover from the effects of occlusion, five minutes were

Time/ mins	
0	Subject enters lab to acclimatise
2	Take written consent
5	Train subject to use the pressure sensor (a,b)
10	Mark the region to be imaged (c)
30	Take the first measurement lasting 30 s
35	Apply 0.1 ml of the product
55	Wait a minimum of 20 mins before the next measurement

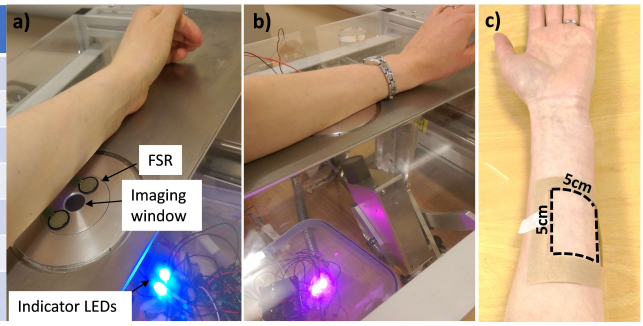

Figure 3.6: Table of the protocol used for *in vivo* skin measurements in this study. a) and b), the experimental setup used with the pressure sensor with applied pressure below the desired limit and within the desired limits respectively (indicated by the blue and pink lights). c) The marked region to be imaged on the volar forearm.

left between the first measurement and the application of the skin product. The skin product was measured in 0.1 ml quantities using a Pos-D micropipette from Mettler Toledo, this volume is sufficient to allow saturation of the 5 by 5 cm region with no excess remaining on the skin. This volume can be changed depending on the products being tested and the ability of the skin to absorb them. The product was rubbed into the skin whilst wearing a latex glove to ensure that none of the product was absorbed by the hand applying it, efforts were also made to ensure that the product was massaged into the skin consistently covering all the marked area. An interval of 20 minutes was left between measurements to allow the water distribution in the skin to recover from the effects of occlusion from the first measurement [77].

The product of interest was only applied to the left arm and the right arm remained untreated to act as a control. This control arm measurement makes it possible to identify which observed changes are the result of the moisturiser product and which are induced by natural variation in the skin with time of day, eating, drinking or other environmental factors as it is understood that these factors will change the skin uniformly across the body. In this study measurements were taken of the treated and control skin regions before the application of the product and 30 minutes, 1 hour, 2 hours and 4 hours after application.

3.3.4 Data Processing

The THz pulses measured in this study were processed using the approach described in Section 2.4, in order to obtain the smooth pulses shown in Figure 3.7 c). Sun *et al.* [72, 77] demonstrated that as the time for which the skin is occluded increases water builds up in the surface of the skin and this can be seen as a decrease in the

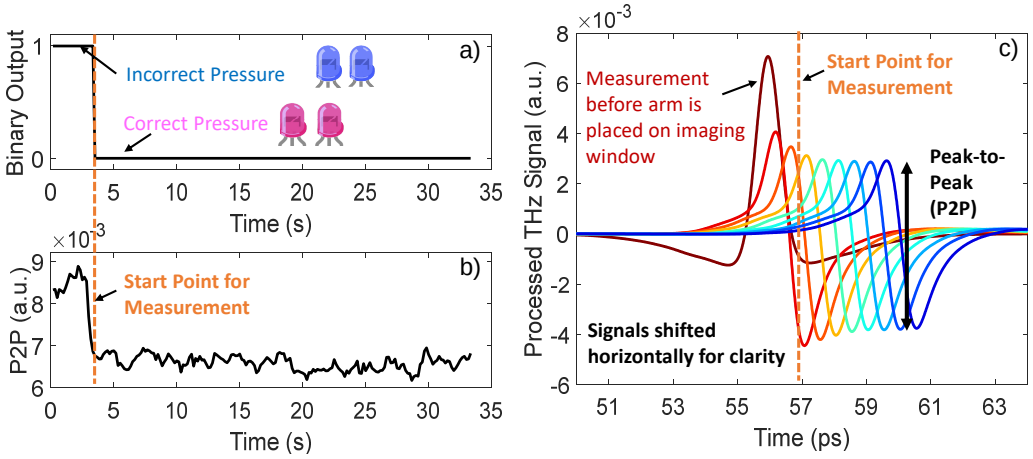

Figure 3.7: The output from a THz measurement of skin. The start point of the measurement where stable contact with the imaging window was reached at the correct pressure, is marked by the orange dashed line. a) the pressure sensor binary output measured throughout the THz measurement, b) the P2P of the processed signal as a function of occlusion time, c) the processed THz signal at the start of the measurement both before and after the contact of the skin with the imaging window. The signals are shifted horizontally for clarity and only one signal of the window before contact with the skin is displayed in red.

Peak-to-Peak (P2P) amplitude of the processed signal as shown in Figure 3.7 c). This is because the increased water content in the skin increases the refractive index of skin, so the reflected THz signal is reduced. Therefore, through this initial study into pressure controlled THz measurements of the effect of applying a moisturiser, a decrease in P2P is understood to indicate an increase in skin hydration.

3.3.5 Using the Pressure Sensor Output

The output from the pressure sensor can be used to identify the point at which the arm makes stable contact with the imaging window and how long the subject took to attain the desired contact pressure. This makes it possible to determine which changes of the THz pulse are due to occlusion and which are due to an incorrect pressure between the arm and the window. Also, any changes throughout the measurement that are the result of a change in pressure can be identified. If the subject failed to reach the correct pressure quickly or the pressure varied significantly throughout the measurement the data are excluded.

The processing and analysis of the measured THz signals using the pressure sensor data are shown in Figure 3.7. The binary output from the pressure sensor as a function of time is displayed in Figure 3.7 a), and the regions of incorrect

pressure are identified. Fig 3.7 b) shows the variation of the P2P as a function of time with the start point corresponding to the correct pressure marked by the orange dashed line. Figure 3.7 c) shows the processed THz response measured at different time intervals into the measurement, including one just before the arm makes contact with the imaging window. The processed signal for the measurement before the arm was placed on the imaging window represents the filter introduced in Equation 2.31 in the time domain, as the sample measurement is identical to the air reference at this time point. These plots are used together to determine the time into the measurement at which the data can be considered useful and consistent with those taken from other subjects. In Figure 3.7 c) the processed signals have been shifted horizontally for clarity.

3.3.6 Normalising Results

In order to eliminate variation in the skin not due to the application of the moisturiser, a variable is defined in Equation 3.2 called the Normalised Relative Change (NRC), in which the change measured in the control region is subtracted from the measured change in the treated region.

$$\text{NRC}(\%) = \frac{(X_{Tt} - X_{T0}) - (X_{Ct} - X_{C0})}{X_{T0} + (X_{Ct} - X_{C0})} \times 100 \tag{3.2}$$

Where X_{Tt} and X_{Ct} are the measured P2P values of the treated and control arms, time t after the application of the product, X_{T0} and X_{C0} are the initial P2P values of both arms. The NRC represents the normalised percentage change in the P2P, resulting from the application of a moisturiser product relative to that of the control arm, which should be representative of the natural variation of the arm caused by environmental factors. It might be expected that (X_{Ct} – X_{C0}) would average to zero but when there is a change in the skin not caused by the moisturiser e.g. due to eating, drinking or a temperature change then this will be non-zero and the effect from it will be removed from the change observed in the treated region.

The more negative the NRC value the more the P2P decreased due to the moisturiser application and therefore the greater the hydration increase in the skin. However, it is also possible that the moisturising product may induce other changes in the skin not linked to hydration that may alter the THz response. Further modelling of the skin is required to identify how much of the observed NRC is caused by changes in skin hydration. The NRC can isolate the change in the THz response of skin induced by the application of the skin product. When the water content of the skin is extracted a similar normalisation process can be carried out

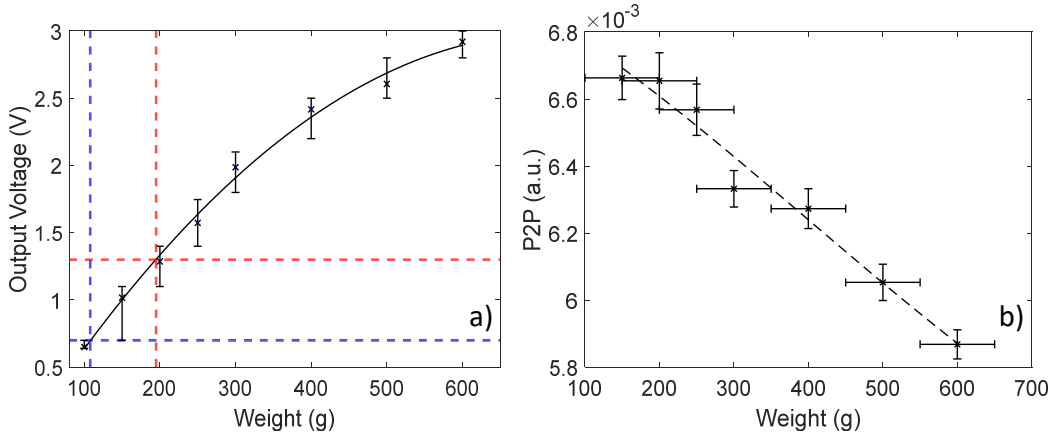

Figure 3.8: a) The calibration of the FSRs using known weights and taking an average of three readings of the output voltage, the error bars are the variation of the voltage with the application of a fixed weight. The blue and red lines mark the lower and upper voltage and weight thresholds for the blue and red lights to turn on used in this study. b) The measured P2P at different pressures, the x error bars correspond to the calibration errors in a) and the y errors come from the standard deviation of the ten measurements that were averaged to give each data point.

to identify the relative hydration change in the skin.

3.4 Results

3.4.1 Calibration of the Pressure Sensor

The FSRs in the circuit give an output voltage that is a function of the pressure applied. In order to extract a meaningful pressure value from this output the circuit must be calibrated through the application of known weights, the result of this is shown in Figure 3.8 a). Each weight was applied to the FSRs three times and the output voltage from the circuit shown in Figure 3.5 was recorded, the weights were removed and replaced between each measurements. These three values were averaged to obtain the results shown in Figure 3.8 a). The red and blue lines mark the upper and lower thresholds respectively that the pressure sensor lights respond to and the error bars display the voltage range output during the application of the fixed weight.

Figure 3.8 b) shows the average of ten consecutive P2P measurements as a function of weight as determined by the calibrated pressure sensor. The x error bars come from the calibration of the pressure sensor and the limit on the range of pressure that the arm can be kept within for sufficient time for the measurement to

be taken. The y error bars are the standard deviation of the ten measurements of the P2P. Figure 3.8 b) shows that when a suitable target pressure range is defined, the variation in the properties of the skin caused by changes in the applied pressure can be smaller than present THz sensitivity. Therefore, using the pressure sensor to limit the variation in pressure to correspond to a weight range of 100 g is enough to significantly reduce variation due to pressure, whilst preventing the subject from moving excessively to attempt to keep within an unattainably small pressure range.

3.4.2 Testing the Technique

To test the capabilities of this protocol for quantifying the effects of moisturisers on the skin, a study was conducted using a commercially available skin moisturising product. Using the protocol described in Section 3.3.3, Vaseline lotion was tested on the same subject three times with one week between each study to allow for recovery of the skin where the moisturiser was applied. The results of this study are shown in Figure 3.9 a), where the changes in the P2P of the control and moisturised arm in three repeat measurements on the same subject can be seen. In this figure the average of ten consecutive P2P measurements taken 25 seconds into the occlusion process is plotted, and the error bars are the standard deviation of these ten values. The dashed lines indicating the control arm in Figure 3.9 a) are largely self-consistent; however, there are some small variations that could be caused by factors other than the application of the moisturiser. If there is an observable change owing to the consumption of food or other factors that influence the skin homogeneously on the left and right arms the use of the NRC variable should remove this effect. Additionally, a large change can be seen between measurements 1, 2 and 3 of the control arms, using the NRC variable will yield a measure of the change of the state of the skin relative to the starting conditions before the application of the product. There is a significant decrease in P2P shown by the solid lines after the application of the Vaseline, this change is large enough that it cannot be accounted for simply by natural variation of the skin, therefore this figure demonstrates that THz measurements of the skin are capable of characterising changes induced by the application of moisturising products.

Figure 3.9 b) shows the result of the three identical studies on the same subject with the treated arm normalised to the control arm, the data point plotted for the value of the NRC before the application of the moisturising product is defined to be zero by Equation 3.2 and therefore has no associated error. A significant change is observed in the skin following the application of the product as none of the results overlap with the dashed line marking out zero NRC. There is a consistent and

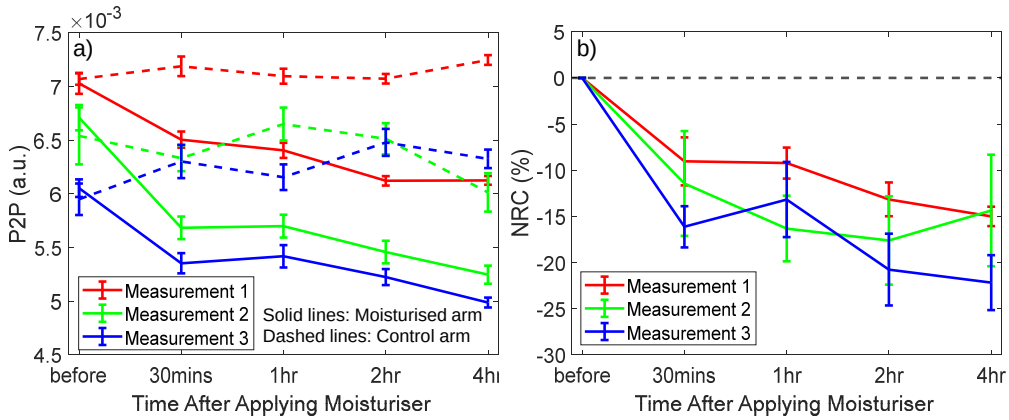

Figure 3.9: The THz response of skin after the application of a commercial skin product. a) The average of ten measurements of the P2P plotted at different time intervals before and after applying moisturiser to one arm. b) The NRC observed after 25 seconds of occlusion in three repeats of the same protocol on the same subject after the application of the product, the data point marked for the NRC value before the application of the sample is defined to be zero by Equation 3.2 and the dashed black line highlights the point for no change observed. In both figures the error bars correspond to the standard deviation.

significant decrease in the NRC of approximately 10−15%, following the application of the product. As all of the normalised results are significantly different from zero this change cannot be attributed to natural variation of the skin.

The results from the pressure sensor were used to identify the start point of the occlusion of the skin, this was then used to align the start points of the data from the control and treated regions. By doing this before calculating the NRC the effect of occlusion is compensated for so this should not contribute to the error bars, which are the standard deviation of the ten consecutive NRC values averaged to give the values in the figure. This figure suggests that after the initial changes observed when the product is applied, further increases in this change can be seen at increasing time after application, suggesting that the changes the product induces in the skin may take some time to begin.

This protocol is shown to be capable of producing repeatable *in vivo* THz skin measurements as the results in Figure 3.9 b) of the percentage NRC of the skin largely agree within their error bars despite the measurements being taken at one week intervals. From these results the NRC of the skin 30 minutes after the application of the skin product, is shown to decrease to 10% and 4 hours after the application of the product this decreases further to 17%. However, further measurements will need to be taken on a range of subjects, in order to be confident

that this trend applies to all skin types in a range of seasons.

This work can be expanded on in the future by applying the protocol to a wider range of subjects and samples to study if a change in the effects can be observed. A model could also be developed to facilitate the extraction of the hydration as a function of depth to allow the observation of the effects of the products deeper into the skin. This would also give greater meaning to the observed changes in the THz signal after the application of the products if they can be expressed in terms of percentage increase in hydration, which will be of more interest to potential skin product customers.

3.5 Summary

In this chapter a protocol has been introduced that can be used to perform THz measurements of the skin that yield repeatable results. This protocol makes it possible to control the effects of pressure and occlusion on the skin and uses the NRC variable to remove the effects of changing environmental conditions on the measured THz response of the skin. In subsequent chapters elements of this protocol and processing technique will be applied to ensure that the results can be compared between subjects.

Chapter 4

Comparison of THz Sensing with Other Approaches to Skin Characterisation

4.1 Introduction

Chapter 3 described a robust protocol that can be used to obtain repeatable results for the THz response of skin following treatment with a commercially available moisturiser on a single subject. In order to further verify the application of THz measurements for *in vivo* hydration assessment it is necessary to compare the results to alternative techniques. In this chapter the THz response of skin was be measured following the application of three types of moisturising products, this is compared to results from two other techniques that are commonly used for skin hydration assessment. The corneometer uses the capacitance of the skin to evaluate the water content and the Tewameter measures the Transepidermal Water Loss (TEWL) of the skin to provide insight to the functionality of the skin barrier for keeping water inside the skin. The effect of the initial hydration state on the response of skin to the application of different moisturiser samples is also investigated.

In order to offer a thorough comparison of the three devices, three common moisturiser components are tested on 20 subjects and the changes in the reflected THz signal, skin capacitance and TEWL are compared. This is the first comprehensive comparison of *in vivo* THz measurements of the skin with TEWL and capacitance measurements of the skin and makes it possible to assess the ability of THz measurements to diagnose the hydration of the SC.

4.2 The Stratum Corneum

4.2.1 The Function of the Stratum Corneum

The SC is the uppermost layer of the skin, followed by the epidermis layer. The SC is less hydrated than the epidermis as it is in direct contact with the external environment and water is continually lost from the SC, the rate of this water loss depends on the health and functionality of the SC and the environmental conditions. The SC is composed of layers of corneocyte cells and lipids, this layered structure was investigated in detail with THz ellipsometry techniques by Chen *et al.* [85].

The primary function of the skin is to form a semi-permeable protective barrier capable of maintaining the required hydration levels inside the body and preventing harmful chemicals from entering. This barrier allows water to enter and leave the body at a controlled rate, some water will be absorbed through washing whilst water can be lost through a process called TEWL. If the skin barrier is healthy this TEWL is controlled, however if there is damage to this barrier the skin can dry out [86].

4.2.2 Percutaneous Absorption

As the SC is semi-permeable, substances can enter the body via the skin, in a process known as percutaneous absorption. Many factors can contribute to the rate of percutaneous absorption including skin hydration, skin health, barrier function and external factors such as washing or exfoliating [87]. Studies have been performed investigating links between percutaneous absorption and skin hydration, and it has been found that excessive hydration can increase absorption as soluble components of the sample can diffuse through the SC more easily [88]. However, poor skin barrier function, which is often linked to dry skin conditions, can also increase absorption rates [89]. One study using normal and cosmetically dry skin to test the difference in barrier function found that the barrier function of normal skin is 40% higher than that of dry skin [90]. This means that naturally dry skin is likely to have higher rates of percutaneous absorption than initially well hydrated skin; this may influence how these different skin types respond to the application of moisturiser samples.

INCI[a]	WO Emulsion	Aqueous System	Anhydrous	Ingredient Effect
Water	qs100	qs100		
Triolein	30%		99%	Emollient, occlusive
Glycerine	10-12%	10-12%		Humectant, NMF[b]
Phenoxyethanol	0.5%	0.5%		Stabiliser
Polyglyceryl-3 Polyricinoleate	2%			Stabiliser
Methyl Glucose Dioleate	2%			Emulsifier
Sphingomonas Ferment Extract		0.3%		Occlusive, humectant
Caprylic/ Capric Triglyceride	1%		1%	Occlusive

Table 4.1: [a]International Nomenclature of Cosmetic Ingredients, [b]Natural Moisturising Factor. A list of the compositions of each sample tested in this study, and a summary of the expected effects of each ingredient on the skin.

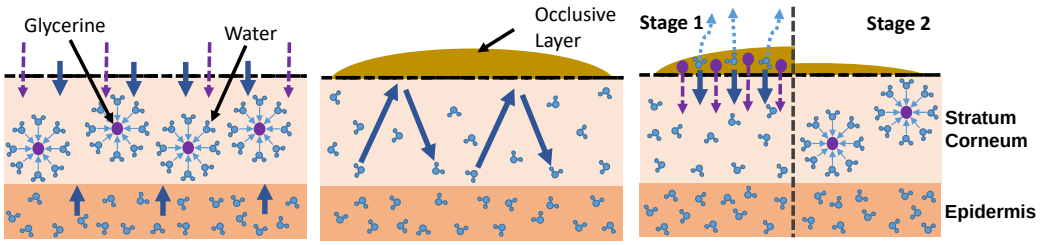

(a) Aqueous (b) Anhydrous (c) WO

Figure 4.1: The mechanisms of the interactions of a) the aqueous sample, b) the anhydrous sample and c) the WO sample with the skin.

4.2.3 Response of the Skin to Different Moisturisers

The three sample types applied in this study are: an aqueous sample primarily consisting of water and glycerine; an anhydrous sample containing triolein and a Water in Oil (WO) emulsion, which is a mixture of both the samples. The compositions of these samples and the anticipated effects of each ingredient are shown in Table 4.1.

An increase in the presence of water is expected to increase the corneometer measurement, but any residue of oil components can interfere with this measurement, decreasing the measured value of skin capacitance. An increase in skin hydration is expected to decrease the amplitude of the reflected THz pulse, as the refractive index of skin increases, as explained in Section 2.5.4. However, oil on the surface of the skin may increase the amplitude of the reflected THz pulse as the refractive index of the surface of the skin may decrease, leading to a larger refractive index contrast at the interface between the quartz imaging window and the surface of the skin, thereby increasing the THz reflectivity. It is expected that samples that repair the skin barrier and prevent water loss will decrease the TEWL measured, however residual samples on the surface of the skin may interfere with the measured TEWL. While TEWL measurements do not give a direct indication of the water content of skin, improving the functionality of the skin barrier can improve the ability of the skin to retain water, allowing the water content of the skin to recover over time.

Figure 4.1 shows the mechanisms through which each of these samples are expected to interact with the skin to increase the hydration. The aqueous sample is shown in Figure 4.1 a), and the main effect arises from the absorption of water and glycerine. Glycerine acts as a humectant meaning that it is able to draw water to itself and bind to it [91]. Therefore, this aqueous sample draws water into the SC from the sample and potentially from deeper layers of the skin, which are more hydrated. When glycerine is applied to the skin with water it can reduce

the diffusivity of water, reducing the rate at which this absorbed water is lost from the surface of the skin [92]. The absorbed water is therefore held in place by the glycerine, increasing the hydration of the SC [93].

The anhydrous sample acts as an emollient softening the skin and forming an occlusive layer on the surface of the skin. The effects of this occlusive layer are demonstrated in Figure 4.1 b); the oil on the surface of the skin forms a water-proof barrier, which traps water inside the skin, allowing the SC hydration to increase [94]. It is possible that the formation of this occlusive layer on the surface of the skin could interfere with the corneometer measurement, making it appear that the skin hydration has not significantly increased. It is expected that on the short timescales being used for this study with just one measurement 20 minutes after treatment, the presence of oil on the surface of the skin will be visible in the THz response of skin leading to an increase in the reflected amplitude.

The interaction of the WO emulsion with the skin is shown in Figure 4.1 c) as a two stage dynamic process, which is a combination of the mechanisms seen in the two other samples. It is understood that initially the water component of the sample will be absorbed into the skin and some will evaporate from the SC (on a timescale of approximately 15 minutes). This will leave the oil components behind on the surface of the skin in what is known as the lipidisation phase [95]. At the point 20 minutes after the treatment when the measurement is performed it is expected that the oil components will dominate the measurement.

4.3 Techniques to Study Human Skin Hydration

In the study described in this chapter three techniques to study the skin are compared: corneometer measurements, TEWL measurements and THz measurements of the skin. This section outlines the key principles behind each of these techniques and how the results obtained link to changes in the structure and properties of the skin. It should be noted that there are many other techniques that are also used to study the properties of the skin such as impedance measurements, a review of some of the developments in this area can be found elsewhere such as in reference [96].

4.3.1 Corneometer Measurements

The capacitance of the surface of the skin is measured using a corneometer, which can be used to infer the relative hydration. Tracks of oppositely charged gold plates are interleaved on the head of the electrode, resulting in a shallow electric field that penetrates into the upper layers of the skin, operating in the frequency range from

0.9 MHz to 1.2 MHz. This measurement can be used to infer the dielectric properties of the surface of the skin, which are correlated to the hydration [97].

The measurements taken by the corneometer are in standard corneometer units, which give a scaled measurement of the capacitance of skin. The range of these values is from 0, which is calibrated as the response where there is no water in the sample, to 120, which is calibrated with pure water [98]. It is possible that if an oily sample is used on the skin and leaves a residue, the response measured may be smaller than expected due to interference caused by the film [99].

The corneometer is an accepted gold standard for quantifying the effect of different skin treatments on the SC hydration [100]. According to the web of science there have been 287 publications referring to the corneometer produced between 1987 and 2020; many of these use the measurements to demonstrate the efficacy of a new type of moisturising sample or a new device for skin measurements.

4.3.2 Transepidermal Water Loss Measurements

TEWL is defined as the rate of diffusion of condensed water vapour through the SC [101]. It is not possible with present techniques to non-invasively measure this variable directly, however using the physical laws that define the diffusion process it is possible to infer it indirectly by measuring the rate of evaporation of water from the surface of the skin, as shown in Equation 4.1 [102], where J is the rate of water leaving the skin in a given area, D is the diffusion coefficient, which can be assumed to be a constant in controlled environmental conditions, c is the concentration of water vapour in the air or humidity and x is the location of the humidity measurements as marked in Figure 4.2. The TEWL measurement has units $\mathrm{gh}^{-1}\mathrm{m}^{-2}$.

$$J = -D\frac{dc}{dx} \tag{4.1}$$

It has been observed that TEWL is correlated with percutaneous absorption as both offer an indication of the skin barrier properties [103], one from the inside of the skin out and the other from the outside in. This means that the initial state of the skin as indicated by the TEWL may influence the way the skin responds to treatment with a topically applied sample and how quickly the sample is absorbed. Studies have also shown correlation between TEWL and the size of the corneocytes at the surface of the skin [104], as shown in Figure 4.2, when the corneocytes are smaller there are more gaps for water to escape through. Additionally, reduced corneocyte size increases the area available within the skin for topically applied samples to be stored as a reservoir, increasing the absorption of the sample by the

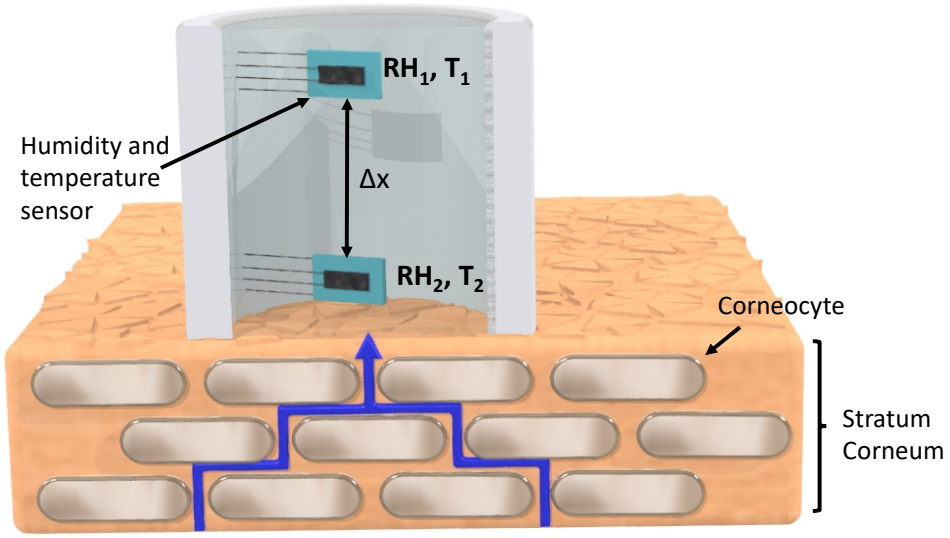

Figure 4.2: The mechanism by which TEWL occurs from the surface of the skin and how this can be measured indirectly with an open chamber device.

skin.

It is expected that when the skin is treated with a sample that is effective at repairing the skin barrier the TEWL should decrease. However, the TEWL device used to take the measurements works on the assumptions that the skin is dry and free from surface moisture, the presence of any water or oil on the surface could lead to an observed increase despite the skin barrier having been repaired following the treatment. It is anticipated that some treatments may act by forming an occlusive barrier on the surface of the skin, leading to a decrease in the TEWL observed as epidermal water is trapped inside the skin, enabling the skin to recover its natural hydration state. Also, treatments that increase the water content of the skin are expected to reduce the TEWL, as the natural humectants inside the corneocytes will absorb water causing the corneocytes to swell, improving the skin barrier [105].

In this study an open chamber device was used to measure TEWL, as shown in Figure 4.2, this has an advantage over closed chamber devices that it does not occlude the skin or disturb the natural microclimate. However, the fact that the chamber is open means that the measurement can be influenced by changes in the environmental conditions such as humidity and airflow [101]. For the study described in this chapter the temperature and humidity were carefully controlled to minimise the impact on the TEWL measurements.

4.3.3 THz Measurements

THz measurements of the skin can be acquired using a reflection geometry to study changes in the hydration levels of skin following treatment with different samples. The various experimental approaches and processing techniques that can be used to study the skin with THz spectroscopy were introduced in Chapter 2. Using these techniques a processed THz time domain signal can be obtained and the amplitude of this signal is used to infer the changes in the skin measured with the THz system. The amplitude of the reflected signal decreases when the hydration of the skin increases, as shown in Section 2.5.4. By measuring the optical properties of the oil based samples, the effect of these samples on the amplitude of the reflected signal can also be predicted. Additionally, the refractive index and absorption coefficient of the skin could be extracted using the techniques introduced in Section 2.4.2.

The modelling approaches introduced in Section 2.5 are not used to extract the changes in the hydration of the skin from the measured changes in the reflected signal as there are too many unknowns after the different samples have been applied, including how deep the moisturiser sample penetrates into the skin and how the thickness of the SC is affected by application of the samples. It is possible that the optical properties of each of the samples could be used with the properties of a biological background and water in the LLL model to represent the addition of the samples to the skin. However, there is not yet enough understanding about the physical changes in the skin to construct an accurate model. The more studies that are performed of this nature the better the foundation that will be available for constructing an accurate model for the treatment of skin with moisturisers in the future.

4.4 Methods

4.4.1 Protocol

20 subjects were studied for the purposes of this investigation (9 males, 11 females) of ages ranging from 21-52. All volunteers gave informed consent to be involved in the study. The protocol for this study is summarised by the table in Figure 4.3. All subjects were measured on the same day to minimise variations caused by external factors such as climate. Allergy tests were performed on all subjects at least 24 hours prior to the measurements by applying a small amount of each sample to the upper arm, no subjects were withdrawn from the study due to a negative response to any of the samples.

Protocol for measurements
Subject enters the lab
Acclimatise to controlled environment for 20 minutes, T= 23^{O}C
Mark 4 3x3 cm region on the volar forearms
Measure the regions with corneometer (a), Tewameter (b) and THz
Apply 0.036ml of each sample to the corresponding region (c)
Wait 20 minutes for sample to be absorbed
Repeat measurements with corneometer, Tewameter and THz for each region
Subject leaves the controlled environment

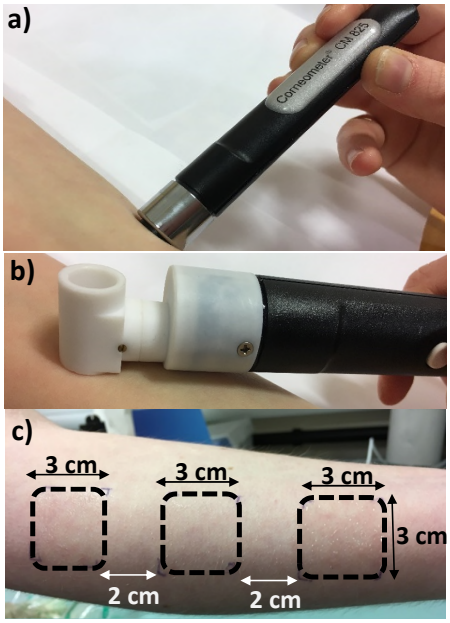

Figure 4.3: Left: a table describing the experimental protocol employed for the measurements. Right: a) The Corneometer CM 825 used to measure the capacitance of the skin. b) The Tewameter TM 300 used to measure the TEWL of each region. c) The regions on the volar forearm to be treated and measured, one region was also marked on the other arm in the centre position, which was not treated and acts as a control.

Each region of the skin was measured with all three techniques before treatment with any products, making it possible to normalise the observed changes in the treated regions to the initial state of the skin and account for any natural variation. Four regions were marked on the arms, three on the left arm to be treated and one on the right arm to remain untreated acting as the control, these regions are shown in Figure 4.3 c).

After the initial measurements of the skin the regions were treated with anhydrous, aqueous and WO samples. The sample volume of 0.036 ml was measured using a micropipette and applied to each region before being rubbed in by the subject whilst wearing a latex glove. This prevented the sample being absorbed by the hand used to rub it in. The subjects then waited 20 minutes for the samples to be absorbed. Following this the four regions were then measured again with all three techniques. The timings of all the measurements were planned to give the skin time to recover from any occlusive effects of prior measurements before the region was measured again.

In this study three samples types were tested: an oil based sample, a water

based sample and a WO emulsion, as introduced in Section 4.2.3. All three samples were common components of commercial moisturisers and act to increase the water content of the skin through various mechanisms.

4.4.2 Capacitance Measurements

Capacitance hydration measurements of the skin were taken using a Corneometer CM825 (Courage + Khazaka Electronic, Cologne, Germany) [98], shown in Figure 4.3 a). The probe was wiped with a dry tissue between each measurement to remove any residual sample remaining on the surface of the skin or other skin lipids, which could interfere with the next measurement.

The measurement with the corneometer is linked to a spring based pressure system, which ensures that the probe is applied to the skin with the desired force of 1 N before the measurement is taken [98]. Once the desired pressure has been reached the measurement is taken, which lasts less than one second.

4.4.3 Transepidermal Water Loss Measurements

The TEWL of the skin was measured using the Tewameter TM 300 (Courage + Khazaka Electronic, Cologne, Germany) [106] shown in Figure 4.3 b), an open chamber device capable of measuring the flow of water from the skin without occluding the region. These measurements were acquired for 20 seconds during which time a stable humidity gradient is established within the chamber. This trend of tending to an equilibrium state can be fit with a biexponential curve to identify the end point that the system is tending towards, as shown by Figure 4.4, where the blue circle indicates the end point that is sampled for that measurement. All measurements were performed in the controlled environmental conditions of the lab as this device is very sensitive to changes in the temperature and humidity of the surroundings.

4.4.4 THz Measurements of the Skin

Point scans of each region were acquired in a reflection geometry using THz light generated and detected using the TeraPulse 4000 system introduced in Section 2.6.1. To control variables such as occlusion and pressure, which have been identified as factors that can influence the THz response of skin, the protocol introduced in Chapter 3 was closely followed, and a pressure sensor system was used to enable repeatability. The pressure sensor allows the subject to observe whether the pressure applied is in the correct range of 1.6-2 Ncm^{-2} and make real time adjustments. This pressure range is chosen so as to be low enough that all subjects are comfortable in

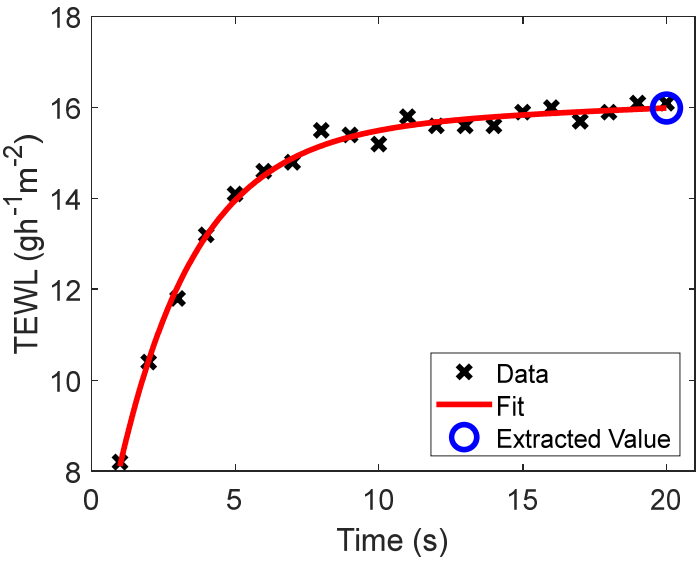

Figure 4.4: The processing technique used to extract a value from the measurements of the TEWL, the red line shows the biexponential fit applied to the data and the blue circle shows the value sampled for the measurement.

maintaining the pressure for the duration of the measurements, whilst high enough to ensure that there is no air gap between the skin and the quartz window [79]. The information recorded by the pressure sensor was exported along with the measured THz pulses, making it possible to exclude data points recorded at the incorrect pressure. This is particularly important for a study involving many subjects who will have less experience in applying the desired pressure during the measurements. Prior to involvement in the study all subjects were asked to spend time practising using the pressure sensor, this ensured that they all had some experience in applying the correct pressure whilst preventing the extra occlusion of the skin during the practice time from affecting the measurements.

To study the dynamic response of skin, 200 measurements were recorded in 33 seconds with an acquisition rate of 30 Hz and five waveforms were averaged to complete a single measurement. For the duration of the measurement the skin was occluded by the quartz window causing the hydration profile of the skin to change. The rapid sampling rate chosen makes it possible to not only observe the initial state of the skin at the start of occlusion but also observe the changes in the skin as a function of time as water builds up in the SC. This occlusion response can be observed in parameters such as the amplitude of the processed THz signal introduced in Section 2.4.

The decrease in the reflected signal as a function of time can be seen in

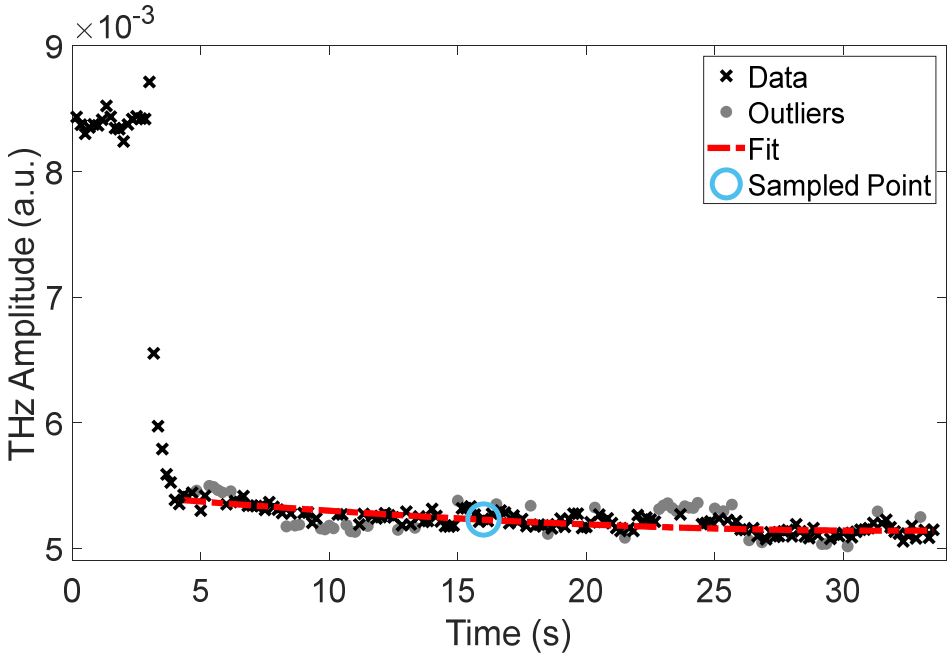

Figure 4.5: Processing the THz signal to remove fluctuations throughout the measurement caused by the subject moving or changing the contact pressure. Time dependent data were fit with a biexponential function (red dashed line) and sampled 12 seconds into the occlusion process (blue circle). Measurements more than one standard deviation away from the fit (grey crosses) were excluded and the fitting was repeated to improve stability.

Figure 4.5, the first five seconds show the very high reflected values before the arm is placed on the window. The output from the pressure sensor is used to find the start of stable occlusion of the skin: this is the point at which the red dashed line fitting to the results begins. To account for the effects of occlusion when comparing results for different measurements, the reflected amplitude must be analysed at the same time into the occlusion process.

The quality of the contact between the skin and the imaging window can often vary throughout the 33 seconds of the measurement leading to occasional fluctuations in the occlusion trend. However, in order to meaningfully compare results at the same time into the occlusion process the data must be extrapolated to remove the effects of these fluctuations. To enable this, a biexponential function was fitted to the occlusion curve data (excluding outliers more than one standard deviation away from the original fit), as shown in Figure 4.5 by the red dashed line [107]. The outliers that are excluded from the fitting are shown by grey circles. This makes it possible to extract a value for the THz measurement at a fixed time

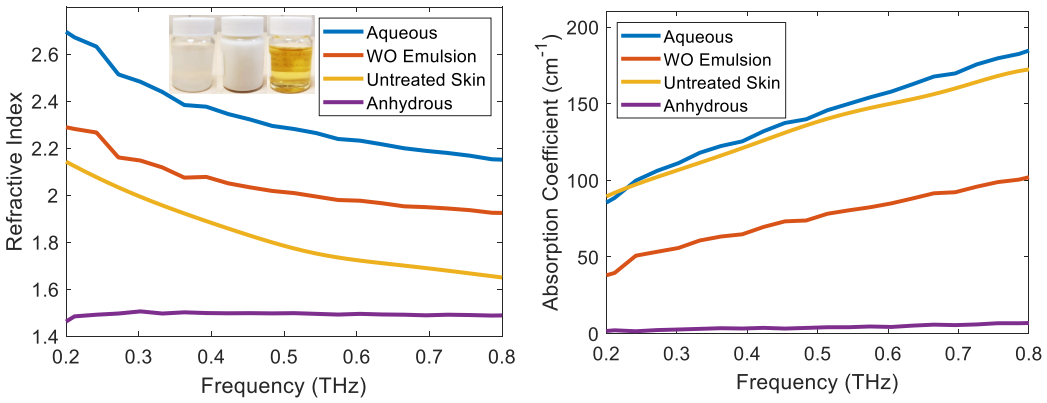

(a) Refractive Index

(b) Absorption Coefficient

Figure 4.6: a) The refractive indices of each sample as measured in a transmission geometry and a refractive index profile for untreated skin measured in reflection geometry. Inset: photograph of each of the samples prior to application. b) The absorption coefficient of each of the samples measured as above, with the profile of untreated skin measured in reflection included for reference.

into the occlusion process without the potential for sampling at an anomaly, this is shown in the figure by the blue circle. For this study the occlusion curve was sampled 12 seconds after the start of occlusion.

4.4.5 THz Measurements of the Moisturisers

The individual samples were measured in the transmission unit of the TeraPulse 4000 THz-TDS system (TeraView Ltd, Cambridge), described in Section 2.6.2. A liquid cell was used in which the samples were sandwiched between two pieces of quartz each 3 mm thick using a 0.1 mm spacer. The thickness of the sample that could be measured was limited by the high absorption coefficient of the aqueous sample. The optical properties were extracted for the thin layers of each sample using the approach introduced in Section 2.3.2. The results for the samples measured in transmission are presented for the frequency range 0.2-0.8 THz to correspond to the usable frequency range for the frequency dependent properties of skin calculated from measurements obtained using a reflection geometry with this system. The extracted refractive indices and absorption coefficients of the samples can be seen in Figure 4.6, in addition to the optical properties of a single *in vivo* measurement of untreated human skin extracted from a measurement performed using a reflection geometry. Note that the optical properties of the skin were extracted using the assumption that the skin is a single homogeneous layer.

Figure 4.6 a) shows that the refractive indices of the aqueous and WO samples

are larger than that of skin, therefore if these samples are present at the surface of the skin the refractive index will increase, leading to a decrease in the amplitude of the THz signal as explained by Section 2.5.4. However, if the anhydrous sample is applied to the skin and remains on the surface the refractive index will reduce, having an effect on the optical properties similar to the dehydration of the skin, causing the amplitude of the THz signal to increase. However, as previously stated an increase in the hydration of the skin will lead to a decrease in the THz amplitude so there will be multiple effects contributing to the changes in the measured THz response of the skin. Using these initial measurements, it is possible to make predictions about the change in the THz response of skin following treatment with these different samples. However, it is also expected that this response will vary between subjects and will depend on how well the sample is absorbed into the skin, as well as the initial refractive index of the skin.

For completeness Figure 4.6 b) shows the extracted absorption coefficients of each of the samples, however there are minimal changes observed in the absorption coefficient of the skin following the application of the samples due to the single layer model used to extract the optical properties. A more complex model of the skin would give greater insight into the changes in the absorption coefficient following application of the samples, however it is not known if a two layer model is sufficient after the samples have been applied. A greater understanding is required about how each of the samples are absorbed into the skin before models of this kind can be effectively applied.

4.4.6 Data Processing

In addition to variables such as pressure and occlusion, which may affect measurements of the skin if not carefully controlled, it is possible that the state of the skin will vary between measurements owing to natural changes caused by eating, drinking or the time of day. It is not possible to prevent the skin changing in this way, instead processing techniques must be used to account for the effects. A variable called the NRC was defined in Section 3.3.6 and is restated in Equation 4.2 more generally for the results of the measurements with any of the three approaches used in this study.

$$\mathrm{NRC}(\%) = \frac{(X_{Tt} - X_{T0}) - (X_{Nt} - X_{N0})}{X_{T0} + (X_{Nt} - X_{N0})} \times 100 \tag{4.2}$$

Where X_{Tt} is the measured parameter at time t following treatment with a sample and X_{T0} is the measured parameter of that same region of skin at t=0, before the skin was treated. X_{Nt} and X_{N0} are these same parameters for the region that was

not treated; the difference between these two parameters acts as a representation of the natural variation of the skin between the measurements and is subtracted from the measured change in the treated region.

This approach to processing the measured responses can be applied to the results from all three techniques used in this study, making it possible to compare the trends seen in response to the three different samples. By taking an average of the NRCs observed in all the individuals following treatment with a specific sample, an overall representation of the responses observed can be found. In this case, the standard deviation of the NRC across all subjects gives an indication of the range of the measured responses of subjects to a sample.

As the data from this study vary due to the changes in the initial state of skin and the way different subjects' skin will respond to the samples, a statistical test is required to see if the changes observed in the skin following treatment are statistically significant. First the data sets were checked using the Shapiro-Wilk test to confirm that the data can be modelled using a normal distribution, which is a requirement for the further statistical tests to be valid [108]. Despite the possibility that the distribution of the NRC in the properties of the skin may not be normally distributed, in this study the distributions were sufficiently close to normal to justify the use of the subsequent statistical tests. Then the one-way Analysis of Varaince (ANOVA) test is used with a 5% threshold to test whether the distributions of NRC responses to each sample are significantly different to one another. The Tukey-Kramer test is used to interpret the results of the ANOVA test and to ensure that the 5% significance threshold is maintained. These statistical tests were chosen to allow the comparison of all three techniques for each of the three moisturisers and to provide an analysis that is comparable with that commonly used by end users within the skin care industry.

4.5 Results

4.5.1 Individual Trends

The NRC for each individual 20 minutes after treatment with the samples, measured with all three devices, is shown in Figure 4.7. The dotted grey lines mark the defined zero NRC point as a guide to the eye and the dashed coloured lines are the average NRCs for all the subjects for that treatment and device.

The clearest and most consistent change induced in the skin visible with all three techniques is that following treatment with the aqueous sample shown in green. In the majority of subjects, the THz response decreases and corneometer

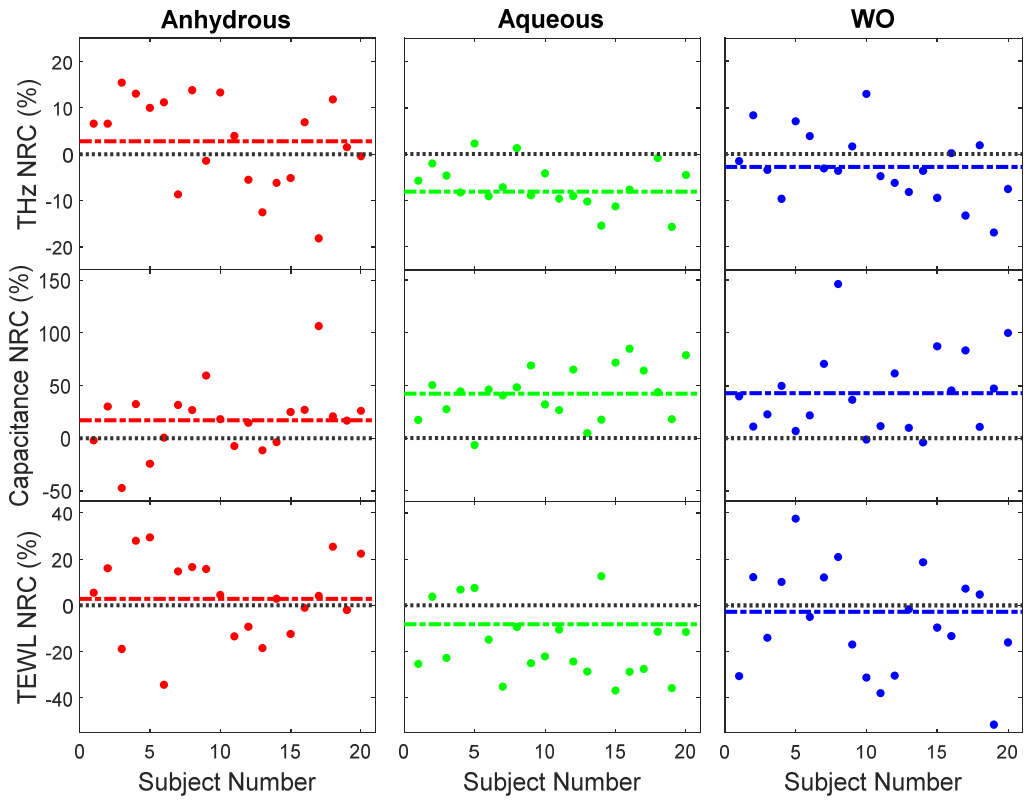

Figure 4.7: The NRC measured with each technique following each treatment for all subjects. The grey dotted line is the zero NRC line for reference and the coloured dashed lines are the average of the NRC values for all subjects.

response increases, both indicate an increase in the water content of SC and the TEWL decreases suggesting that the skin barrier has been repaired.

The anhydrous and WO samples lead to a wider range of responses from the subjects in comparison, which can be seen from the distribution of the points about the coloured average line. The observed response to the anhydrous sample is a marginally positive NRC from the corneometer and THz measurements, but for THz there is a large variation as some subjects have a positive and others a negative NRC following treatment. Following application of both the anhydrous and WO samples the TEWL measurements show a mix of positive and negative responses with inconclusive results, this suggests that the presence of residual oil on the surface of the skin may have interfered with the measurement of the rate of water loss from the skin.

Treatment with the WO sample leads to an increase in the measured capacitance on a comparable level to the aqueous sample, although the distribution of the

points about the average is much larger. The THz responses show a negative NRC following treatment with the WO sample, but again the distribution of the points is much larger compared to the aqueous sample with a range of positive and negative values, suggesting that subjects' skin responded in a range of ways to the oil-based samples but more consistently to the aqueous one.

4.5.2 Overall Results

A summary of the results is presented in Figure 4.8 using box plots for the average percentage change measured in the skin with the three different approaches. The centre lines through the boxes mark the median response for all subjects, with the horizontal edges of the boxes marking the 25^{th} and 75^{th} percentiles indicating the width of the distribution of responses. The whiskers on the box plots mark the upper and lower limits of the measurements and any outliers are shown by black crosses. Here the trends inferred from Figure 4.7 are clearer.

The THz and capacitance measurements show that the distribution of the responses to the aqueous sample is the smallest as shown by the small height of the boxes, while there is a wider range of responses from the samples containing oil components. For some samples the average response is close to zero however, this is not because the most common response is no change following treatment with the sample; there are a range of responses to treatment with positive and negative values. The TEWL measurements have a wide range of values for each of the samples. As noted above there is a clear decrease in the TEWL following the application of the aqueous sample, suggesting that the skin barrier has been strengthened by the sample.

By studying the percentage change in this figure rather than the NRC it is possible to also observe the change in the untreated region between the two measurements, giving an insight into the repeatability of the technique. Whilst it is anticipated that there may be some natural variation in the untreated skin between measurements, these changes should be small compared to the changes induced by the treatments. For a technique with high repeatability between measurements it is expected that the percentage difference will be close to zero for the control region for the majority of subjects.

The THz responses shown in Figure 4.8 a) follow what can be predicted using the optical properties of the samples relative to those of untreated skin, with the anhydrous sample increasing the reflected signal, the aqueous sample reducing it and the WO emulsion doing likewise but to a lesser extent. The large variation in responses particularly to the anhydrous sample could be explained by changes in

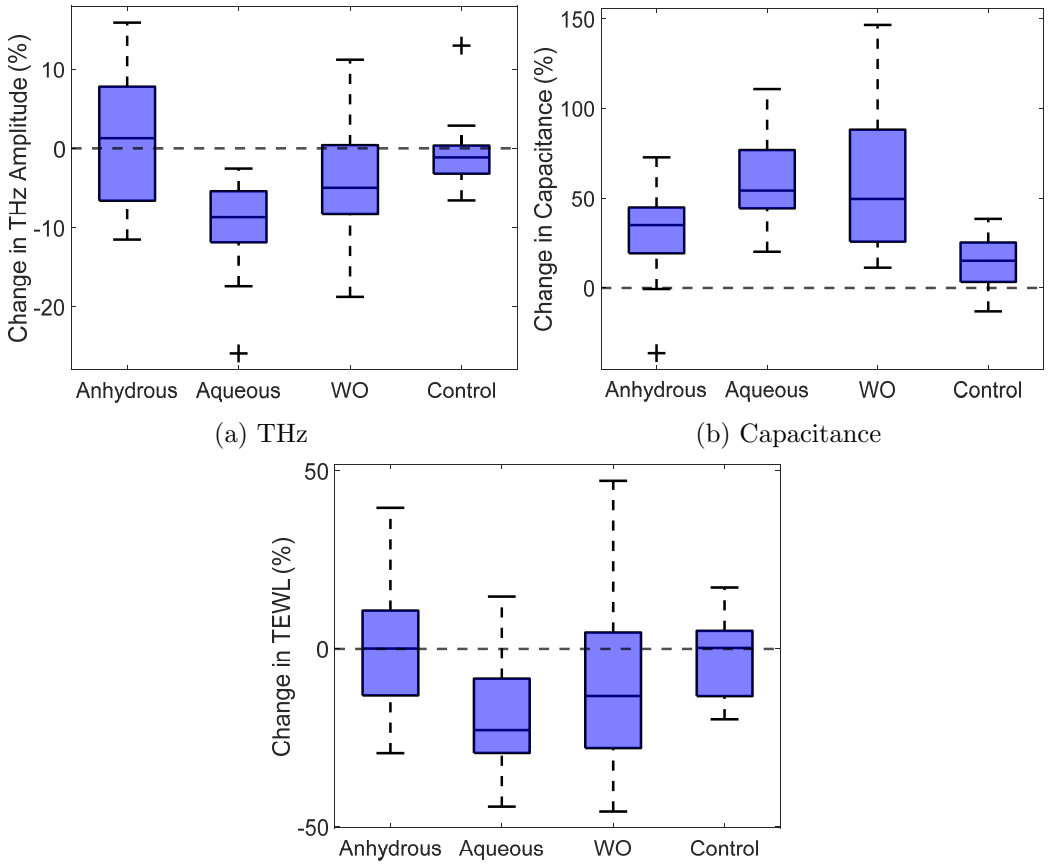

(a) THz

(b) Capacitance

(c) TEWL

Figure 4.8: Box plots of the percentage change measured in a) THz amplitude and b) capacitance and c) TEWL for the three volar forearm regions following treatments with anhydrous, aqueous and WO samples and the change measured in the untreated control region. The top and bottom of the box indicate the 75^{th} and 25^{th} percentiles of the data, the whiskers mark the extent of the range of the data and the black crosses show any outliers.

the rate of absorption of the oily residue by different subjects' skin. The change in control region overlaps with the zero change line and has a much smaller range than the changes seen in response to the treatments. This confirms that the wide range of observed responses is caused by different skin responses to the samples, not a lack of repeatability in the THz measurements of the skin, this verifies the success of the robust protocol for *in vivo* THz measurements of the skin introduced in Chapter 3.

The capacitance measurements of the responses to the treatments shown in Figure 4.8 b) show a positive average percentage change for all three samples, with very similar responses for the aqueous and WO samples, suggesting that the corneometer is not able to distinguish between samples of these types. The measured

increase in hydration induced by the anhydrous sample is smaller than from the other two samples, it is possible that this could be caused by the oil on the surface of the skin interfering with the capacitance measurement. The capacitance measurements of the control region are close to zero and have a smaller range than the other samples, however this distinction is less obvious than in the THz measurements in Figure 4.8 a), meaning that the THz measurements of the skin have the potential to be more repeatable than those taken with the corneometer.

The measurements of the TEWL in Figure 4.8 c) show the least significant differences between the measured responses to the samples. There is a broad distribution across the subjects for all samples and the control region suggesting that there is a problem with the repeatability of this technique. While the average trends shown by the lines through the boxes for the responses to the aqueous and WO samples suggest that the TEWL did decrease following treatment with these samples, this change is not as significant as that observed with the other two techniques. It could be that the 20 minutes between sample application and skin measurement was not enough time for this device to observe the changes in the skin barrier function or there may have been environmental factors that influenced the TEWL measurements such as changes in the air flow caused by the movement of other subjects in the room. The limited repeatability of the TEWL measurements shown by the large distribution of responses of the control region suggest that variation in the environmental conditions may have interfered with the acquisition of the TEWL measurements. Although it appears that there may be some correlation between the TEWL results and the trend observed in the measured THz response of the skin following the application of the samples the uncertainty associated with the TEWL measurements is too high to confirm this correlation. Therefore, the following sections will only compare the results from the corneometer and THz measurements. However, further measurements should be performed comparing TEWL measurements performed with different devices (that is, closed chamber, open chamber and condenser) with THz measurements of the skin.

With all three devices it is possible to observe variation between subjects for each sample, as different skin types may react in a range of ways to the samples. This will be investigated further in Section 4.5.5, where the significance of the initial hydration state of the skin in determining the response of the skin to the application of the sample is discussed.

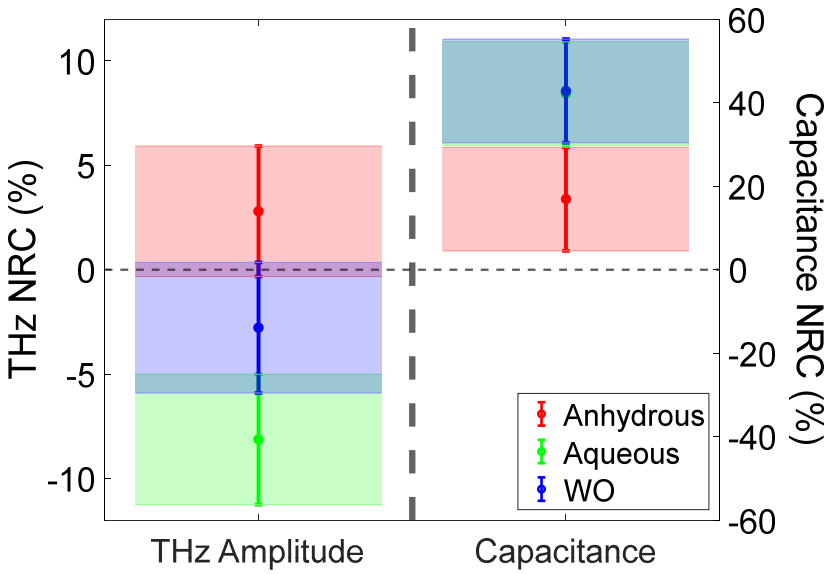

Figure 4.9: Results of performing the one-way ANOVA test, showing the estimated mean of the distribution, the shaded error bars are the result of the Tukey-Kramer test, overlapping bars suggest that the changes observed are not statistically different. The left y axis corresponds to the NRC in the amplitude of the reflected THz signal and the right y axis to the capacitance NRC. Note: the data point for the capacitance measurements of the aqueous sample is obscured by the marker for the WO sample.

4.5.3 Statistical Tests

The outcomes of the ANOVA statistical test comparing the results from the corneometer and THz measurements are shown in Figure 4.9, where the location of the dots mark the estimated mean of the distribution of responses to that treatment and the shaded error bars show the upper and lower confidence limits at a 95% level. Where these comparison intervals overlap, the two responses cannot be described as significantly different from one another. These results were obtained using the Tukey-Kramer test on the output of a one-way ANOVA test. This approach makes it possible to statistically compare the responses to treatments with all three samples measured with a certain technique to one another simultaneously.

The NRC of the THz responses in regions treated with the anhydrous and aqueous samples shown on the left of the figure by the red and green regions respectively, are found to be significantly different to one another. The THz response of skin to the WO sample was observed to be overlapping with the aqueous and anhydrous samples, which is unsurprising as the WO sample is a combination of the key components of the aqueous and anhydrous samples.

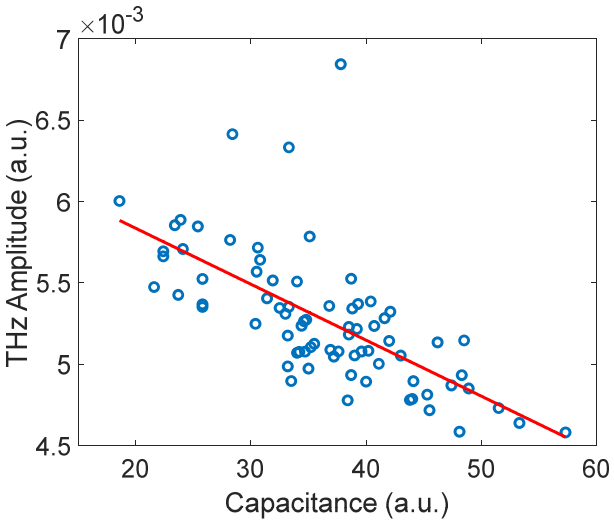

Figure 4.10: A demonstration of the correlation between the THz amplitude and capacitance measurements of untreated skin. The red line shows the line of best fit, correlation coefficient of r = −0.66.

The responses measured by studying the capacitance of skin are quite different to the THz responses of skin, the WO and aqueous measurements are both significantly different to the response of the region treated with the anhydrous sample. However, the WO and aqueous regions overlap almost entirely suggesting that there is very little difference between the capacitance measurements for these two types of samples. The corneometer is primarily sensitive to changes in water content but less so to other changes in the skin, it appears that the aqueous and WO samples increase the water content by similar amounts but no more can be learnt about the interaction of these samples with the skin.

4.5.4 Correlation Testing

Figure 4.10 shows the THz amplitude measured in the four regions of untreated skin measured at the start of the study plotted against the capacitance measurements of the same regions. One subject was excluded from this study as it is thought that hair on the arms of the subject prevented good contact with the imaging window for the THz measurements. The correlation coefficient of the relationship between the THz amplitude and the capacitance is $r = -0.66$, this trend is negative as an increase in hydration is indicated by a decrease in the THz amplitude and an increase in capacitance.

Initially Dry		Initially Hydrated	
Capacitance (a.u.)	THz Amplitude* (a.u.)	Capacitance (a.u.)	THz Amplitude* (a.u.)
34.1	5.33	36.3	5.29
22.2	5.80	39.0	4.93
35.1	6.01	52.6	4.63
28.1	5.66	42.1	4.90

Table 4.2: The capacitance and THz amplitude measurements of untreated skin for the eight subjects categorised as having dry or well hydrated skin prior to treatment. *Factor of 10^{-3} removed from values.

4.5.5 Effect of Initial Hydration of Skin on the Responses to the Samples

The measurements of the skin taken before treatment can be used to characterise the skin regions as dry or well hydrated. This initial state can influence the response of the region to the different treatments, to demonstrate this four subjects were chosen from each category as shown in Table 4.2. Well hydrated skin was defined as having a capacitance value of over 36 and a reflected THz amplitude below 5.3×10^{-3} and the excluded region defines dry skin.

Figure 4.11 shows the NRC in the measured THz and capacitance responses of skin following treatment with each of the samples for the groups of subjects with initially dry or well hydrated skin, where the error bars are the standard deviation within each group.

In Figure 4.11 a) the difference in the THz responses between the two groups is particularly clear for the oil based samples. The increase in the THz response following treatment with oil based samples in the well hydrated skin group could be caused by slow absorption of oil into the skin, meaning that an oily residue remains on the surface when the follow up measurements are taken 20 minutes later. The presence of oil on the surface of the skin is expected to increase the amplitude of the reflected THz pulse by reducing the refractive index of the surface of the skin. However, for subjects with initially dry skin it is expected that their skin will quickly absorb the sample removing any oil from the surface, so the increase in the water content can be observed as a decreased THz amplitude. This difference in absorption rate can also explain the larger decrease in the THz amplitude in the dry skin group following treatment with the aqueous sample. It is possible that the aqueous sample

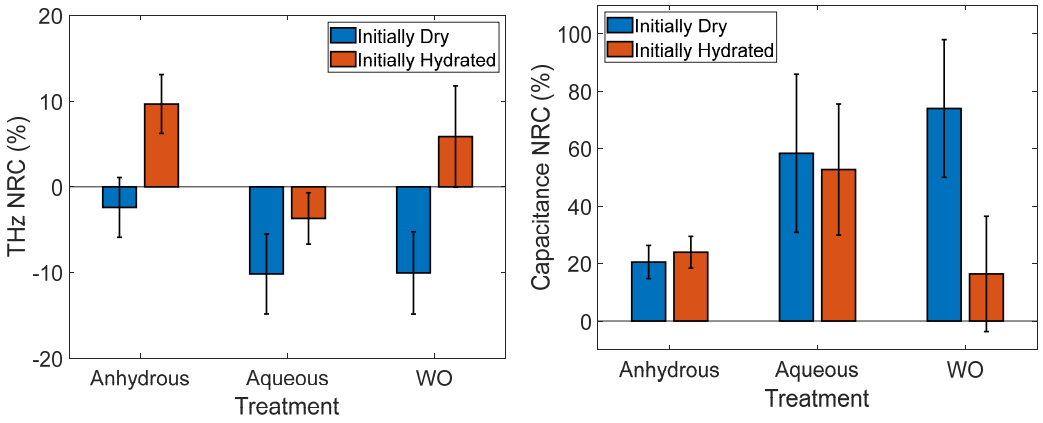

(a) THz

(b) Capacitance

Figure 4.11: The NRC in the a) THz and b) capacitance measurements of the skin following treatment with each of the samples. The data are separated into the responses of subjects with initially dry and initially well hydrated skin shown by the blue and red bars respectively, with four subjects in each category. The error bars are the standard deviation of the responses from the four subjects in each group.

will be absorbed more rapidly by dry skin, meaning that a larger amount of water will be gained by the dry skin than the initially well hydrated skin, which may be slow to absorb the water allowing more of it to escape into the environment.

In comparison to the THz responses there is little difference in the capacitance measurements of dry and well hydrated skin responses to treatment with anhydrous and aqueous samples, shown in Figure 4.11 b). There is however a difference in the responses to the WO sample; the initially dry skin shows a larger increase in capacitance than the well hydrated skin. It is suspected that the well hydrated skin may have some oil residue remaining on the surface of the skin at the time of measurement, which could interfere with the capacitance measurement, reducing the perceived hydration of the skin. Whereas, the dry skin is less likely to have this oil on the surface of the skin, so the large increase in skin hydration can be seen in the capacitance measurement.

These results suggest that the initial hydration state of the skin can have a large effect on the way in which the skin responds to different samples and the time scale on which these changes occur. From the results shown in Figure 4.11, it appears that THz measurements of the skin are more sensitive to these differences caused by the initial state and make it possible to infer more about the mechanisms of the interactions of the samples with the skin.

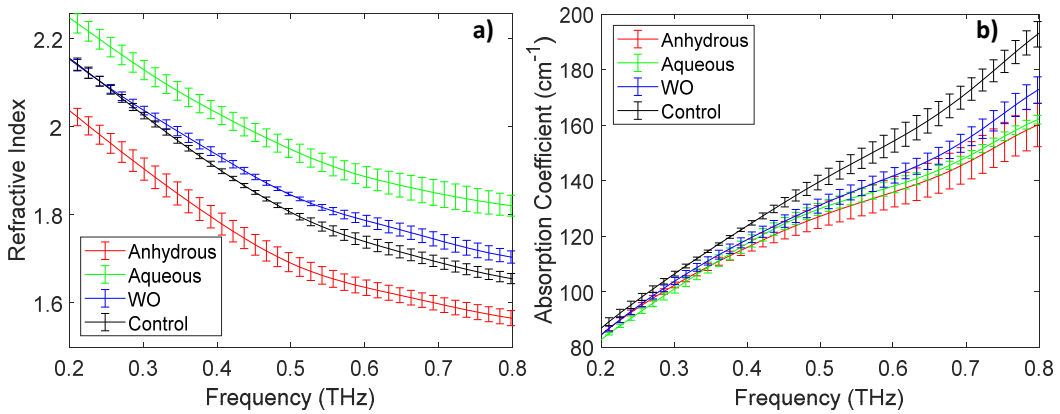

Figure 4.12: An example of a) the refractive index and b) the absorption coefficient of the skin following each of the treatment options for a single subject. The plotted values are the average of five consecutive results, the error bars are the standard deviation of these five results.

4.5.6 Frequency Dependent Properties of the Skin

Finally, in Figure 4.12 an example is given of the extracted refractive index and absorption coefficient of the skin following the application of each of the samples. This figure shows the changes in the frequency dependent properties for a single subject acquired 20 seconds into the occlusion process, the results from five consecutive repeat scans were averaged to give the plotted results and the error bars are the standard deviation. It can be seen that the application of the samples has a more significant effect on the refractive index than the absorption coefficient. The refractive index of the skin increases following the application of the aqueous and WO samples and decreases after the application of the anhydrous sample, confirming the trends observed in the amplitude of the THz signal. As with the time domain variable studied above there is significant variation in the way different subjects' skin responds to the samples so it is not meaningful to average these spectra to present the results for multiple subjects.

The technique for extracting these properties was explained in Section 2.4.2, it is important to note that this approach assumes that the skin is a single homogeneous layer. This assumption may not be accurate after applying the products to the skin, but it gives an indication of the macroscopic changes occurring.

4.6 Discussion

The effects of each sample can be discerned through the observations made in this study. Firstly, the aqueous sample had the most significant effect on the skin when measured with all three devices. The corneometer observed an increase in the response from the skin as expected, due to its calibration using water to define the upper limit of possible responses. The THz reflection measurements showed a significant decrease following treatment with the aqueous sample, this observation has been seen in several other studies using treatments that increase the skin hydration, so was an expected result. A decrease in the TEWL was observed in the regions treated with the aqueous sample suggesting that the skin barrier function had improved.

The effects of the anhydrous sample on the skin were more varied across the different subjects, it can be seen that the response could depend on the initial hydration state of the subject's skin. The capacitance measurements of the skin showed a slight increase following treatment with the anhydrous sample, indicating that the water levels had improved, but not as significantly as with the two other samples. This increase of water in the skin was caused by an occlusive layer trapping water inside the surface, but it is possible that the hydration increased more than this and the oily residue interfered with the measurement. The THz measurements showed an average increase in the reflected signal, caused by the presence of oil in the upper layers of the skin, though some subjects showed a decrease possibly because their skin had fully absorbed the oil so the resulting increase in hydration could be observed. The TEWL measurements were not able to give conclusive results for the two oil based samples, this is possibly because the presence of oil on the surface of the skin interfered with the measurement, preventing observations of the state of the skin barrier following treatment.

The treatment of the skin with the WO emulsion induced a range of responses across the subjects, which could also be associated with the initial hydration state of the skin. The WO sample is thought to most closely replicate the majority of commercial products with a mixture of both oil and water phases present. The THz measurements of the skin following treatment with the WO sample are not significantly different from those of skin treated with anhydrous and aqueous samples but lie between the two, this could be expected as the composition of the WO sample is a combination of the two other samples. Whereas, the capacitance measurement of the WO sample on the skin is nearly identical to the response from the aqueous sample. This shows the difference in the way the measurements work, suggesting

that both the WO and aqueous samples increase the water content of the skin by approximately the same amount.

It is possible to infer that the corneometer is an effective technique for evaluating skin hydration, while THz measurements can also be sensitive to the effects induced in the skin by a range of sample types. THz measurements were also more sensitive to the different responses to the samples observed by the hydrated and dry skin categories and were able to identify whether the oil had been completely absorbed. However, another technique to assess the surface lipids is needed to verify this hypothesis.

The correlation testing part of the study was carried out on untreated skin so that the presence of the samples on the skin did not influence the observations. The results show that there is moderate correlation between the THz and corneometer measurements with $r = -0.66$ [109]. Neither of the techniques measure the skin hydration directly but measure capacitance and THz reflectivity. Capacitance measurements of the skin are known to be affected by more than just skin hydration, so perfect correlation between the two devices is not expected. The fact that there is moderate correlation with the current gold standard for measuring skin hydration suggests THz sensing has great potential for studying skin *in vivo*.

It has previously been demonstrated that THz measurements of the skin have the potential to provide more quantitative information about the hydration profile of the skin than can be obtained by a corneometer [72]. Additionally, there are known weaknesses of the corneometer including its lack of specificity to skin water content and the limited ability to link the measured result to changes in the skin, it is hoped that THz sensing will be able to overcome both of these problems. Measurements of the TEWL can be heavily dependent on the environmental conditions in which they are performed, therefore repeatability of the results obtained is limited. Furthermore, the cost and size of THz systems are decreasing and it is envisaged that THz sensing will become affordable for many future applications including high precision diagnosis and evaluation of skin conditions, leading to the prescription of more effective treatment options.

4.7 Conclusion

This study presents the first known comparison of *in vivo* measurements of human skin taken using THz-TDS with the present gold standard for skin hydration assessment, the corneometer. Additionally, measurements were taken of the TEWL to assess the skin barrier function, however these had limited repeatability for un-

treated skin regions. The measurements were taken of untreated skin as well as skin treated with three samples; aqueous, anhydrous and a WO emulsion. The corneometer is very sensitive to water content and shows the greatest changes, it can be most useful in studies where different amounts of water are applied, however it is not able to distinguish between the response of the skin to the WO and aqueous samples. The THz measurements compare well with this commercial technique, and the results are very positive for a relatively new technique. Some of the changes observed in the THz response were subtle and ways to enhance the contrast of these measurements should be sought. However, THz measurements came closer to distinguishing the responses of the three samples and show a strong sensitivity to the properties of the surface of the skin beyond hydration effects, as well as an ability to identify the different responses of dry and hydrated skin to the samples. Additionally, the study of the correlation between the techniques assists in the validation of *in vivo* THz measurements of the skin as a means of highly quantitative skin assessment. It is hoped that with the expansion of this work through further modelling, THz measurements of the skin could develop into a useful technique for skin characterisation beyond simple hydration measurements.

Chapter 5

Monitoring the Effect of Patches for Transdermal Drug Delivery on Skin Using THz Sensing

5.1 Introduction

In addition to assessing changes in the water content of skin to quantify the efficacy of skin care products, there are many other cases in which it is important to be able to assess the hydration of the skin. For example, water content of the skin is an important parameter for controlling the penetration rate of chemicals through the skin barrier, therefore in order for patches designed for transdermal drug delivery to be successful, the effects of the patches on the water content of the skin must be understood.

In this chapter THz measurements of the skin are used to observe the effect of partially and fully occlusive transdermal drug patches on the THz response of the skin after the patches had been applied for 24 hours. It was possible to observe an increase in the water content of the skin following the application of the patches and identify that the skin remains hyper-hydrated for at least four hours after the removal of the fully occlusive patches. Herein it is shown that THz spectroscopy has potential for increasing the understanding of how transdermal drug patches affect the skin, how long the skin takes to recover following patch removal and what implications these factors might have for how transdermal drug patches are designed and used.

5.1.1 Patches for Transdermal Drug Delivery

Transdermal drug delivery is used for an increasing number of applications to provide alternatives to oral and intravenous administration, with over 1 billion patches being manufactured each year [110]. Administration of drugs through the skin can be a useful option to avoid potential metabolism of the drug in the liver or gastric side effects and to avoid the use of needle penetration. It can also allow for the controlled release of a drug into the body at a more consistent rate than orally administered drugs over the entire time window of drug requirement [111]. A primary factor that can influence the rate of drug delivery through the patch is the hydration of the skin, it is therefore important that the effect of patches on the skin is understood as much as possible [112]. Additionally, the way in which the skin recovers following the removal of the patches is important as it can inform the advice given to patients about how often to apply patches and how often the application site should be rotated.

Some of the earliest treatments that were delivered through patches include the prevention of motion sickness [113, 114] and nicotine to aid smoking cessation [115]. Patches have also been developed for hormone replacement therapy [116], localized pain relief using diclofenac [117] or fentanyl [118] and for controlling the symptoms of chronic conditions such as Parkinson's [119] or Alzheimer's [120] disease. Transdermal drug patches can be very beneficial in the cases where the patient may lack the capacity to take medication by themselves as the patches can be easily applied and replaced by a carer and deliver the required dosage for a longer period of time than oral medication.

There are many aspects to be considered when designing patches for transdermal drug delivery including the choice of adhesive and backing material. Changing the backing material can alter the occlusive nature of the patch and change how the skin responds to the application of the patch. In some cases, such as with fentanyl patches where the drug is highly potent and potentially toxic if administered to the wrong person, it is important that a fully occlusive backing is used to prevent the leaking and transfer of the drug [121]. However, it has also been observed that long term application of fully occlusive patches can cause skin irritation due to the buildup of water at the surface of the skin [122].

Some studies have been performed to assess the effects of occlusion on the water content of the skin and the function of the skin barrier. For example, Aly *et al.* observed an increase in the TEWL measured following 24 hours of occlusion with plastic [123]. They then observed that the TEWL had returned to its previous levels 18 hours after the removal of the plastic, suggesting that the occlusion of the skin

had increased the levels of water in the skin but that there had been no significant damage to the skin barrier. A subsequent study by Faergemann *et al.* measured an increase in the water content of the skin with a dielectric probe following occlusion with a plastic layer [124]. An increase in the bacteria count was also observed with increasing occlusion time suggesting that in some cases long term occlusion of the skin can increase the risk of bacterial infections.

5.1.2 Using THz Imaging for Assessing the Efficacy of Transdermal Drug Delivery Techniques

Previous studies have found that the strong sensitivity of THz light to the water content of skin can also be used to observe changes induced by occlusive materials, which prevent the natural loss of water through the skin barrier. This was identified as a potential problem when performing THz measurements that involve contact between the skin and an imaging window, as introduced in Chapter 3. However, Wang *et al.* demonstrated that this sensitivity to the effects of occlusion on the skin can also be a strength [51]. They successfully used THz measurements to observe changes in the skin following the application of silicone gel sheeting, which is commonly used to treat severe burns by occluding the skin and increasing the water content.

THz spectroscopy and imaging techniques have previously been applied to assess the efficacy of various approaches to transdermal drug delivery. For example, Kim *et al.* were able to measure the penetration of a sample containing ketoprofen through excised mouse skin by taking THz images of the underside of the skin sample [125]. Wang *et al.* then investigated the effects of approaches to enhance the penetration of the samples through the skin barrier such as micro and nano needle patches. They performed *ex vivo* measurements using porcine skin and observed that there is a significant change in the measured THz response of a sample that was treated with a nanoneedle patch prior to drug application compared to skin that received no extra treatment before the drug was applied [33]. THz measurements have also been used to quantify the amount of nicotine that has left a nicotine patch by measuring the patch before and after it was applied for different durations, showing that it is possible to use THz spectroscopy to verify the rate of drug delivery through a patch membrane [126]. These studies focused on the penetration of the drug through the skin, whereas in this chapter the effect of patches on the skin is investigated in order to learn how different patches can influence the rate of drug delivery through the skin barrier. However, it is possible that in the future the approach highlighted in this chapter could be combined with those mentioned

above to use THz spectroscopy and imaging techniques to obtain a more complete picture of the dynamic response of the skin to the application of patches containing active drug ingredients.

This study investigates the ability of *in vivo* THz measurements of the skin to identify the changes induced in the skin by patches for transdermal drug delivery by analyzing THz light reflected from the surface of the skin. Two types of patches are tested: one backed with a Polyethylene Terephthalate (PET) film, which is fully occlusive, and the other that is backed with a woven material, which is semi-occlusive. Three percentages of excipients were tested for each type of patch and the properties of the skin were measured immediately after the removal of the patches following application for 24 hours. Additionally, the recovery of the skin was monitored by taking subsequent measurements 30 minutes and four hours after the removal of the patches. In this study *in vivo* THz measurements are used to identify changes in the water content of skin treated with different types of patches and observe the changes further induced in the skin when it is occluded by a quartz imaging window during the measurement following the removal of the patches.

5.2 Methods

5.2.1 Skin Patches for Assessment

This study investigates the effects of drug in adhesive patches for transdermal drug delivery on the THz response of the skin. To isolate the effects of the patch from the effects of the drugs, the active ingredient was not present in these patches. Two different types of backing materials were used to investigate the effect of the occlusive nature of the patch backing on the THz response of skin, a fully occlusive PET film backing and a partially occlusive fabric woven PET fiber backing. An example of the patches applied to the volar forearm can be seen in Figure 5.1 a). It is expected that the woven backed patch will allow some water loss from the skin through the adhesive and out from the backing, whilst the PET film backed patch will prevent all water loss from the surface of the skin as it is impermeable to water vapour, as shown in Figure 5.1 b) and c).

In addition to changing the backing material of the patches, three excipient compositions were tested with 0%, 3% and 6% propylene glycol, which is commonly added to transdermal drug patches in order to enhance the penetration of drugs through the skin barrier. These concentrations of propylene glycol were chosen to replicate the concentrations typically used in a transdermal drug patch, making it possible to investigate the potential effects of these different adhesive compo-

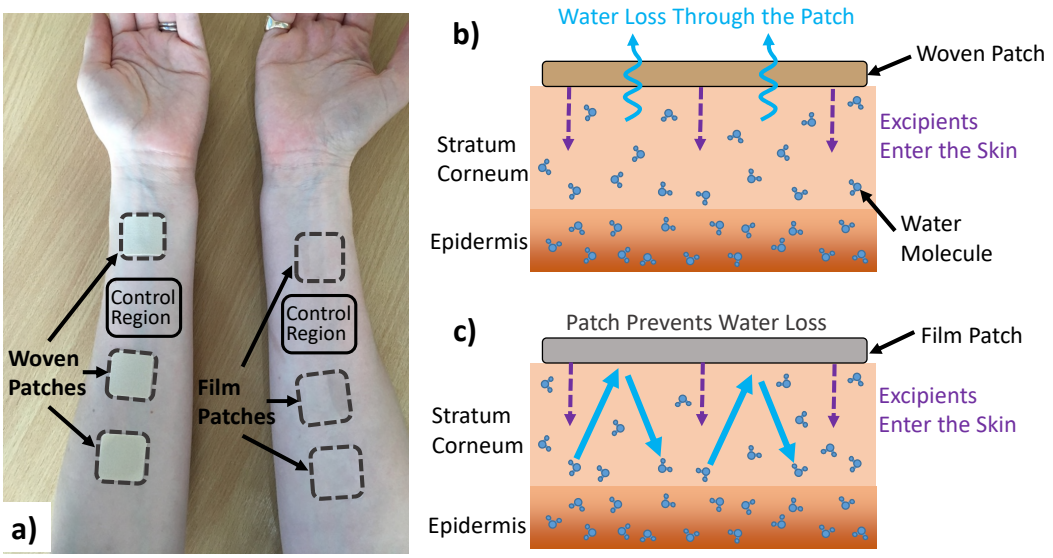

Figure 5.1: a) The volar forearms of a subject with the woven and film backed patches applied with a control region left untreated on each arm. b) and c) show the mechanisms by which the woven and film backed patches affect the movement of water in the skin.

sitions on the hydration of the skin. The adhesive of all the patches contained 10% transcutol, another common component of transdermal drug patches [127]. Both propylene glycol and transcutol are FDA approved excipients for transdermal and topical medicines and are used to increase the diffusion of the drug across the skin. Frequently the effects of these approved excipients vary from the active pharmaceutical ingredient and have cooperative effects. The adhesive used was a proprietary polyurea crosslinked thermoset mainly composed of a high percentage weight of siloxy terminated poly(propylene glycol) prepolymer chain extended with isophorone diisocyanate and crosslinked and cured with the excipients in place by exposure to 100% humidity for five minutes at 70°C [128, 129]. The patches used in this study were all produced by Medherant Ltd and were donated free of charge.

5.2.2 THz Measurements of the Skin

The THz measurements of the skin were acquired using the TeraSmart THz spectrometer from Menlo systems introduced in Section 2.6.1, using a reflection geometry with pressure sensors positioned either side of the imaging window. The system is capable of acquiring THz pulses at a rate of four pulses per second. In each skin measurement, 240 pulses were measured, meaning that the skin was in contact with the imaging window for one minute at each time point. This relatively long mea-

surement duration was chosen in order to measure the response of the skin to the occlusive effects of the imaging window and to observe how this changed following the application of the different types of patches.

5.2.3 Protocol for Skin Measurements

To test the effect of the patches on the skin, three patches backed with woven PET fibers and three PET film backed patches were applied to the volar forearms of five human subjects. The subjects involved in this study were four males and one female in the age range 24-34, all of the subjects had healthy skin in the regions in which the measurements were performed. Written informed consent was obtained from each subject prior to their involvement in the study. The patches were applied for 24 hours before being removed and then the skin was assessed. THz measurements were performed on each region prior to the application of the patch, in addition to a control region on both forearms that remained untreated throughout the study. The regions were subsequently measured with THz light immediately following the removal of each patch and 30 minutes and four hours after patch removal and the change in the reflected light was measured in order to observe the recovery of the skin. The control regions were also measured at each time point.

To ensure that the results were as repeatable as possible, the measurements were performed according to the robust protocol for THz measurements of the skin, introduced in Chapter 3. As part of this the subjects were asked to spend 30 minutes in the lab prior to each measurement, to give the skin time to acclimatize to the controlled environmental conditions of the lab. Additionally, pressure sensors were positioned either side of the quartz imaging window, this is part of the pressure sensor system described in Section 3.3.2. The pressure sensor was connected directly to the THz system to provide a real time output that was visible to the participants to help them keep the applied pressure within the desired range. The measured output from the pressure sensors was also recorded so that these values could be used to help with the processing of the results, making it possible to reject measurements acquired at the incorrect pressure. The target pressure range defined for this study was 1.6-2.0 N cm^{-2}, this was found to be a large enough pressure to reduce the risk of air gaps being present between the skin and the imaging window during the measurements, whilst being low enough that it can be comfortably maintained by the subject throughout the measurement. The pressure sensors were also used to start the THz measurement, as soon as the pressure sensors detected any contact the measurement began, this ensures that the time for which the skin is in contact with the imaging window is controlled for all subjects.

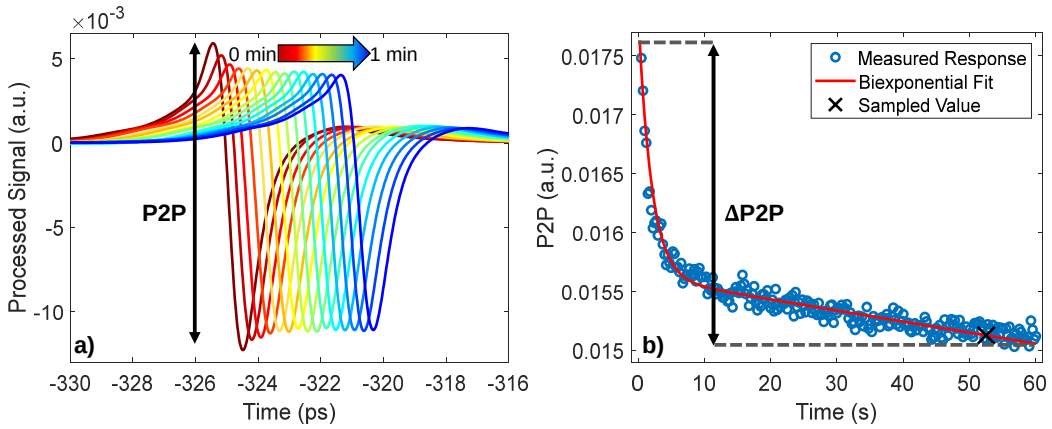

Figure 5.2: a) The processed THz signals measured from the untreated skin of a single subject, the colour gradient shows increasing occlusion time. The pulses are plotted every second for the first three seconds then every five, they have been shifted horizontally for clarity. The P2P variable is shown on the plot. b) P2P plotted as a function of occlusion time, fitted with a biexponential function shown by the red line and sampled 52 seconds into occlusion as shown by the black cross. The definition of the ΔP2P variable is shown as the difference between the value of the fit at the start and end of occlusion.

5.2.4 Approach to Data Processing

The processing techniques introduced in Section 2.4 were used in this study to obtain a processed time domain signal and the optical properties of the skin from the THz measurements. Examples of the processed time domain signal are shown in Figure 5.2 a). In this figure the signals are plotted every second for the first three seconds of the measurement and every five seconds for the remainder of the one-minute measurement. The pulses are shifted horizontally in the figure for clarity. The P2P variable used previously to quantify the THz response of the sample is indicated in the figure.

The amplitude of the processed THz signal decreases throughout the one minute measurement as shown in Figure 5.2 a), due to the occlusive effect of the imaging window. The decrease in the amplitude is associated with an increase in the water content and monitoring changes in P2P makes it possible to quantify changes in the water content of skin caused by the application of the patches. For each measurement, the results recorded by the pressure sensor were used to remove measurements that were recorded when the incorrect pressure was being applied. After the measurements were filtered to select only the values obtained at the correct pressure a biexponential fitting was applied and the value of the fit was sampled 52 seconds into occlusion, as shown in Figure 5.2 b), using the approach introduced in

Chapter 4.

The application of fully or partially occlusive transdermal drug patches changes the distribution of water in the skin, this changes the way in which the skin will respond to occlusion by the imaging window. In order to quantify this change in the response to occlusion, the variable ΔP2P is defined as the difference between the value of the biexponential fit at the start and end of occlusion, as shown in Figure 5.2 b). This variable can then be used to observe whether the application of the patches increases or decreases the gradient of the occlusion curve observed throughout the one minute measurement. In addition to using the amplitude of the time domain signal, the frequency dependent optical properties of the sample were calculated using a single layer model of the skin as described in Section 2.4.2.

The NRC defined in Section 3.3.6 was also calculated in order to remove the effect of natural variation of the skin between measurements that is not caused by the treatment of the skin. In this study the use of the NRC to characterize the changes observed in the skin is particularly important due to the relatively long time for which the patches are applied, giving the skin time to change significantly due to exposure to other environmental factors.

The one-way ANOVA test was used to evaluate if the changes observed are statistically significant. These results were analysed with the Tukey-Kramer test to ensure that the threshold of 5% significance was maintained. These results can be used to see if the changes observed in the skin following the application of the patches are significant and to see if the patches produce significantly different results from one another.

5.3 Results

5.3.1 Average Changes in the Skin Following Patch Application

The average change in the reflected THz signal following the removal of each of the patches is shown in Figure 5.3, where the error bars indicate the standard error on the mean. The figure shows the NRC in the amplitude of the THz pulse, sampled by fitting the occlusion curve with a biexponential function and sampling the value from the fit 52 seconds into occlusion. A decrease in P2P is associated with an increase in the water content of the skin. The left- and right-hand sides of the figure show the responses observed following treatment with the woven and film backed patches respectively for the three excipient levels contained in the patches. The recovery of the skin following the removal of the patches can be observed from the results showing the measured properties of the skin 30 minutes and four hours

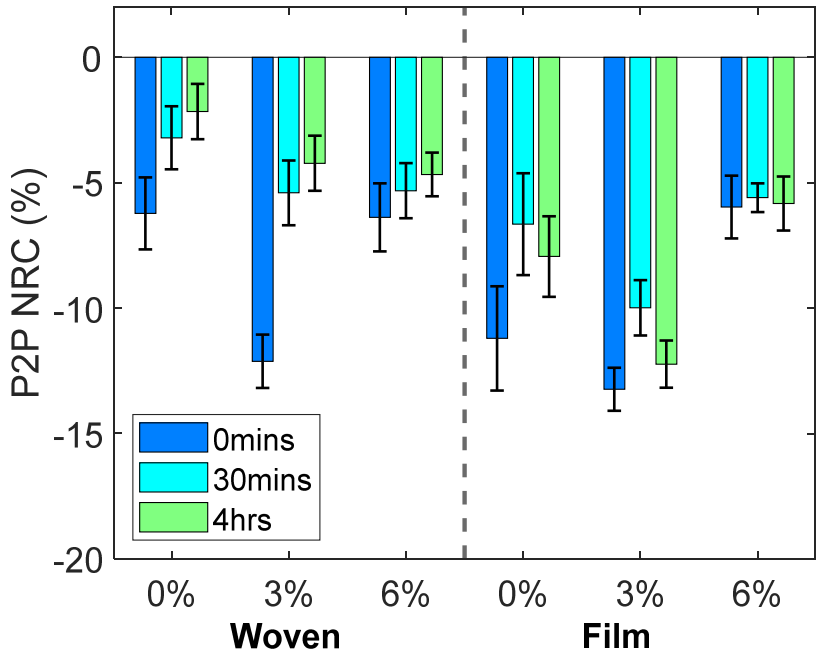

Figure 5.3: The average NRC in the P2P sampled 52 seconds into occlusion, observed in all five subjects at 0 minutes, 30 minutes and four hours following the removal of the woven and film backed patches containing 0%, 3% and 6% propylene glycol. The error bars are the standard error on the mean.

after the patch was removed, in addition to the measurements taken immediately following patch removal.

For all of the patches a decrease in P2P was observed suggesting that the hydration levels of the skin had increased following application of each of the patches for 24 hours. These changes appear to persist in the skin for at least four hours following the removal of the patches. The results show that the film backed patches induced a larger change in the skin than the woven patches and that the rate of recovery of the skin treated with the PET film backed patches was reduced compared to the partially occlusive woven patches. Additionally, patches with 3% excipient levels seem to have the largest impact on the THz response of the skin, however measurements on more subjects will be needed to draw further conclusions about the significance of this observation.

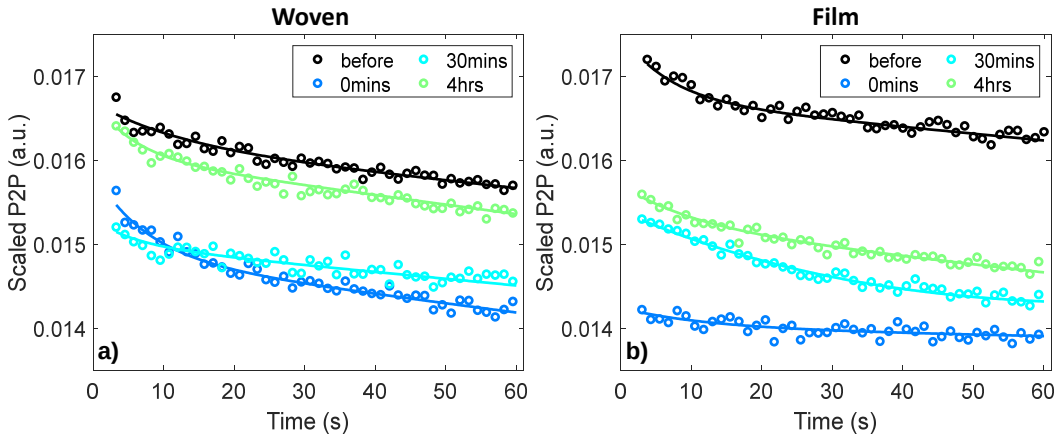

Figure 5.4: An example of the occlusion curves observed for a single subject following the application of a) woven and b) film backed patches, every fifth data point is plotted and the biexponential fits are shown by the solid lines. The results have been scaled by subtracting the change in the control region between the initial measurement and the measurement taken at that time point.

5.3.2 Effect of Patch Application on the Response of Skin to Occlusion

In addition to sampling the value of P2P measured at a particular time point using a biexponential function as shown in Figure 5.2, it is possible to use the observed occlusion curve to learn about the changes in the water distribution in the skin caused by the application of the patches. It was shown in Figure 5.2 that in untreated skin it is possible to observe a decrease in the amplitude of the processed signal throughout a skin measurement due to the occlusive effect of the imaging window. However, if the water content in the skin has been disrupted, it is expected that this could be observed as a change in the way the skin responds to the one minute of occlusion throughout the THz measurement.

Figure 5.4 shows an example of the occlusion curves observed in a single subject following the application of a woven and film backed patch by plotting the change in P2P measured throughout the one minute measurement. Every fifth data point is plotted and the biexponential fit for the data set is shown by the solid lines. All of these curves have been scaled to account for the natural variation of the skin between measurements, this was done by subtracting the difference in the control region between the initial measurement and the measurement taken at that time point, as sampled after one minute of occlusion. The black curves in each plot show the measured response of the region prior to the application of the patches. The coloured curves show the response of the skin to occlusion 0 minutes, 30 minutes

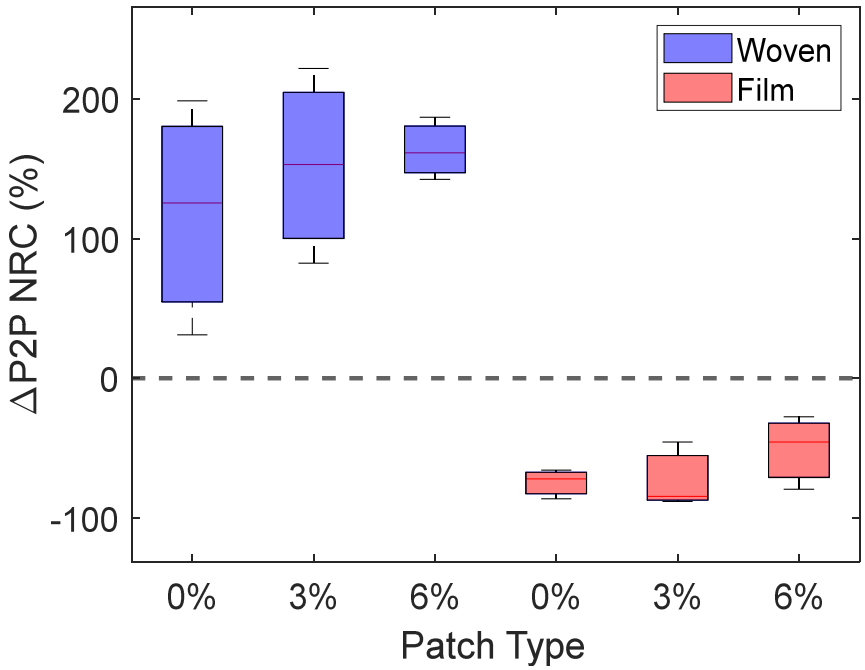

Figure 5.5: A box plot of the NRC in ΔP2P, a variable defined to give an indication of the change induced in the skin by one minute of occlusion by the quartz imaging window immediately after the removal of the patches. This figure shows the results in the three subjects who were able to keep the applied pressure within the desired range for the most time points. The red lines inside the boxes indicate the median response observed, while the upper and lower edges of the boxes show the upper and lower quartiles of the measured responses.

and four hours after the patches were removed.

The dark blue curve in Figure 5.4 a), which indicates the occlusion curve measured immediately following the removal of the woven backed patch, appears to show a greater change in P2P than that observed prior to patch application. Whereas the dark blue curve in Figure 5.4 b) indicating the response following the removal of the film backed patch is much flatter than the response of untreated skin. The flattening of the occlusion curve suggests that the skin is already saturated with water due to the occlusive effect of the film backed patch, so occlusion by the imaging window has little effect on the hydration of the skin. The steepening of the occlusion curve following removal of the woven backed patch is harder to explain without further modelling of the skin.

It can be seen that 30 minutes and four hours after the removal of both patches the behavior of the skin in response to occlusion by the imaging window has

returned to what it was before the patches were applied as the slopes return to the same shape. However, the P2P measured remains lower than that of untreated skin suggesting that there is an increase in the water content of the skin. The recovery of the skin with increasing time after the patches were removed can be seen as the occlusion curves rise back up towards the black curves measured before the patches were applied. It appears that it takes the skin longer to recover from the application of the film backed patches than the woven backed patches.

In order to visualize the change in the response to occlusion, Figure 5.5 shows the NRC of ΔP2P, as defined in Figure 5.2 b). A positive NRC in ΔP2P indicates that the application of the patch increased the amount that P2P changes during one minute of occlusion and that the occlusion curve steepens. This approach gives a way to quantify the qualitative changes observed in the occlusion curves, shown in Figure 5.4. In the boxplot, shown in Figure 5.5, the blue and red boxes show the response to the woven and film backed patches respectively, where the upper and lower limits of the boxes indicate the upper and lower quartiles of the data set and the red lines through the boxes show the median. This plot only uses the data from the three subjects who were able to keep the applied pressure within the desired range for the most time points. It is necessary to only study the subjects with the most consistent pressure to investigate ΔP2P as the occlusion curve is very sensitive to changes in pressure and any bumps in the data caused by movement of the subject or incorrect pressure are harder to account for.

A clear divide can be seen between the effects of the woven and film backed patches in Figure 5.5. The woven backed patches appear to increase the change in the skin under one minute of occlusion while the film backed patches decrease this change. This confirms the qualitative trend observed in Figure 5.4. It does not appear that the percentage of propylene glycol excipient in the patch affects ΔP2P significantly. It seems that the dominant factor that influences the way skin responds to occlusion is whether the patch applied was fully or partially occlusive, this would determine whether the surface layers of the skin are already saturated with water prior to the occlusion of the skin by an imaging window.

5.3.3 Changes in Optical Properties

Up until this point all of the results presented have involved analysis of how the amplitude of the processed time domain signal changes following the application of the patches. However, it is also possible to extract the frequency dependent optical properties using the approach described in Section 2.4.2. Figure 5.6 shows the refractive index and absorption coefficient of the skin of a single subject for untreated

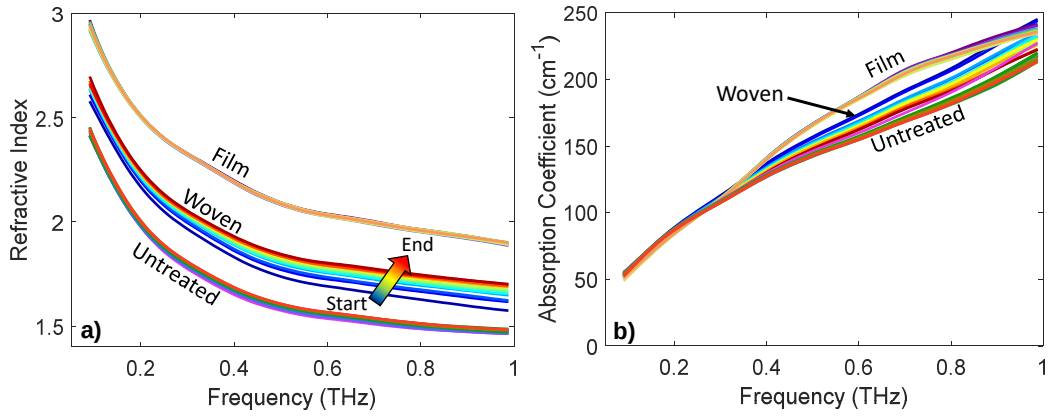

Figure 5.6: An example of a) the refractive index and b) the absorption coefficient as a function of frequency for untreated skin and immediately following the removal of film and woven backed patches. The colour gradients indicate increasing occlusion time, making it possible to observe the effect of the changing response of the skin to occlusion on the optical properties of skin.

skin and skin immediately following the removal of film and woven backed patches. The colour gradient indicates measurements being plotted later into occlusion with the coloured arrow showing the direction of increasing occlusion time and the lines are plotted every five seconds into occlusion.

It is clear from Figure 5.6 a) that there is a large difference in the refractive index of untreated skin and skin that has had a film or woven backed patch applied. The application of the patches increases the refractive index suggesting that the water content of the skin has increased due to the patch application. The film backed patch has the largest impact on the refractive index, suggesting that it caused the largest increase in the water content of the skin. Looking at the width of the distribution of the lines plotted with the colour gradient it is possible to observe how much the refractive index of the skin changes throughout the one minute of occlusion by the quartz imaging window throughout the THz measurement. The largest distribution is shown by the skin that was treated with the woven backed patch, this matches the trend observed in the time dependent variable. This figure shows that throughout occlusion the refractive index of skin increases across the whole frequency range from 0.1-1 THz, this suggests that water builds up in the surface layers of the skin. The smallest distribution of lines corresponding to the smallest change in the refractive index of the skin during occlusion is shown by skin treated with the film backed patches, confirming that the skin is already saturated with water so does not change any more in response to further occlusion by the

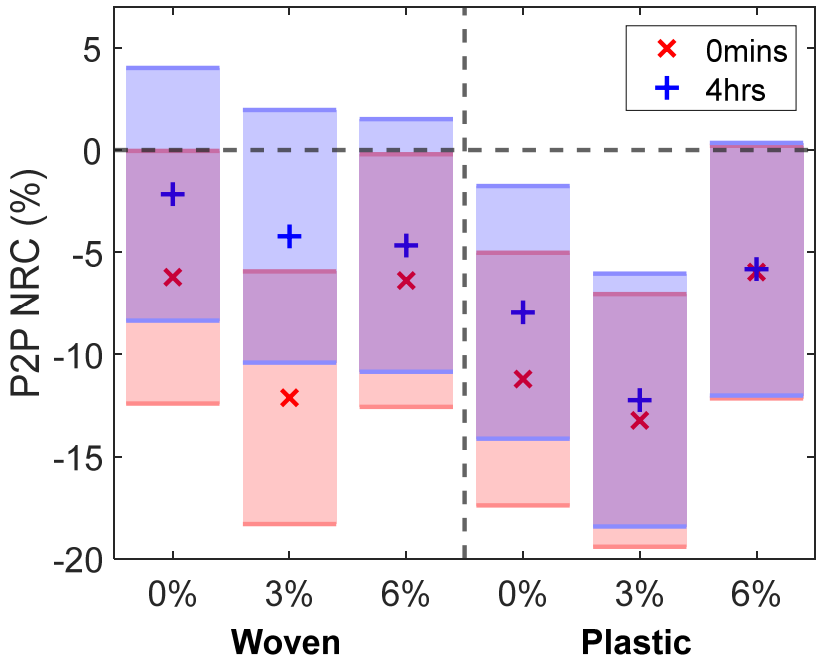

Figure 5.7: The results of performing the one-way ANOVA test on the NRC in the P2P sampled 52 seconds into occlusion for all subjects, 0 minutes and four hours after patch removal as shown by the red and blue regions respectively, the markers show the estimated mean of the distribution of responses to the patches, the shaded bars are the 95% confidence intervals calculated using the Tukey-Kramer test.

imaging window.

For completeness the same results are shown for the absorption coefficient of the skin in Figure 5.6 b). The differences between the untreated skin and the skin treated with the different patches is less clear in this plot. There is some separation between the different treatments at higher frequencies, but less can be learned about the effect of the patches on the skin from this plot.

5.3.4 Statistical Analysis

Finally, the statistical significance of the changes observed in the skin is tested using the one-way ANOVA test and the Tukey-Kramer test [130]. The results of these statistical tests are shown in Figure 5.7, for the NRC in the P2P measured 0 minutes and four hours after the removal of the patches, where the shaded bars indicate Tukey's minimal significant difference at a 5% significance level. Where the bars do not overlap with the dashed line indicating zero change this means that there is a significant difference in the skin following treatment with the patches. The

markers inside the bars indicate the estimated mean of the distribution of changes in the skin induced by each patch.

Studying the red regions in Figure 5.7, which indicate the results immediately after the patches were removed, reveals that all patches result in a significant change in P2P. The patches with 3% propylene glycol led to the largest changes in the measured response of the skin for both patch types. The film backed patches induce a larger change in the skin than the woven backed patches. The blue regions show the results four hours after the patches were removed, these show that the changes in all regions of the skin treated with woven backed patches are no longer significant, as all blue regions on the left-hand side of the plot overlap with the dashed zero line. While the skin treated with the 0% and 3% propylene glycol patches backed with the PET film maintain a significant difference and the result for the 6% film backed patch just touches the zero line. This confirms that the changes induced in the skin by the film backed patches persist for much longer than those induced by the woven backed patches.

5.4 Discussion

In this study it was found that THz reflection measurements can be used to observe changes in the skin induced by the application of transdermal drug patches. It was possible to observe these changes in the time and frequency dependent properties, particularly in the amplitude of the processed THz signal reflected from the surface of the skin and the refractive index of the skin in the frequency range from 0.1 to 1 THz. The measured responses suggest that the 24 hour application of the different patches all increased the water content of the skin.

The ability of the THz-TDS system used in this study to take rapid repeated measurements of the skin whilst it remains in contact with an imaging window makes it possible to learn more about the effect of patch application on the distribution of water in the upper layers of the skin. The flattening of the occlusion curve observed in skin that had been treated with a film backed patch suggests that the PET film fully occluded the skin preventing the natural loss of water, causing the water levels in the skin to increase. Therefore, when the skin was occluded by the imaging window in order to perform the THz measurements there was little change observed in the THz response of the skin as the upper layers of the skin were already saturated with water.

Surprisingly, a change was also observed in the response of skin treated with a woven backed patch to occlusion as the occlusion curve became steeper. Further

studies are required to learn more about the cause of this effect, however it is possible that the patch is interfering with the ability of the skin barrier to keep water in the skin, therefore when the skin is occluded water rapidly builds up.

As the skin was measured 0 minutes, 30 minutes and four hours after the removal of the patches it was possible to investigate how rapidly the properties of the skin return to their untreated state. It was found that the regions treated with the film backed patches remained significantly more hydrated than the initial state of the skin after four hours, whereas the regions treated with woven backed patches had begun to return to their initial state after four hours. Measurements were also performed to test the effects of patches with different percentages of propylene glycol, it appeared that the patches with 3% propylene glycol led to the largest increase in skin hydration. However, these differences between propylene glycol content were smaller than the changes between the two backing materials. To explore the effect of different excipients further a larger scale study should be conducted using more subjects to obtain significant results.

The ability to quantify the hydrating effects of patches for transdermal drug delivery and how long these effects last is important when designing patches to deliver drugs at a fixed rate as the rate of drug absorption through the skin barrier is closely linked to skin hydration. If the skin hydration increases due to the application of the patch, then the rate of drug delivery could also change and risk leaving the therapeutic window. Equally, it is important that the rate of recovery of the skin following the removal of the patches is well understood, as this can influence how soon patches can be safely reapplied to the same area and how long a patch can be left on the skin. Excess hydration of the skin due to prolonged patch application can lead to skin irritation and if a patch is reapplied to the same region, then the hydration levels will be different from untreated skin, meaning that the initial rate of drug delivery will also be affected. THz measurements of the skin can therefore give important insight into the distribution of water in the skin following the application of different types of patches. Unlike other approaches that have been used to test the skin such as TEWL measurements, THz measurements can give a direct indication of the water content of skin and can be used to observe the dynamic response of skin to occlusion. Many other approaches to testing the effects of patches are performed on animals or on excised tissue [131], these studies do not give the same insight to the response of living human skin to the application of the patches.

This study offers a proof of concept showing that THz technology has promising potential in this field and could be used to help develop more complex transdermal drug patches by increasing understanding of how patches influence the skin. To

develop this work further larger scale studies should be performed with more participants and a wider range of patch types with different excipients. Additionally, patches containing active ingredients should be tested to explore what effects these may have, particularly in cases where there is the potential for skin irritation. This study used THz point scans meaning that each measurement only observed a single location within the region of interest, as imaging speeds increase for THz systems it would be beneficial to obtain THz images of regions treated with patches to explore the spatial uniformity of the responses to the patches, for example if the change in the skin is different near the edges of the patch. Finally, further work should be done to develop a model that can be used to investigate the effect of patch application on the diffusivity of water within the skin such as that performed by Sun *et al.* [72]. However, this would require more complex models, as the skin is often assumed to be made of water and a biological background, if drugs and excipients are entering the skin then the models would need to be adapted to account for this.

5.5 Conclusion

In this study THz measurements of the skin have been used to quantify the response of skin to the application of fully and partially occlusive transdermal drug patches. It is possible to observe the increase in water content caused by both patch types and that the skin treated with a film backed patch remained at an increased hydration level four hours after the removal of the patch. It was also observed that the response of skin to occlusion by the imaging window altered depending on which patch had been applied, giving further insight into the effect of patches on the distribution of water in the skin. The results of this study suggest that THz measurements of the skin could be used when developing patches for transdermal drug delivery, to understand the effect of different patch backings on the water content of skin and therefore the rate of drug delivery.

Chapter 6

Testing the Effect of Skin Tone and Sex on the Properties of the Skin Measured with THz Spectroscopy

6.1 Introduction

In previous chapters in which the results of *in vivo* measurements of the skin are reported there was no investigation into the effect of the skin tone or sex of the subject on the THz response of untreated skin or how the skin responds to the application of the samples. If THz techniques are to be successfully applied for the diagnosis of diseases such as skin cancer, suitable ranges must be identified for the measured parameters of healthy skin. It is therefore important to be aware of any other variables that can influence the measured THz response of human skin such as the skin tone and sex of the subject. Additionally, the identification of trends in which types of moisturisers are more effective for different skin types could be useful for the development of personalised skin treatment plans, particularly for the treatment of skin diseases such as eczema or psoriasis.

In this chapter the results of a study involving THz measurements of the skin of 34 subjects before and after the application of various moisturisers are presented. The skin tone of the subjects was quantified using the Fitzpatrick scale and the subjects were also asked to report their biological sex. The results of this study found that all three types of commercial moisturisers tested in the study increased the water content of the skin on average across all the subjects. However, no significant

distinction in the measured responses was observed when the results were split according to Fitzpatrick group or sex. This suggests that if there are differences caused by factors such as skin tone and sex, they are smaller than the present sensitivity of THz skin measurements.

6.1.1 The Effect of Skin Tone and Sex on the Properties of the Skin

Despite a growing understanding of the properties of the skin there is still uncertainty about the effect of skin tone and sex. Many studies have been performed investigating how parameters such as skin hydration and barrier function are affected by skin tone and sex, with some studies observing a difference while others conclude that there is no difference. These studies use widely accepted techniques for skin characterisation, such as measurements of the TEWL and capacitance demonstrated in Chapter 4.

A study performed by Diridollou *et al.* characterised skin dryness of the volar and dorsal forearm using capacitance measurements of the skin [132]. The study measured 311 American women from four ethnic groups; African American, Chinese, Caucasian and Mexican. The study found that subjects with lighter skin had drier skin on the sun exposed dorsal forearm than the relatively sheltered volar forearm, this difference was not observed in subjects with darker skin tones. They observed no significant difference in the dryness of skin for the different ethnicities in subjects below the age of 50. However, they found the dryness of skin for the different ethnicities diverged with age, as African American and Caucasian women over 50 had drier skin than Mexican and Chinese women over 50.

Sivamani *et al.* measured the friction and electrical impedance of the volar forearms of 59 healthy volunteers and found that there was no significant difference with skin tone or sex [133]. Additionally, they observed no significant difference with skin tone in the way these properties of the skin changed following the application of moisturisers.

Gunathilake *et al.* measured the number of tape strips needed to increase the TEWL to three times its initial value and the rate of skin barrier recovery following this for subjects with different skin tones [134]. They measured 110 subjects with light skin tones and 129 subjects with dark skin tones. The study found that darker skin exhibited a stronger skin barrier and faster barrier recovery rate following tape stripping. These observations of stronger skin barrier for darker skin were replicated by similar smaller scale studies [135, 136]. However, other studies that have also investigated the skin barrier properties as a function of skin tone have found no

significant differences [137, 138].

Several studies have investigated the differences in the properties of the skin with sex, yielding mixed results with some finding that there is no significant difference with sex [104, 139]. While the study by Hadi *et al.*, found that the skin on the volar forearms of female subjects was on average more hydrated and had a higher TEWL than the male subjects [140]. It is possible that some differences could be caused by structural variations in the skin such as the presence of more hair on the arms of male subjects than female subjects, which could interfere with some of the measurements.

Peralta *et al.* performed a study investigating the effect of melanin on the THz response of skin tissue models [141]. They developed pigmented skin models for Asian, Black and Caucasian skin, which were given 16 days for the cells to differentiate. THz measurements were performed of the samples using a transmission geometry and the refractive index and absorption coefficient were extracted in the frequency range from $0.4-1.4$ THz. They observed that the refractive index and absorption coefficient of the Caucasian skin model were significantly lower than those of the Black and Asian models. The Black and Asian models exhibited similar optical properties to one another, however on Day 16 the refractive index and absorption coefficient of the Asian model were significantly higher than those of the Black model. From this the authors conclude that melanin is not the only factor which influences the THz optical properties of the skin models.

In this study THz measurements were performed of the volar forearm of 34 subjects with a range of skin tones in order to assess whether skin tone and sex have a significant effect on the THz response of the skin. The untreated skin was characterised for the different subject groups using variables such as the amplitude of the processed THz signal, the response of the skin to occlusion and the reflectivity, in order to see if there are any significant differences. Additionally, three commercially available moisturisers were tested on each of the subjects, in order to investigate whether skin tone or sex affects the way in which the skin responds to the application of different types of moisturiser.

6.2 Methods

6.2.1 THz Measurements of the Skin

The THz measurements of the skin performed in the study described in this chapter used the TeraSmart spectrometer from Menlo Systems that was introduced in Section 2.6.1. The configuration was the same as that used to measure the regions of the

skin following the application of the patches for transdermal drug delivery described in Chapter 5. For each skin measurement 120 consecutive pulses were recorded at a rate of four pulses per second, meaning that each skin measurement took 30 seconds. The skin remained in contact with the quartz imaging window throughout the duration of this measurement. Pressure sensors were positioned either side of the imaging window and connected to the THz system in order to show the subjects a real time indication of whether they needed to apply more or less pressure, the values of the pressure applied throughout each measurement were recorded to aid data processing. The pressure sensors were also used to start the measurement, as soon as contact was detected the measurements began, this ensured that the time for which the skin was occluded was the same for all measurements.

6.2.2 Moisturisers to be Tested

This study builds upon the investigations described in Chapter 4, which explored the ability of THz measurements to differentiate between the effects of different types of moisturisers on the THz response of the skin. The moisturisers chosen for this study are of similar types to those tested in Chapter 4 and it is expected that they will interact with the skin through the same mechanisms as those introduced in Section 4.2.3. However, the samples used in the study described in Chapter 4 were common components of commercial moisturisers, whereas in the study described in this chapter the samples are all commercially available moisturisers. Three types of commercially available moisturisers were tested: an oil based sample, a water based sample and a WO emulsion.

The water based sample used in this study was Clinique Moisture Surge^{TM} Hydrating Supercharged Concentrate, the primary ingredients are water and glycerin. The oil based sample was Eucerin Elasticity + Filler Facial Oil, the primary ingredient is octyldodecanol. The WO emulsion was Liz Earle Skin Repair Moisturiser^{TM} - Dry/Sensitive, where the key ingredients are water and capric triglyceride. These samples were chosen as they are expected to interact with the skin through mechanisms similar to those of the moisturiser components tested in Chapter 4.

THz measurements were carried out for each of the moisturising samples prior to their application using a transmission geometry. These measurements used the main unit of the Teraview system introduced in Section 2.6.2, and the unit was purged with Nitrogen gas for the duration of the measurement to prevent water vapour from interfering with the measurements. The samples were sandwiched between two pieces of quartz with thickness 3 mm, with a spacer of 0.1 mm thickness

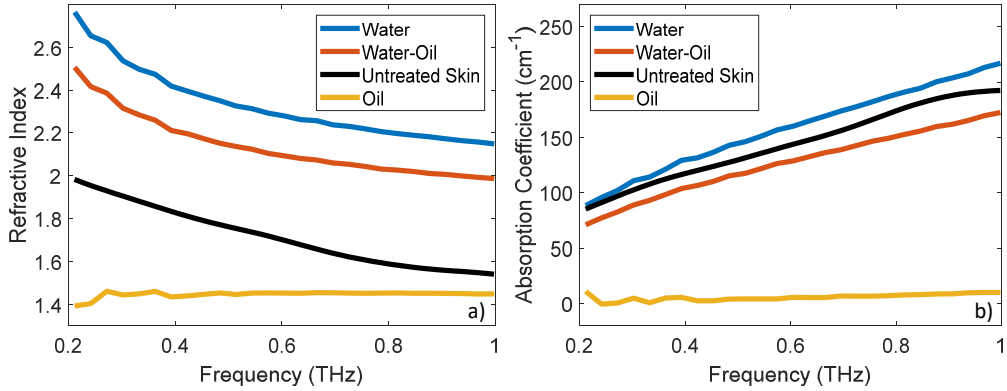

Figure 6.1: a) The refractive indices and b) the absorption coefficients of each of the moisturiser samples measured with a transmission geometry, with an example of untreated skin measured in reflection included for comparison.

used to control the width of the moisturiser sample being measured. From these measurements the refractive index and absorption coefficient of the samples were extracted using the processing techniques introduced in Section 2.3.2. The optical properties of the moisturiser samples are shown in Figure 6.1 for a frequency range from 0.2−1 THz, these results confirm that the THz properties of the samples are similar to the samples tested in Chapter 4. The properties of the water based and WO samples are similar to one another, whilst the oil based sample has a much lower refractive index and an absorption coefficient close to zero.

6.2.3 Protocol for Skin Measurements

Upon arrival in the lab the subjects were asked to complete a survey recording information such as their age and sex, they were also asked a series of questions in order to classify their skin type using the Fitzpatrick scale. The Fitzpatrick scale groups the skin types using factors such as hair colour, skin tone and how prone the subject is to sunburn. The scale has six groups where group I includes subjects with very pale skin and group VI includes subjects with very dark skin. The Fitzpatrick scale is demonstrated in Figure 6.2, which shows images of the forearms of subjects measured in this study from each of the six Fitzpatrick groups. Table 6.1 shows a summary of the demographics of the subjects recruited for this study. A total of 34 subjects participated in this study, with a range of ages from 19 to 31. All subjects were asked to give their informed consent before their participation in the study.

A summary of the protocol followed to perform the measurements of the skin described in this study is given by the table in Figure 6.3. In order to follow the

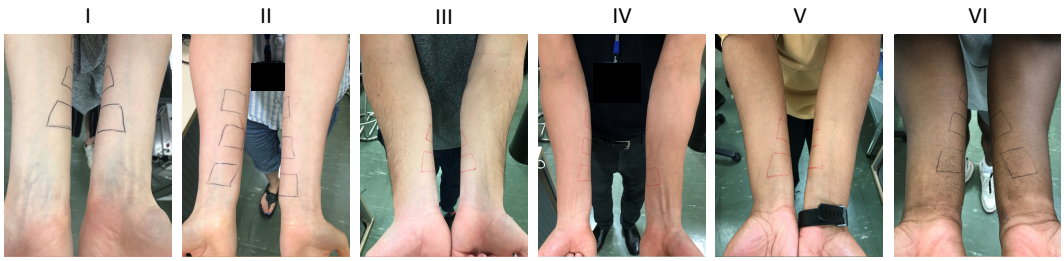

Figure 6.2: Images of the forearms of subjects showing examples for each Fitzpatrick group number.

Title	**Category**	**Number of Subjects**
Age Range	19−31	34
Sex	Male	19
	Female	15
Fitzpatrick No.	I	5
	II	1
	III	9
	IV	7
	V	5
	VI	7

Table 6.1: A summary of the demographics of the subjects measured in this study.

robust protocol for skin measurements introduced in Chapter 3 the subjects were asked to arrive in the lab 30 minutes prior to the first measurement to allow their skin to acclimatise to the controlled environmental conditions of the lab. During this time the subjects were given the opportunity to practice using the pressure sensor to apply the correct pressure with their forearm on the imaging window. For this study the target pressure range was $1.6 - 2.0$ N cm^{-2}, in order to maintain the balance of being comfortable for the subject to maintain throughout the measurement, whilst minimising the risk of air gaps between the skin and the imaging window.

During the acclimatisation time six regions were marked on the volar forearms of the subjects, with dimensions of 3×3 cm with 2 cm spacing between each region, three regions were placed on each arm, as shown in Figure 6.3 a). The three regions on the left arm remained untreated throughout the duration of the study

Time	Protocol
0 mins	Subject enters lab to acclimatise to controlled environmental conditions
	Informed consent obtained
	Mark six 3x3cm regions on the arms a)
	Pressure sensor training
30 mins	THz measurements of all six untreated regions
35 mins	Apply 0.036ml of the oil b), WO c) and water d) based samples
50 mins	Dab treated regions to remove excess sample
60 mins	THz measurements of all six regions
65 mins	Subject leaves the controlled environment

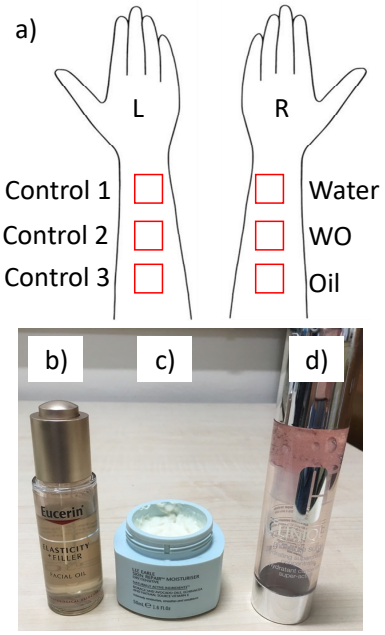

Figure 6.3: Table of the protocol used to perform the measurements of the skin. a) the locations of the control and treated regions on the volar forearms of the subjects. The b) oil, c) WO and d) water based commercial moisturisers tested in the study.

in order to act as a control for the corresponding regions on the right arm and to enable the calculation of the NRC variable introduced in Chapter 3.

THz measurements were performed of all six regions prior to the application of the samples. After the regions had been measured, 0.036 ml of each of the three samples was measured using a micropipette and applied to the corresponding regions as indicated by Figure 6.3 a). Pictures of the samples that were applied are shown in Figure 6.3 b)-d). The samples were rubbed into the marked regions whilst wearing a latex glove. The subjects were then asked to sit still to allow the skin to absorb the samples and to ensure that the samples were not removed due to contact with another surface, such as the subject's clothing. After 15 minutes the regions in which the samples were applied were lightly dabbed with a piece of dry tissue in order to remove the excess sample remaining on the surface of the skin. The subjects then waited a further ten minutes before THz measurements were repeated of all six regions.

6.2.4 Data Processing

As in the studies described in previous chapters, one of the key parameters that was used to quantify the changes in the skin observed with THz measurements is the amplitude of the processed signal introduced in Section 2.4. As in previous chapters this P2P parameter was evaluated by fitting the occlusion curve with a biexponential function. In order to account for the effects of pressure, only P2P values obtained when the applied pressure was in the desired range were considered when applying the fitting. The biexponential function obtained by the fitting process was sampled 25 seconds into occlusion. These P2P values can be used to evaluate the properties of untreated skin in addition to finding the percentage change and the NRC arising from the application of the different moisturisers.

Other approaches were also used to assess the properties of untreated skin in order to check for differences caused by skin tone or sex. The ΔP2P parameter introduced in Chapter 5 was used to test if there were differences in the response of different skin types to the occlusion caused by the imaging window throughout the measurement. This ΔP2P was calculated by sampling the biexponential fit of the P2P occlusion curve 2 seconds and 30 seconds into occlusion and calculating the difference. The 2 seconds delay in starting the sampling was to account for the fact that some of the subjects did not immediately achieve stable contact between their skin and the imaging window. The data from five subjects could not be included in this analysis as the occlusion curves measured were not stable enough due to excessive movement of the subject throughout the measurement.

Another approach that was used to evaluate the properties of the untreated skin of each subject was the calculation of the reflectivity. The reflectivity is a frequency dependent parameter and is defined in Equation 6.1, where r_{qs} and r_{qa} are the Fresnel coefficients for the quartz-skin and quartz-air interfaces respectively and M_{meas} is the measured sample to reference ratio.

$$\text{Reflectivity} = |r_{qs}|^2 = |r_{qa}M_{meas}|^2 \tag{6.1}$$

The reflectivity can be used to give an indication of the frequency dependent properties of the skin and is not dependent on an assumed structure of the skin.

Finally, the one-way ANOVA test was used to explore the statistical significance of the differences observed in the properties of untreated skin and in the changes in the P2P following the application of the moisturisers. The Tukey-Kramer test was used to confirm that the 5% threshold for significance was met.

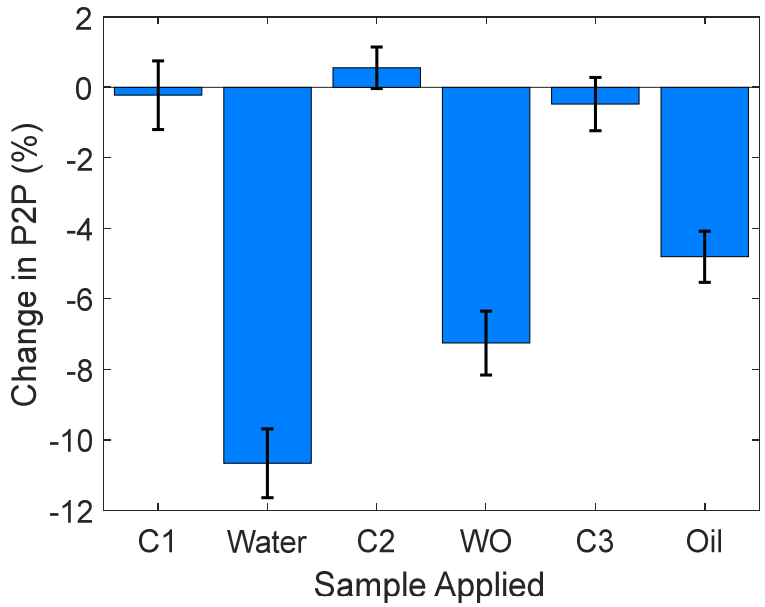

Figure 6.4: The average percentage change in the P2P for all subjects following the application of the samples and for the three control regions (C1, C2 and C3). The error bars are the standard error on the mean.

6.3 Results

6.3.1 Average Response to the Application of the Samples

The average percentage change in the P2P of the processed THz signal for all subjects sampled 25 seconds into occlusion is shown in Figure 6.4, following the application of the three types of moisturisers and for the three control regions (C1, C2 and C3). In this plot the error bars are the standard error on the mean for each measurement. The percentage change is plotted here instead of the NRC as it gives an insight into the repeatability of the measurements of the untreated regions, for which the changes are expected to be small compared to the changes induced by the samples. All three control regions show an average percentage change consistent with zero within the error bars, suggesting that this protocol gave good repeatability of THz measurements on average.

This figure shows that on average all three moisturiser samples decreased the P2P of the processed signal, suggesting that the water content of the skin increased following the application of the samples. This can be compared to the results obtained in Chapter 4 with similar samples, in which an increase in the P2P was observed for some subjects following treatment with the oil based samples. This

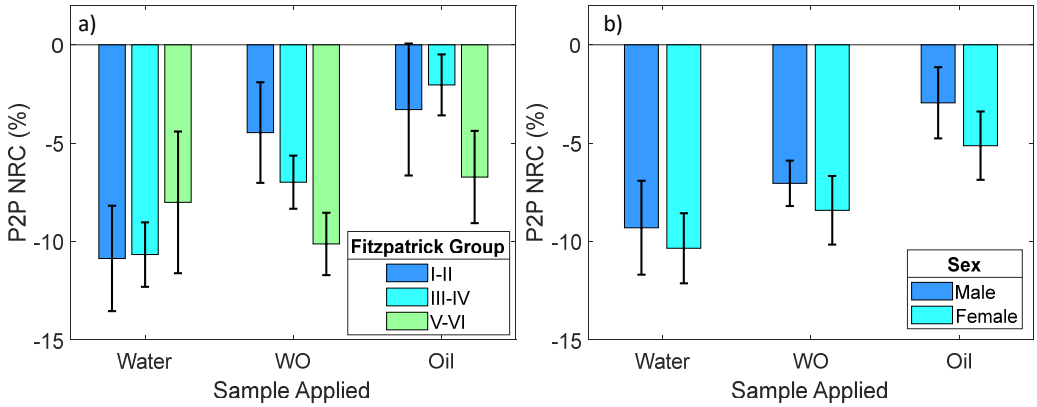

Figure 6.5: The average NRC in the P2P following the application of the three types of samples. The responses are split by a) the Fitzpatrick group and b) the sex of the subjects. The error bars are the standard error on the mean for each group.

difference can be attributed to the change in the protocol between the two studies; in the study in Chapter 4 excess sample was not removed from the surface of the skin prior to the THz measurements, whereas in this study the treated regions were lightly dabbed with a tissue to remove excess sample before being measured. This change in the results reinforces the hypothesis in Chapter 4 that the increase in the P2P observed for some subjects following treatment with the oil based samples was due to residual oil remaining on the surface of the skin. The results in Figure 6.4 suggest that all three samples increase the water content of the skin, with the water based sample causing the largest increase and the oil based sample the smallest increase.

Figure 6.5 shows the NRC in the P2P sampled 25 seconds into occlusion following the application of each of the three samples, where Figure 6.5 a) gives the results split by the Fitzpatrick group of the subject and Figure 6.5 b) gives the results split by the sex of the subject. In both figures the error bars are the standard error on the mean. These plots give an indication of whether skin tone or sex affect the way in which the skin responds to the application of different types of moisturising samples.

In Figure 6.5 a) the subjects are grouped by two Fitzpatrick group numbers, with the dark blue indicating groups I-II, the light blue groups III-IV and the green groups V-VI, this is to account for the fact that some groups had fewer subjects, such as group II for which only one subject was measured. Fitzpatrick groups I-II and III-IV show trends similar to those observed in Figure 6.4, with the largest decrease in the P2P being seen for the regions treated with the water based sample and the

smallest decrease for the oil based sample. However, subjects in Fitzpatrick groups V-VI appear to show a more uniform response to the three samples. This figure could give the first indications of a preference for oil based samples for increasing the hydration of the skin of subjects with darker skin tones, while water based samples are more effective for lighter skin tones. However, results for more subjects are needed in order for such conclusions to be made, if these differences are present they are small relative to the overall change in skin following the application of the samples.

Figure 6.5 b) shows that in the sex disaggregated data, the overall trend seen for the average of all subjects in Figure 6.4 persists. It appears that the P2P decreased more for the female subjects in response to the application of all three samples than for the male subjects, suggesting a greater hydrating effect for female subjects. However, this difference is within the error bars so cannot be confirmed from this plot. It does not appear from these results that differences in sex lead to a preference for a type of moisturiser that is more effective at increasing the hydration of the skin.

6.3.2 Properties of Untreated Skin

In addition to studying the changes induced in the skin by the application of each of the moisturisers and how this varies with the skin tone and sex of the subject, the properties of untreated skin can also be compared for each of the subject groups. In the study each of the three control regions were measured twice and the three treated regions were measured once prior to sample application, this means that for each subject nine measurements of untreated skin were performed.

Figure 6.6 shows the average P2P of the nine measurements of untreated skin obtained for each subject split by the sex and Fitzpatrick group of the subject, where the error bars are the standard error on the mean for the nine measurements. The size of the error bars on this plot give a clear indication of the repeatability of the measurements of untreated skin performed in this study, with the majority of subjects showing a strong repeatability. Two male subjects have results with large P2P values and large error bars, it is possible that this is the result of the presence of hair on the region being measured preventing consistent contact between the skin and imaging window. The results in this figure do not suggest that there is a significant difference in the P2P of untreated skin caused by the sex or Fitzpatrick group number of the subject.

The frequency dependent properties of untreated skin can also be investigated to see if these properties vary with the sex or Fitzpatrick group of the sub-

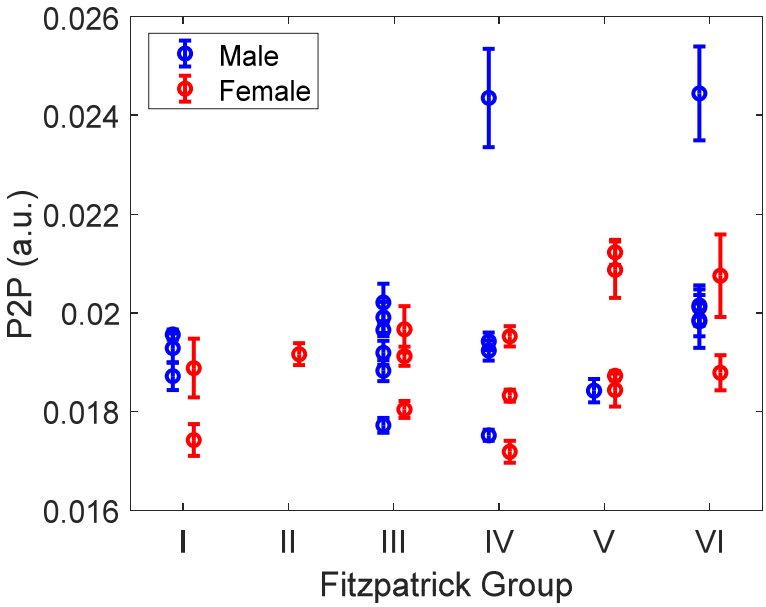

Figure 6.6: The average of the P2P of the nine measurements of untreated skin obtained for each subject, disaggregated by the skin tone and sex of the subject. The error bars are the standard error on the mean for the nine measurements of untreated skin.

ject. Figure 6.7 shows the reflectivity of untreated skin in the frequency range from 0.15−0.8 THz, where the solid and dashed lines indicate the responses from male and female subjects respectively and red, green and blue colours indicate the I-II, III-IV and V-VI Fitzpatrick groups. To obtain this plot the reflectivity curves for the nine untreated regions of skin were averaged for each subject, these responses of the individual subjects were averaged for all the subjects in each group to obtain the curves shown in the figure. The error bars are the standard error on the mean for the measurements of all the subjects included in each group, the error bars are plotted at 0.2 THz intervals for clarity. Note that the slight increase in the reflectivity at frequencies above ∼0.5 THz is likely caused by the presence of air either owing to poor contact between the skin and the imaging window or furrows in the skin.

The results in Figure 6.7 show an increase in the reflectivity of untreated skin with increasing Fitzpatrick number in both male and female subjects and the reflectivity of the skin of the female subjects appears to be lower than that of the male subjects. These changes are largest at higher frequencies in the range from 0.5−0.8 THz. It should be noted that these observations are not yet significant results due to the large size of the error bars, however with further studies involving

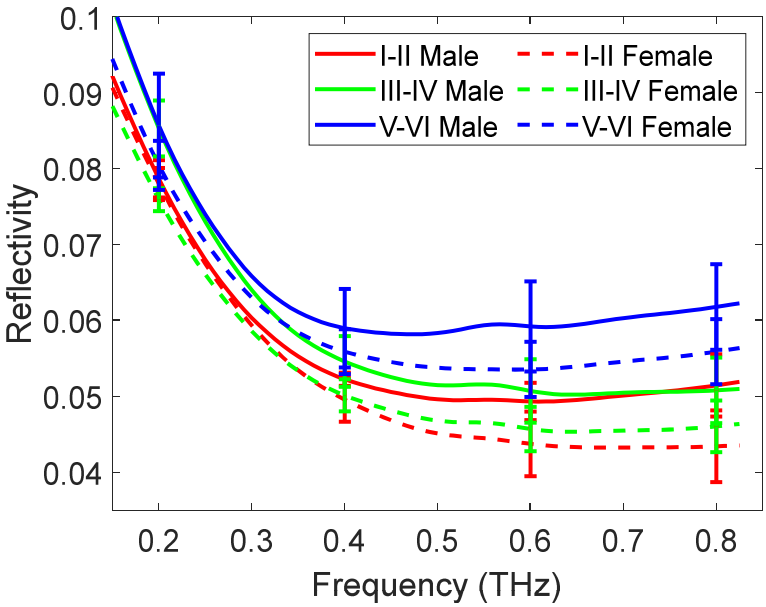

Figure 6.7: The reflectivity of untreated skin as a function of frequency, for subjects split by skin tone and sex. The plotted curves are the average of the measured responses for all the subjects in that category. The solid and dashed lines show the results for male and female subjects respectively, and the colours show the different Fitzpatrick groups of the subjects. The error bars are the standard error on the mean, these are plotted at intervals of 0.2 THz for clarity.

more subjects this trend could be clarified. This plot suggests that there may be a difference in the reflectivity of untreated skin caused by the skin tone and sex of the subject, however this change may be small enough to be concealed within the current levels of repeatability of THz measurements.

6.3.3 The Response of Skin to Occlusion

As introduced in Section 3.2.1, when the skin is in contact with the imaging window water begins to build up at the surface of the skin changing the measured THz properties of the skin. The measurements of the skin performed in this study each lasted 30 seconds, during which time 120 THz pulses were sampled. This is sufficient time for there to be changes induced in the water content of the skin, in previous chapters it has been shown that the change in the P2P with occlusion time takes the form of a biexponential curve. To further investigate the effect of skin tone and sex on the properties of the skin, the response of untreated skin to 30 seconds of occlusion by the imaging window can be studied.

Figure 6.8 a) shows the average occlusion curve obtained by plotting the

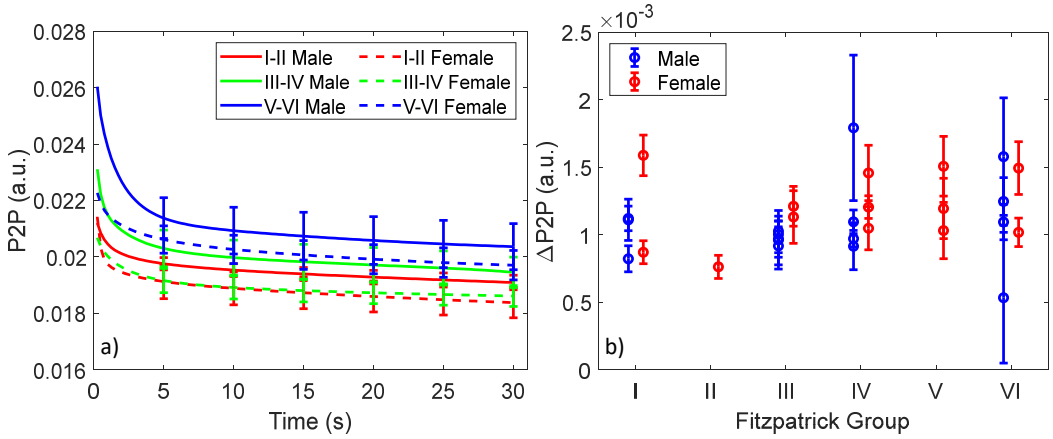

Figure 6.8: The responses of untreated skin to occlusion by the imaging window, split by skin tone and sex. a) shows the average occlusion curves in the P2P as a function of increasing occlusion time, here the solid and dashed lines show the average responses for male and female subjects respectively, while the colors show the different Fitzpatrick groups of the subjects. b) shows the average ΔP2P of untreated skin during 30 seconds of occlusion for each subject, split by skin tone and sex. In both plots the error bars are the standard error on the mean. Five subjects were excluded from these plots as the occlusion curves were not stable enough to be consistently fitted.

change in the P2P of the processed THz signal as a function of occlusion time. These occlusion curves were obtained by fitting the change in the P2P with occlusion time with a biexponential function for each of the nine measurements of untreated skin obtained for each subject. These occlusion curves were then averaged to obtain a single occlusion curve for each subject. The occlusion curves shown in the figure are the average of the occlusion curves for all subjects within each of the demographic groups, where the error bars are the standard error on the mean for all the subjects in each group. In this figure the solid and dashed lines show the average for the male and female subjects respectively, while the red, green and blue colours indicate the Fitzpatrick group number of the subjects. As seen in the previous figures there is a slight increase in the P2P for subjects with higher Fitzpatrick numbers and for males compared to females, this causes the offset in the position of the curve. However, it can be seen that the shapes of the occlusion curves are consistent between the different subject groups, suggesting that the response of the skin to occlusion is not significantly affected by changes in sex or skin tone.

In addition to plotting the whole occlusion curve as in Figure 6.8 a), it is also possible to characterise the curve using the ΔP2P parameter introduced in Chapter 5. For this investigation ΔP2P was obtained by fitting the change in the P2P with

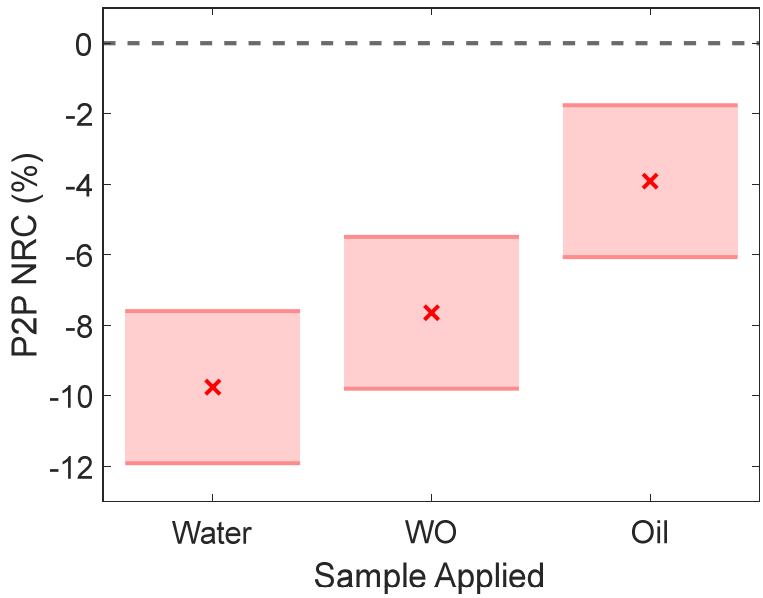

Figure 6.9: The results of performing the one-way ANOVA test on the NRC of the P2P for all the subjects following the application of the each of three samples, sampled 25 seconds into occlusion. The markers show the estimated mean of the distribution of responses to the samples and the shaded regions show the 95% confidence limits calculated with the Tukey-Kramer test.

a biexponential function and sampling this fit two seconds into occlusion and 30 seconds into occlusion and calculating the difference. The two seconds start point was chosen to account for subjects who did not immediately achieve consistent contact between their skin and the imaging window, leading to variation in the occlusion curve for the first second of the measurement. The ΔP2P values for each measurement of untreated skin were averaged for each subject to obtain the results shown in Figure 6.8 b), where the error bars are the standard error on the mean of the ΔP2P value for each subject. Five subjects were not included in this investigation as there was too much movement throughout the measurement meaning that no occlusion curve could be identified. The results in Figure 6.8 b) confirm what was observed in Figure 6.8 a), that there is no significant change in the response of the skin to occlusion caused by the skin tone or sex of the subject.

6.3.4 Results of Statistical Analysis

As with the studies described in previous chapters a statistical analysis was then performed on the results using the one-way ANOVA test with the Tukey-Kramer

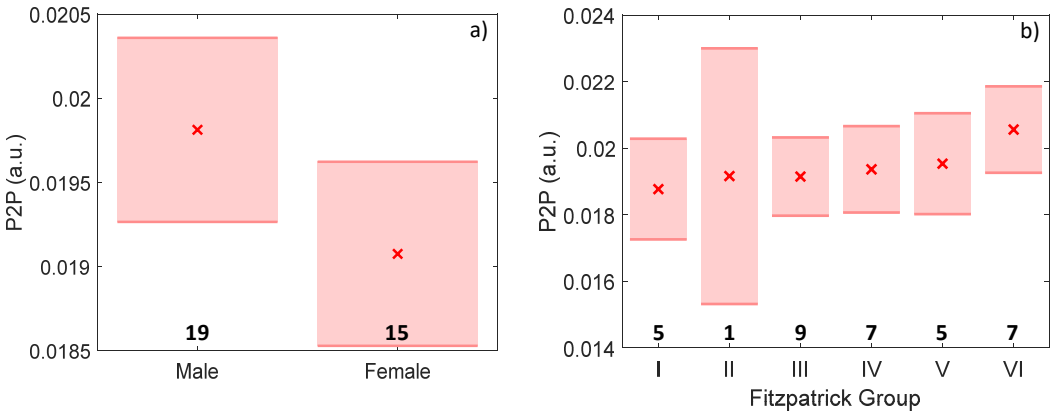

Figure 6.10: The results of performing the one-way ANOVA test on the P2P of untreated skin to check for significant differences in the properties of untreated skin caused by a) the sex or b) the skin tone of the subject. The markers show the estimated mean of the distribution of responses to the samples and the shaded regions show the 95% confidence limits calculated with the Tukey-Kramer test. The numbers in black indicate the number of subjects in each group.

test to see if there are significant changes between any of the measurements. First, statistical tests were performed on the NRC of the P2P for all subjects following the application of the samples to see if the samples induced significant changes in the skin and if the changes in the properties of the skin are significantly different for each of the samples. The results of this are shown in Figure 6.9, where the markers indicate the estimated mean of the distribution of responses and the shaded regions are obtained from the Tukey-Kramer test and indicate the 95% confidence limits, a dashed line is marked for zero change as a guide to the eye. This figure shows that all three samples lead to a significant reduction in the P2P. There is also a significant difference between the response of the skin to the application of the water and oil based samples, with the water based sample leading to a significantly greater decrease in the P2P than the oil based sample. The WO sample leads to a significant decrease in the P2P, however it is not significantly different from the responses of the other two samples. It is perhaps to be expected that the change in the skin arising from the application of the WO sample is somewhere between those from the water and oil based samples as it has a composition similar to a mix of the two samples.

In addition to testing if the changes induced in the skin by the application of the samples are significant, similar tests are also performed to see if changes in sex and skin tone lead to significantly different properties of untreated skin. Figure 6.10 shows the results of the one-way ANOVA test for changes in the P2P of untreated

skin caused by a) the sex and b) the Fitzpatrick group number of the subjects. The numbers in black at the bottom of the plot show the number of subjects in each group. As before the markers show the location of the estimated mean of the P2P of untreated skin for each group and the shaded regions show the confidence limits obtained from the Tukey-Kramer test. Figure 6.10 a) shows that while the P2P of untreated skin of male subjects appears to be slightly higher than that of female subjects, this change is not significant. Figure 6.10 b) shows a slight increase in the P2P with increasing Fitzpatrick group number, but again this difference is not significant between any of the groups. The confidence limits for group II are large because there is only one subject in this group. This analysis suggests that whilst there may be a slight trend caused by sex and skin tone this change is too small to be significant with the sample size measured in this study.

6.4 Discussion

This study showed that the three commercial moisturiser samples tested all decreased the measured P2P, suggesting that the water content of the skin had increased. This adds to the findings described in Chapter 4 in which similar samples were tested but an increase in the P2P was observed for some subjects after the application of the oil based samples. These observations were attributed to the presence of oil on the surface of the skin that was not absorbed in the time between sample application and skin measurement. In the study described in this chapter the protocol was modified in order to investigate this, so the skin was gently wiped with a tissue to remove excess sample from the surface of the skin. The fact that all three sample types decreased the measured P2P in this study confirms that it is likely that the increase in the P2P observed for some subjects in Chapter 4 was due to the presence of the samples remaining on the surface of the skin. However, the results presented in this study are not able to reveal whether the smaller change observed in the P2P following the application of the oil based sample compared to the water based sample is due to the oil causing a smaller change in the water content of the skin or whether some of the oil remains in the surface layers of the skin contributing to the observed THz response of the skin. In order to investigate this further more complex modelling approaches are required that are able to calculate how deep each of the samples penetrate into the skin and to distinguish the changes in the water content of the skin caused by the application of the sample from the effects of the samples remaining in the skin. Additionally, measurements of the skin could be performed on a longer time scale many hours after the application of the

sample or following regular usage of the sample by subjects over several weeks.

The measurements of untreated skin performed in this study did not reveal significant changes arising from differences in skin tone or sex. However, there were indications that the P2P is higher for subjects with higher Fitzpatrick group numbers and for male subjects compared to female subjects. This trend was also observed in the reflectivity of untreated skin, particularly at higher frequencies. At present the differences in the skin arising from skin tone and sex are smaller than the sensitivity of the THz measurements that were performed for a study involving 34 subjects. Therefore, it is not an immediate concern for THz classification of the skin, however as the sensitivity of the measurement techniques improve it may become a factor that needs to be considered in the future. If THz measurements are ever to be used clinically for skin cancer assessment it is vital that the ranges of parameters for healthy and cancerous skin are well understood for all skin types.

Investigations into the effect of skin tone and sex on the way that the skin responds to 30 seconds of occlusion by the imaging window, suggested that there was no difference in the shape of the occlusion curves observed for the different subject groups. This means that characterising the occlusion curve with THz measurements of the skin could give a set of patient invariant parameters for healthy skin. Future studies should investigate whether the presence of cancer on the skin affects the way in which skin responds to occlusion. If so occlusion parameters could be a vital part of developing THz techniques for skin cancer assessment.

Within the six Fitzpatrick groups used to classify the skin in this study there remains variation in the skin tone, therefore a classification technique should be used that can fully evaluate the gradient of skin tones of the subjects, for example the measurement of the luminosity of the skin as suggested by Peralta *et al.* [141]. In order for the full gradient of skin tones to be studied a much larger scale study should be performed to ensure that there is sufficient population of each group. This study shows that if there are changes in the THz properties of the skin arising from skin tone and sex, these changes are small, therefore many measurements will be required in order for significant results to be obtained. Also, the subjects involved in this study were from a narrow age range of $19-31$, so for a more complete understanding these changes must also be investigated over the full range of ages. Further investigation should also be carried out into whether other approaches to skin classification can be used to confirm whether there are changes in the THz response of the skin caused by skin tone and sex, for example the extraction of the Double Debye parameters.

6.5 Conclusion

This study used *in vivo* THz measurements of the skin to investigate the effects of water, WO and oil based moisturiser samples on the skin, and it was found that all three samples significantly decreased the P2P of the skin. No significant differences were observed in the response of the skin to the different types of samples arising from differences in the skin tone or sex of the subject. No significant differences were observed in the THz properties of untreated skin for different skin tones or for male and female subjects. However, a small increase in the P2P was observed with increasing Fitzpatrick number and for male subjects compared to female subjects, therefore larger scale studies are required to confirm whether these differences are significant. No changes were observed with skin tone or sex in the response of the skin to 30 seconds of occlusion, so the classification of the occlusion response could be a patient invariant parameter, useful for identifying healthy or diseased skin in future studies.

Chapter 7

Further Work and Summary

In this thesis THz spectroscopy and imaging techniques are applied to a selection of biomedical applications, utilizing the sensitivity of THz light to the water content of human skin. Primarily, this work focuses on establishing a robust technique for performing *in vivo* measurements of the skin using THz light and applying this technique to explore the ability of THz measurements to identify changes in the skin caused by the application of various samples such as moisturisers. This chapter gives a summary of the key findings of this thesis and presents suggestions for areas of future work in this field.

7.1 Summary of Thesis

In Chapter 1 the current state of the field of biomedical applications of THz technology was summarised. This section introduced THz-TDS as a technique for imaging and spectroscopy and explained some of the wide range of applications that have been investigated. Additionally, there was a detailed review of the *in vivo* and *ex vivo* studies using THz light that have been carried out to date. In Chapter 2 the theoretical ideas used throughout the thesis were described including the behaviour of light at interfaces, dielectric models for the skin and approaches for data processing. The experimental setups used to perform the measurements described in this thesis were also introduced.

Chapter 3 presented a robust protocol for performing *in vivo* THz measurements of the skin by controlling the effects of pressure and occlusion. It was demonstrated that by using this protocol and by applying a processing technique to account for the effect of natural variation of the skin, repeatable measurements of the THz response of the skin following the application of a moisturiser could be

performed. The study in Chapter 3 involved a single subject, therefore in Chapter 4 this protocol was applied to a larger scale study involving 20 participants in which three common moisturiser components were applied to skin and the hydration of the skin was tested using THz, TEWL and corneometer measurements. The results of this extended study showed that THz measurements of the skin could be used to observe differences in the changes in the skin following the application of the different types of samples.

Chapter 5 described the results of a study exploring the effects of different types of patches for transdermal drug delivery on the THz response of the skin. It was found that both partially and fully occlusive patches increased the water content of the skin for at least four hours after the removal of the patches. It was also observed that the way in which skin responds to occlusion by the imaging window during the THz measurement changed following the application of the patches. These results suggested that the application of the fully occlusive patch led to the surface layers of the skin becoming fully saturated with water. Finally, in Chapter 6 the effect of the skin tone and sex of the subject on the measured THz response of the skin was investigated by performing measurements on 34 participants with a range of Fitzpatrick skin types. This study did not find any significant differences in the THz response of the untreated skin of subjects with different skin types or in the way in which the skin of these subjects responded to the application of different types of moisturisers.

7.2 Future Work

7.2.1 Increasing Imaging Speeds

In order for THz measurements to be used in a clinical setting for the diagnosis of diseases such as skin cancer it is important that an image can be acquired rather than a point scan of a single location on the surface of the skin. For this to be achievable with living human subjects, the imaging speed capabilities need to be significantly improved. Present techniques require the raster scanning of the THz emitter and detector to measure each location in the region to be imaged. This process can take a long time, meaning that it is difficult for subjects to remain still for the duration of the measurement and that there are large variations in the water content of the skin across the images caused by the occlusive effect of the imaging window. In order to reduce the time required to take a THz image of a region, techniques that remove the need for raster scanning must be developed.

One promising technique capable of reducing imaging speeds is single pixel

imaging. This approach involves encoding a spatial pattern in the THz beam that can be measured using a single detector. This technique is capable of rapidly acquiring images whilst retaining the phase and amplitude information that makes THz-TDS techniques desirable for *in vivo* imaging. Statchev *et al.* demonstrated the success of such an approach by using it to acquire a 32×32 pixel image at a rate of six images per second [142]. Such a technique would enable the imaging of the entire region of interest at the same time into the occlusion process, removing the need to subtract the changes due to occlusion from the image with post processing techniques. However, further work is required in order to incorporate such a technique into a reflection geometry that is suitable for *in vivo* measurements.

7.2.2 Non-Contact Imaging Techniques

Another way to remove the effects of variables such as occlusion and pressure during THz measurements of the skin is to develop a technique that does not require an imaging window. Presently, an imaging window is used to flatten the surface of the skin and to enable calibration and alignment during the measurement. For example, the baseline reflection from the underside of the imaging window is used throughout this thesis to account for fluctuations in the incident THz pulse. However, developing a non-contact imaging system would not only remove the effects of variables such as pressure and occlusion it would also facilitate the measurement of a wider range of regions on the body, especially if the size of the imaging setup can be reduced so that the system can be hand-held or mounted on a robot.

Non-contact THz measurements have been performed when measuring static samples, for example to test the thickness of paint layers on a car [143]. When measuring a region on a living subject, which will move throughout the measurement, such an approach is more challenging. During THz measurements it is essential that the sample is in the correct position so that the THz beam is focused on the sample surface, as movement of the order of micrometers can result in significant changes in the measured THz amplitude. Additionally, when the sample is curved, as with much of the human body, a small shift can prevent the majority of the reflected THz pulse being received by the THz detector. Sung *et al.* successfully used a non-contact system to obtain THz images of the human cornea through *in vivo* measurements [58]. The technique used in this study utilised the relatively uniform spherical shape of the human eye to aid alignment. Applying such an approach to imaging other regions of the body that are harder to model and have greater variation between subjects will be challenging. In order to address such challenges approaches to track the movement of the subject and rapidly move the THz system

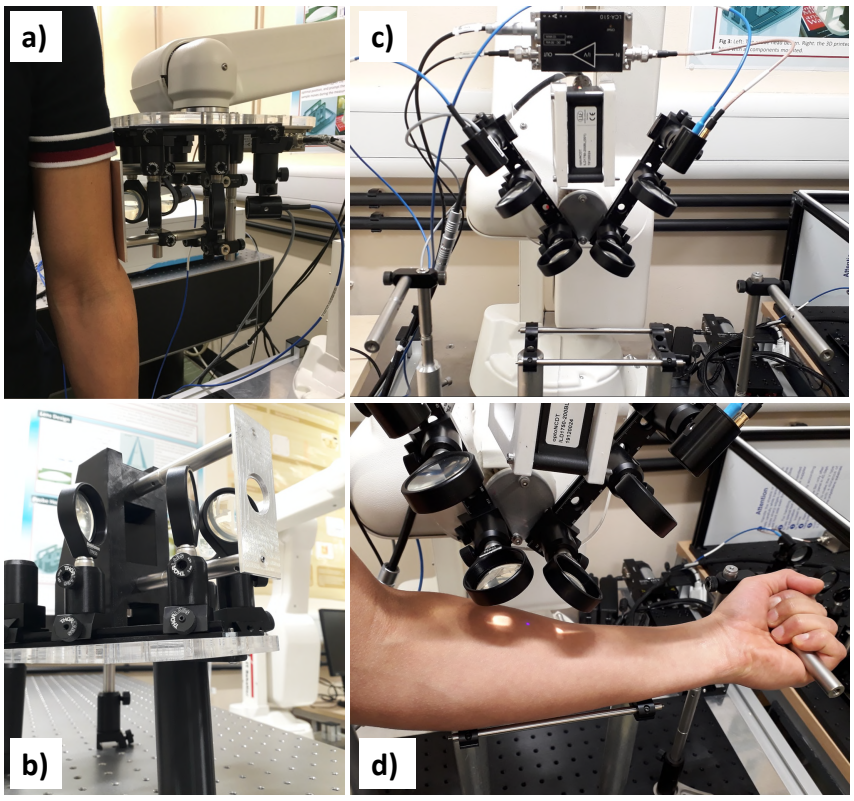

Figure 7.1: Examples of the new geometries being developed by the MacPherson research group to facilitate the *in vivo* measurement of a wider range of regions on human subjects. a) Robot mounted contact geometry, b) handheld contact geometry, c) and d) both show a robot mounted non-contact imaging system.

in response must be developed, alternatively a way to prevent all movement of the subject could be used.

Recent work by the MacPherson research group has involved the development of new systems that have greater versatility and can be used to measure a wider range of regions on the human body, rather than being limited to the volar forearm. Examples of some of these new systems are shown in Figure 7.1, with a) and b) showing robot mounted and handheld contact systems respectively, which can be used to perform measurements similar to those described in this thesis in a wider range of locations. This is an important development in order to test the contrast caused by cancer at THz frequencies, as skin cancer is often found in locations such as the head and neck. Meanwhile, Figure 7.1 c) and d) show a robot mounted non-contact imaging setup that uses a proximity sensor to align the optics relative to the location of the region being measured. However, at present more work is needed to improve the response of the robot to the constant movement of a living subject,

in order to maintain alignment throughout the measurement.

7.2.3 Skin Modelling Approaches

Finally, another area for further work is the development of the models for the dielectric properties of the skin introduced in this thesis. Presently, there is tension between the desire for simple, robust models and more sophisticated models that can bring greater insight into the changes in the structure and properties of the skin but that have a greater number of fitting parameters and can be harder to implement. Chen *et al.* used an ellipsometry system in order to obtain four complementary sets of spectral ratios, making it possible to use a more complex model for the skin to extract extra information about the structural properties of the skin on a cellular level [85]. However, at present such experimental setups are complicated to produce and use and the processing techniques can be time consuming, these must be simplified before they can be considered as a potential technique for clinical skin assessment.

The development of further models that can be used to identify changes in the structure and water profile in the skin following treatment with a range of different samples would offer greater insight into how such samples are absorbed by the skin. For example, a model that could track the movement of drugs from a transdermal drug patch through the layers of the skin would be beneficial for developing patches with known rates of drug delivery.

Of course, one of the primary goals of research such as this is that THz imaging techniques could be used to aid the diagnosis of the diseases such as skin cancer. This thesis has identified that there is great potential in the ability of THz spectroscopy and imaging techniques to observe changes in the properties of human skin through *in vivo* measurements. It is hoped that through the combination of these elements of further research and other approaches that have not yet been identified, THz imaging could be used in a clinical setting to impact the way in which skin diseases are diagnosed and treated.

Bibliography

[1] D. H. Auston. Picosecond optoelectronic switching and gating in silicon. *Applied Physics Letters*, 26(3):101–103, 1975.

[2] D. H. Auston and K. P. Cheung. Coherent time-domain far-infrared spectroscopy. *Journal of the Optical Society of America B*, 2(4):606, 4 1985.

[3] Martin van Exter, Ch. Fattinger, and D. Grischkowsky. Terahertz time-domain spectroscopy of water vapor. *Optics Letters*, 14(20):1128, 1989.

[4] Jens Neu and Charles A Schmuttenmaer. Tutorial: An introduction to terahertz time domain spectroscopy (THz-TDS). *Journal of Applied Physics*, 124(231101):1–14, 2018.

[5] Yun-Shik Lee. *Principles of Terahertz Science and Technology*. Springer, 2009.

[6] Joshua Freeman, Harvey Beere, and David Ritchie. Generation and Detection of Terahertz Radiation. In Peiponen Kai-Erik, J. Axel Zeitler, and Makoto Kuwata-Gonokami, editors, *Terahertz Spectroscopy and Imaging*, pages 1–14. Springer, 1 edition, 2013.

[7] S. S. Dhillon, M. S. Vitiello, E. H. Linfield, A. G. Davies, Matthias C. Hoffmann, John Booske, Claudio Paoloni, M. Gensch, P. Weightman, G. P. Williams, E. Castro-Camus, D. R.S. Cumming, F. Simoens, I. Escorcia-Carranza, J. Grant, Stepan Lucyszyn, Makoto Kuwata-Gonokami, Kuniaki Konishi, Martin Koch, Charles A. Schmuttenmaer, Tyler L. Cocker, Rupert Huber, A. G. Markelz, Z. D. Taylor, Vincent P. Wallace, J. Axel Zeitler, Juraj Sibik, Timothy M. Korter, B. Ellison, S. Rea, P. Goldsmith, Ken B. Cooper, Roger Appleby, D. Pardo, P. G. Huggard, V. Krozer, Haymen Shams, Martyn Fice, Cyril Renaud, Alwyn Seeds, Andreas Stohr, Mira Naftaly, Nick Ridler, Roland Clarke, John E. Cunningham, and Michael B. Johnston. The 2017 terahertz science and technology roadmap. *Journal of Physics D: Applied Physics*, 50(4), 2017.

[8] Qiushuo Sun, Yuezhi He, Kai Liu, Shuting Fan, Edward P. J. Parrott, and Emma Pickwell-MacPherson. Recent advances in terahertz technology for biomedical applications. *Quantitative Imaging in Medicine and Surgery*, 7(3):345–355, 2017.

[9] Hai Bo Liu, Yunqing Chen, and X. C. Zhang. Characterization of anhydrous and hydrated pharmaceutical materials with THz time-domain spectroscopy. *Journal of Pharmaceutical Sciences*, 96(4):927–934, 2007.

[10] Vincent P. Wallace, Philip F. Taday, Anthony J. Fitzgerald, Ruth M. Woodward, Julian Cluff, Richard J. Pye, and Donald D. Arnone. Terahertz pulsed imaging and spectroscopy for biomedical and pharmaceutical applications. *Faraday Discussions*, 126(1):255–263, 2004.

[11] Robert K. May, Michael J. Evans, Shuncong Zhong, Ian Warr, Lynn F. Gladden, Yaochun Shen, and J. Axel Zeitler. Terahertz in-line sensor for direct coating thickness measurement of individual tablets during film coating in real-time. *Journal of Pharmaceutical Sciences*, 100(4):1535–1544, 2011.

[12] J. Axel Zeitler, Yaochun Shen, Colin Baker, Philip F. Taday, Michael Pepper, and Thomas Rades. Analysis of coating structures and interfaces in solid oral dosage forms by three dimensional terahertz pulsed imaging. *Journal of Pharmaceutical Sciences*, 96(2):330–340, 2007.

[13] Ke Su, Yao Chun Shen, and J. Axel Zeitler. Terahertz sensor for non-contact thickness and quality measurement of automobile paints of varying complexity. *IEEE Transactions on Terahertz Science and Technology*, 4(4):432–439, 2014.

[14] I. Amenabar, F. Lopez, and A. Mendikute. In introductory review to THz non-destructive testing of composite mater. *Journal of Infrared, Millimeter, and Terahertz Waves*, 34(2):152–169, 2013.

[15] Irl Duling and David Zimdars. Terahertz imaging: Revealing hidden defects. *Nature Photonics*, 3(11):630–632, 2009.

[16] Christopher Stoik, Matthew Bohn, and James Blackshire. Nondestructive evaluation of aircraft composites using reflective terahertz time domain spectroscopy. *Optics Express*, 16(21):17039–17051, 2008.

[17] Wendao Xu, Lijuan Xie, and Yibin Ying. Mechanisms and applications of terahertz metamaterial sensing: A review. *Nanoscale*, 9:13864–13878, 2017.

[18] A. M. Gomez-Sepulveda, A. I. Hernandez-Serrano, R. Radpour, C. L. Koch-Dandolo, S. C. Rojas-Landeros, L. F. Ascencio-Rojas, Alvaro Zarate, Gerardo Hernandez, R. C. Gonzalez-Tirado, M. Insaurralde-Caballero, and E. Castro-Camus. History of Mexican Easel Paintings from an Altarpiece Revealed by Non-invasive Terahertz Time-Domain Imaging. *Journal of Infrared, Millimeter, and Terahertz Waves*, 38(4):403–412, 2017.

[19] Corinna L. Koch-Dandolo, Troels Filtenborg, Kaori Fukunaga, Jacob Skou-Hansen, and Peter Uhd Jepsen. Reflection terahertz time-domain imaging for analysis of an 18th century neoclassical easel painting. *Applied Optics*, 54(16):5123, 2015.

[20] Junliang Dong, J. Bianca Jackson, Marcello Melis, David Giovanacci, Gillian C. Walker, Alexandre Locquet, John W. Bowen, and D. S. Citrin. Terahertz frequency-wavelet domain deconvolution for stratigraphic and subsurface investigation of art painting. *Optics Express*, 24(23):26972, 2016.

[21] Kaori Fukunaga, Yuichi Ogawa, Shin'ichiro Hayashi, and Iwao Hosako. Terahertz spectroscopy for art conservation. *IEICE Electronics Express*, 4(8):258–263, 2007.

[22] David Zimdars and Jeffrey S. White. Terahertz reflection imaging for package and personnel inspection. *Terahertz for Military and Security Applications II*, 5411(September 2004):78, 2004.

[23] William R. Tribe, David A. Newnham, Philip F. Taday, and Michael C. Kemp. Hidden object detection: security applications of terahertz technology. *Terahertz and Gigahertz Electronics and Photonics III*, 5354:168, 2004.

[24] Ingmar Kallfass, Jochen Antes, Thomas Schneider, Fabian Kurz, Daniel Lopez-Diaz, Sebastian Diebold, Hermann Massler, Arnulf Leuther, and Axel Tessmann. All active MMIC-based wireless communication at 220 GHz. *IEEE Transactions on Terahertz Science and Technology*, 1(2):477–487, 2011.

[25] Guillaume Ducournau, Pascal Szriftgiser, Fabio Pavanello, Emilien Peytavit, Mohammed Zaknoune, Denis Bacquet, Alexandre Beck, Tahsin Akalin, Jean François Lampin, and Jean François Lampin. THz Communications using Photonics and Electronic Devices: the Race to Data-Rate. *Journal of Infrared, Millimeter, and Terahertz Waves*, 36(2):198–220, 2015.

[26] James M. Schleicher, Shayne M. Harrel, and Charles A. Schmuttenmaer. Effect of spin-polarized electrons on terahertz emission from photoexcited GaAs. *Journal of Applied Physics*, 105(11), 2009.

[27] Masatsugu Yamashita, Chiko Otani, Toru Matsumoto, Yoshihiro Midoh, Katsuyoshi Miura, Koji Nakamae, Kiyoshi Nikawa, Sunmi Kim, Hironaru Murakami, and Masayoshi Tonouchi. THz emission characteristics from p/n junctions with metal lines under non-bias conditions for LSI failure analysis. *Optics Express*, 19(11):10864, 2011.

[28] R. Huber, F. Tauser, A. Brodschelm, M. Bichler, G. Abstreiter, and A. Leitenstorfer. How many-particle interactions develop after ultrafast excitation of an electron-hole plasma. *Nature*, 414(6861):286–289, 2001.

[29] Cameron M. Hough, David N. Purschke, Chenxi Huang, Lyubov V. Titova, Olga Kovalchuk, Brad J. Warkentin, and Frank A. Hegmann. Biological effects of intense THz pulses on human skin tissue models. In *2017 42nd International Conference on Infrared, Millimeter, and Terahertz Waves (IRMMW-THz)*, pages 1–3. IEEE, 8 2017.

[30] Olga P. Cherkasova, Danil S. Serdyukov, Eugenia F. Nemova, Alexander S. Ratushnyak, Anna S. Kucheryavenko, Irina N. Dolganova, Guofu Xu, Maksim Skorobogatiy, Igor V. Reshetov, Peter S. Timashev, Igor E. Spektor, Kirill I. Zaytsev, and Valery V. Tuchin. Cellular effects of terahertz waves. *Journal of Biomedical Optics*, 26(09), 9 2021.

[31] Yuan Gao, Mohammad Tayeb Ghasr, Michael Nacy, and Reza Zoughi. Towards Accurate and Wideband In Vivo Measurement of Skin Dielectric Properties. *IEEE Transactions on Instrumentation and Measurement*, 68(2):512–524, 2 2019.

[32] Arezoo Modiri, Sally Goudreau, Asal Rahimi, and Kamran Kiasaleh. Review of breast screening: Toward clinical realization of microwave imaging. *Medical Physics*, 44(12):e446–e458, 12 2017.

[33] Jiarui Wang, Hannah Lindley-Hatcher, Kai Liu, and Emma Pickwell-MacPherson. Evaluation of transdermal drug delivery using terahertz pulsed imaging. *Biomedical Optics Express*, 11(8):4484–4490, 2020.

[34] Daniela I Ramos-Soto, Abhishek K Singh, Edgar Saucedo-Casas, Enrique Castro-Camus, and Mariana Alfaro-Gomez. Visualization of moisturizer ef-

fects in stratum corneum in vitro using THz spectroscopic imaging. *Applied Optics*, 58(24):6581–6585, 2019.

[35] Z. D. Taylor, R. S. Singh, M. O. Culjat, J. Y. Suen, W. S. Grundfest, H. Lee, and E. R. Brown. Reflective terahertz imaging of porcine skin burns. *Optics Letters*, 33(11):1258, 2008.

[36] Ruth M. Woodward, Vincent P. Wallace, Richard J. Pye, Bryan E. Cole, Donald D. Arnone, Edmund H. Linfield, and Michael Pepper. Terahertz pulse imaging of ex vivo basal cell carcinoma. *Journal of Investigative Dermatology*, 120(1):72–78, 2003.

[37] Faustino Wahaia, Irmantas Kasalynas, Rimvydas Venckevicius, Dalius Seliuta, Gintaras Valusis, Andrzej Urbanowicz, Gediminas Molis, Fatima Carneiro, Catia D Carvalho Silva, and Pedro L Granja. Terahertz absorption and reflection imaging of carcinoma-affected colon tissues embedded in paraffin. *Journal of Molecular Structure*, 1107:214–219, 2016.

[38] Anthony J. Fitzgerald, Vincent P. Wallace, Mercedes Jimenez-Linan, Lynda Bobrow, Richard J. Pye, Anand D. Purushotham, and Donald D. Arnone. Terahertz Pulsed Imaging of Human Breast Tumors. *Radiology*, 239(2):533–540, 2006.

[39] Tyler C. Bowman, Magda El-Shenawee, and Lucas K. Campbell. Terahertz Imaging of Excised Breast Tumor Tissue on Paraffin Sections. *IEEE Transactions on Antennas and Propagation*, 63(5):2088–2097, 2015.

[40] Tyler Bowman, Magda El-Shenawee, and Lucas K. Campbell. Terahertz transmission vs reflection imaging and model-based characterization for excised breast carcinomas. *Biomedical Optics Express*, 7(9):3756, 2016.

[41] Yookyeong Carolyn Sim, Kang Min Ahn, Jae Yeon Park, Chan Sik Park, and Joo Hiuk Son. Temperature-dependent terahertz imaging of excised oral malignant melanoma. *IEEE Transactions on Terahertz Science and Technology*, 3(4):368–373, 2013.

[42] Yookyeong Carolyn Sim, Jae Yeon Park, Kang-Min Ahn, Chansik Park, and Joo-Hiuk Son. Terahertz imaging of excised oral cancer at frozen temperature. *Biomedical Optics Express*, 4(8), 2013.

[43] Qiushuo Sun, Kai Liu, Xuequan Chen, Xudong Liu, A. I. Hernandez-Serrano, and Emma Pickwell-MacPherson. Utilizing multilayer structures to enhance

terahertz characterization of thin films ranging from aqueous solutions to histology slides. *Optics Letters*, 44(9):2149, 2019.

[44] Stanley Sy, Shengyang Huang, Yi Xiang J. Wang, Jun Yu, Anil T. Ahuja, Yuan Ting Zhang, and Emma Pickwell-MacPherson. Terahertz spectroscopy of liver cirrhosis: Investigating the origin of contrast. *Physics in Medicine and Biology*, 55(24):7587–7596, 2010.

[45] Shuting Fan, Benjamin Ung, Edward P.J. Parrott, and Emma Pickwell-Macpherson. Gelatin embedding: A novel way to preserve biological samples for terahertz imaging and spectroscopy. *Physics in Medicine and Biology*, 60(7):2703–2713, 2015.

[46] Priyamvada Tewari, James Garritano, Neha Bajwa, Shijun Sung, Haochong Huang, Dayong Wang, Warren Grundfest, Daniel B Ennis, Dan Ruan, Elliott Brown, Erik Dutson, Michael C Fishbein, and Zachary Taylor. Methods for registering and calibrating in vivo terahertz images of cutaneous burn wounds. *Biomedical Optics Express*, 10(1):322–337, 2019.

[47] Neha Bajwa, Shijun Sung, Daniel B. Ennis, Michael C. Fishbein, Bryan N. Nowroozi, Dan Ruan, Ashkan MacCabi, Jeffry Alger, Maie A.St John, Warren S. Grundfest, and Zachary D. Taylor. Terahertz Imaging of Cutaneous Edema: Correlation with Magnetic Resonance Imaging in Burn Wounds. *IEEE Transactions on Biomedical Engineering*, 64(11):2682–2694, 2017.

[48] M. Hassan Arbab, Dale P. Winebrenner, Trevor C. Dickey, Antao Chen, Matthew B. Klein, and Pierre D. Mourad. Terahertz spectroscopy for the assessment of burn injuries in vivo . *Journal of Biomedical Optics*, 18(7):077004, 2013.

[49] Omar B. Osman, Timothy Jack Tan, Sam Henry, Adelaide Warsen, Navid Farr, Abbi M. McClintic, Yak-Nam Wang, Saman Arbabi, and M. Hassan Arbab. Differentiation of burn wounds in an in vivo porcine model using terahertz spectroscopy. *Biomedical Optics Express*, 11(11):6528, 2020.

[50] Shuting Fan, Benjamin S Y Ung, Edward P J Parrott, Vincent P Wallace, and Emma Pickwell-Macpherson. In vivo terahertz reflection imaging of human scars during and after the healing process. *J. Biophotonics*, 10:1143–1151, 2017.

[51] Jiarui Wang, Qiushuo Sun, Rayko I Stantchev, Tor-Wo Chiu, Anil T Ahuja, and Emma Pickwell-Macpherson. In vivo terahertz imaging to evaluate

scar treatment strategies: silicone gel sheeting. *Biomedical Optics Express*, 10(7):3584–3590, 2019.

[52] Neha Bajwa, Joshua Au, Reza Jarrahy, Shijun Sung, Michael C. Fishbein, David Riopelle, Daniel B. Ennis, Tara Aghaloo, Maie A. St. John, Warren S. Grundfest, and Zachary D. Taylor. Non-invasive terahertz imaging of tissue water content for flap viability assessment. *Biomedical Optics Express*, 8(1):460, 2017.

[53] G. G. Hernandez-Cardoso, S. C. Rojas-Landeros, M. Alfaro-Gomez, A. I. Hernandez-Serrano, I. Salas-Gutierrez, E. Lemus-Bedolla, A. R. Castillo-Guzman, H. L. Lopez-Lemus, and E. Castro-Camus. Terahertz imaging for early screening of diabetic foot syndrome: A proof of concept. *Scientific Reports*, 7(42124):1–9, 2017.

[54] Kirill I Zaytsev, Nikita V Chernomyrdin, Konstantin G Kudrin, Arseniy A Gavdush, Pavel A Nosov, Stanislav O Yurchenko, and Igor V Reshetov. In vivo terahertz pulsed spectroscopy of dysplastic and non-dysplastic skin nevi. *J Phys Conf Ser*, 735(12076):1–4, 2016.

[55] V. P. Wallace, A. J. Fitzgerald, S. Shankar, N. Flanagan, R. Pye, J. Cluff, and D. D. Arnone. Terahertz pulsed imaging of basal cell carcinoma ex vivo and in vivo. *British Journal of Dermatology*, 151(2):424–432, 2004.

[56] Hua Chen, Yu Zhang, Xiao Li, Xiaofeng Chen, Shihua Ma, Xiumei Wu, Tianzhu Qiu, and Weifeng Zhang. In vivo Non-invasive Diagnosis of Glucose Level in Type-2 Diabetes Mouse by THz Near-Field Imaging. *Journal of Infrared, Millimeter, and Terahertz Waves*, 40:456–465, 2019.

[57] Zachary D. Taylor, James Garritano, Shijun Sung, Neha Bajwa, David B. Bennett, Bryan Nowroozi, Priyamvada Tewari, James W. Sayre, Jean-Pierre Hubschman, Sophie X. Deng, Elliott R. Brown, and Warren S. Grundfest. THz and mm-Wave Sensing of Corneal Tissue Water Content: In Vivo Sensing and Imaging Results. *IEEE Transactions on Terahertz Science and Technology*, 5(2):184–196, 3 2015.

[58] Shijun Sung, Skyler Selvin, Neha Bajwa, Somporn Chantra, Bryan Nowroozi, James Garritano, Jacob Goell, Alexander D. Li, Sophie X. Deng, Elliott R. Brown, Warren S. Grundfest, and Zachary D. Taylor. THz Imaging System for in vivo Human Cornea. *IEEE Transactions on Terahertz Science and Technology*, 8(1):27–37, 2018.

[59] Limin Wu, Degang Xu, Yuye Wang, Bin Liao, Zhinan Jiang, Lu Zhao, Zhongcheng Sun, Nan Wu, Tunan Chen, Hua Feng, and Jianquan Yao. Study of in vivo brain glioma in a mouse model using continuous-wave terahertz reflection imaging. *Biomedical Optics Express*, 10(8):3953, 2019.

[60] J. D.E. McIntyre and D E Aspnes. Differential reflection spectroscopy of very thin surface films. *Surface Science*, 24(2):417–434, 1971.

[61] Xuequan Chen. *Devices and Methods for Accurate Terahertz Time-Domain Spectroscopy and Imaging*. PhD thesis, 2018.

[62] Shengyang Huang, Philip C. Ashworth, Kanis Wai Chi Kan, Yang Chen, Vincent P. Wallace, Yuan-ting Zhang, and Emma Pickwell-MacPherson. Improved sample characterization in terahertz reflection imaging and spectroscopy: erratum. *Optics Express*, 19(24):24782, 11 2011.

[63] Xuequan Chen, Edward P.J. Parrott, Benjamin S.Y. Ung, and Emma Pickwell-Macpherson. A Robust Baseline and Reference Modification and Acquisition Algorithm for Accurate THz Imaging. *IEEE Transactions on Terahertz Science and Technology*, 7(5):493–501, 2017.

[64] Jiarui Wang, Hannah Lindley-Hatcher, Xuequan Chen, and Emma Pickwell-MacPherson. THz Sensing of Human Skin: A Review of Skin Modeling Approaches. *Sensors*, 21(11):3624, 5 2021.

[65] E Pickwell, B E Cole, A J Fitzgerald, M Pepper, and V P Wallace. In vivo study of human skin using pulsed terahertz radiation. *Physics in Medicine and Biology*, 49(9):1595–1607, 2004.

[66] E. Pickwell, B. E. Cole, A. J. Fitzgerald, V. P. Wallace, and M. Pepper. Simulation of terahertz pulse propagation in biological systems. *Applied Physics Letters*, 84(12):2190–2192, 2004.

[67] Bao C.Q. Truong, Hoang Duong Tuan, Ha Hoang Kha, and Hung T. Nguyen. Debye parameter extraction for characterizing interaction of terahertz radiation with human skin tissue. *IEEE Transactions on Biomedical Engineering*, 60(6):1528–1537, 2013.

[68] Bao C.Q. Truong, H. D. Tuan, Anthony J. Fitzgerald, Vincent P. Wallace, and H. T. Nguyen. High correlation of double Debye model parameters in skin cancer detection. In *2014 36th Annual International Conference of the IEEE Engineering in Medicine and Biology Society, EMBC 2014*, 2014.

[69] K. I. Zaytsev, I. N. Dolganova, N. V. Chernomyrdin, G. M. Katyba, A. A. Gavdush, O. P. Cherkasova, G. A. Komandin, M. A. Shchedrina, A. N. Khodan, D. S. Ponomarev, I. V. Reshetov, V. E. Karasik, M. Skorobogatiy, V. N. Kurlov, and V. V. Tuchin. The progress and perspectives of terahertz technology for diagnosis of neoplasms: a review. *Journal of Optics*, 22(1):013001, 1 2020.

[70] Yuezhi He, Kai Liu, Corinna Au, Qiushuo Sun, Edward P J Parrott, and Emma Pickwell-MacPherson. Determination of terahertz permittivity of dehydrated biological samples. *Physics in Medicine & Biology*, 62(23):8882–8893, 11 2017.

[71] Goretti G. Hernandez-Cardoso, Abhishek K. Singh, and Enrique Castro-Camus. Empirical comparison between effective medium theory models for the dielectric response of biological tissue at terahertz frequencies. *Applied Optics*, 59(13):D6, 5 2020.

[72] Qiushuo Sun, Rayko I. Stantchev, Jiarui Wang, Edward P.J. Parrott, Alan Cottenden, Tor-Wo Chiu, Anil T. Ahuja, and Emma Pickwell-MacPherson. In vivo estimation of water diffusivity in occluded human skin using terahertz reflection spectroscopy. *Journal of Biophotonics*, 12(2):e201800145, 2019.

[73] David B. Bennett, Wenzao Li, Zachary D. Taylor, Warren S. Grundfest, and Elliott R. Brown. Stratified media model for Terahertz reflectometry of the skin. *IEEE Sensors Journal*, 11(5):1253–1262, 2011.

[74] Mariko Egawa, Tetsuji Hirao, and Motoji Takahashi. In vivo Estimation of Stratum Corneum Thickness from Water Concentration Profiles Obtained with Raman Spectroscopy. *Acta Dermato-Venereologica*, 87(1):4–8, 2007.

[75] Jane Sandby-Moller, Thomas Poulsen, and Hans Christian Wulf. Epidermal Thickness at Different Body Sites: Relationship to Age, Gender, Pigmentation, Blood Content, Skin Type and Smoking Habits. *Acta Dermato-Venereologica*, 83(6):410–413, 11 2003.

[76] Dominique Batisse, Roland Bazin, and Thérèse Baldeweck. Influence of age on the wrinkling capacities of skin. *Skin Research and Technology*, 8(3):148–154, 8 2002.

[77] Qiushuo Sun, Edward P.J. Parrott, Yuezhi He, and Emma Pickwell-MacPherson. In vivo THz imaging of human skin: Accounting for occlusion effects. *Journal of Biophotonics*, 11(2):e201700111, 2018.

[78] Bryan E. Cole, Ruth M. Woodward, David A. Crawley, Vincent P. Wallace, Donald D. Arnone, and Michael Pepper. Terahertz imaging and spectroscopy of human skin in vivo. In Richard F. Haglund, Jr., Joseph Neev, and Richard F. Wood, editors, *Commercial and Biomedical Applications of Ultrashort Pulse Lasers; Laser Plasma Generation and Diagnostics*, volume 4276, pages 1–10, 5 2001.

[79] Jiarui Wang, Rayko I. Stantchev, Qiushuo Sun, Tor-Wo Chiu, Anil T. Ahuja, and Emma Pickwell MacPherson. THz in vivo measurements: the effects of pressure on skin reflectivity. *Biomedical Optics Express*, 9(12):6467, 2018.

[80] G. W. Nam, J. H. Baek, J. S. Koh, and J.-K. Hwang. The seasonal variation in skin hydration, sebum, scaliness, brightness and elasticity in Korean females. *Skin Research and Technology*, 21(1):1–8, 2 2015.

[81] K.A. Engebretsen, J.D. Johansen, S. Kezic, A. Linneberg, and J.P. Thyssen. The effect of environmental humidity and temperature on skin barrier function and dermatitis. *Journal of the European Academy of Dermatology and Venereology*, 30(2):223–249, 2 2016.

[82] Sunhee Lim, Jihye Shin, Yunhi Cho, and Kun-Pyo Kim. Dietary Patterns Associated with Sebum Content, Skin Hydration and pH, and Their Sex-Dependent Differences in Healthy Korean Adults. *Nutrients*, 11(3):619, 3 2019.

[83] Mary Matsui, Edward Pelle, Kelly Dong, and Nadine Pernodet. Biological Rhythms in the Skin. *International Journal of Molecular Sciences*, 17(6):801, 5 2016.

[84] Interlink Electronics. FSR ® 400 Series Data Sheet Human - Machine Interface Solutions for a Connected World FSR ® 400 Series Data Sheet. 2015.

[85] Xuequan Chen, Qiushuo Sun, Jiarui Wang, Hannah Lindley-Hatcher, and Emma Pickwell-MacPherson. Exploiting Complementary Terahertz Ellipsometry Configurations to Probe the Hydration and Cellular Structure of Skin In Vivo. *Advanced Photonics Research*, 2(1):2000024, 2021.

[86] Kathi C. Madison. Barrier function of the skin: "La Raison d'Être" of the epidermis. *Journal of Investigative Dermatology*, 121(2):231–241, 2003.

[87] Rebecca M. Law, Mai A. Ngo, and Howard I. Maibach. Twenty Clinically Pertinent Factors/Observations for Percutaneous Absorption in Humans. *American Journal of Clinical Dermatology*, 21(1):85–95, 2020.

[88] Mai A. Ngo, Michael O'Malley, and Howard I. Maibach. Percutaneous absorption and exposure assessment of pesticides. *Journal of Applied Toxicology*, 30(2):91–114, 2010.

[89] Magdalena Hoppel, Kristina Kwizda, Dieter Baurecht, Manuel Caneri, and Claudia Valenta. The effect of a damaged skin barrier on percutaneous absorption of SDS and skin hydration investigated by confocal Raman spectroscopy. *Experimental Dermatology*, 25(5):390–392, 2016.

[90] Nandou Lu, P. Chandar, D. Tempesta, C. Vincent, J. Bajor, and H. McGuiness. Characteristic differences in barrier and hygroscopic properties between normal and cosmetic dry skin. I. Enhanced barrier analysis with sequential tape-stripping. *International Journal of Cosmetic Science*, 36(2):167–174, 2014.

[91] Sylvie Verdier-Sévrain and Frederic Bonté. Skin hydration: A review on its molecular mechanisms. *Journal of Cosmetic Dermatology*, 6(2):75–82, 2007.

[92] S. A. Ventura and G. B. Kasting. Dynamics of glycerine and water transport across human skin from binary mixtures. *International Journal of Cosmetic Science*, 39(2):165–178, 2017.

[93] J. W. Fluhr, R. Darlenski, and C. Surber. Glycerol and the skin: Holistic approach to its origin and functions. *British Journal of Dermatology*, 159(1):23–34, 2008.

[94] Mark D.A. Van Logtestijn, Elisa Domínguez-Hüttinger, Georgios N. Stamatas, and Reiko J. Tanaka. Resistance to water diffusion in the stratum corneum is depth-dependent. *PLoS ONE*, 10(2):1–12, 2015.

[95] C. W. Blichmann, J. Serup, and A. Winther. Effects of single application of a moisturizer: Evaporation of emulsion water, skin surface temperature, electrical conductance, electrical capacitance, and skin surface (emulsion) lipids. *Acta Dermato-Venereologica*, 69(4):327–330, 1989.

[96] Fei Lu, Chenshuo Wang, Rongjian Zhao, Lidong Du, Zhen Fang, Xiuhua Guo, and Zhan Zhao. Review of Stratum Corneum Impedance Measurement in Non-Invasive Penetration Application. *Biosensors*, 8(2):31, 3 2018.

[97] Maria-Magdalena Constantin, Elena Poenaru, Calin Poenaru, and Traian Constantin. Skin Hydration Assessment through Modern Non-Invasive Bioengineering Technologies. *Maedica*, 9(1):33–38, 2014.

[98] Courage-Khazaka. Corneometer® CM 825 Courage + Khazaka electronic GmbH. Available at: http://www.courage-khazaka.de/index.php/en/products/scientific/55-corneometer. [Accessed March 2020].

[99] J. M. Crowther. Understanding effects of topical ingredients on electrical measurement of skin hydration. *International Journal of Cosmetic Science*, 38(6):589–598, 2016.

[100] Enzo Berardesca, Marie Loden, Jorgen Serup, Philippe Masson, and Luis Monteiro Rodrigues. The revised EEMCO guidance for the in vivo measurement of water in the skin. *Skin Research and Technology*, 24(3):351–358, 2018.

[101] R. E. Imhof, M. E.P. De Jesus, P. Xiao, L. I. Ciortea, and E. P. Berg. Closed-chamber transepidermal water loss measurement: Microclimate, calibration and performance. *International Journal of Cosmetic Science*, 31(2):97–118, 2009.

[102] Francesco Gioia and Leonardo Celleno. The dynamics of transepidermal water loss (TEWL) from hydrated skin. *Skin Research and Technology*, 2002.

[103] C. Lotte, A. Rougier, D. R. Wilson, and H. I. Maibach. In vivo relationship between transepidermal water loss and percutaneous penetration of some organic compounds in man: effect of anatomic site. *Archives of Dermatological Research*, 279(5):351–356, 1987.

[104] A. Rougier, C Lotte, P Corcuff, and H. Maibach. Relationship between skin permeability and corneocyte size according to anatomic site, age, and sex in man. *Journal of the Society of Cosmetic Chemists*, 39(1):15–26, 1988.

[105] Chunsik Choe, Jürgen Lademann, and Maxim E. Darvin. Depth profiles of hydrogen bound water molecule types and their relation to lipid and protein interaction in the human stratum corneum in vivo. *Analyst*, 141(22):6329–6337, 2016.

[106] Courage-Khazaka. Tewameter® TM 300 Courage + Khazaka electronic GmbH. Available at: http://www.courage-

khazaka.de/index.php/en/products/scientific/139-tewameter. [Accessed March 2020].

[107] MathWorks. Remove outliers. Available at: https://uk.mathworks.com/help/curvefit/removing-outliers.html [Accessed June 2020].

[108] S S Shapiro and M B Wilk. An Analysis of Variance Test for Normality (Complete Samples). *Biometrika*, 52(3/4):591–611, 1965.

[109] M. M. Mukaka. Statistics corner: A guide to appropriate use of correlation coefficient in medical research. *Malawi Medical Journal*, 24(3):69–71, 2012.

[110] Mark R. Prausnitz and Robert Langer. Transdermal drug delivery. *Nature Biotechnology*, 26(11):1261–1268, 11 2008.

[111] Othman A. Al Hanbali, Haji Muhammad Shoaib Khan, Muhammad Sarfraz, Mosab Arafat, Shakeel Ijaz, and Abdul Hameed. Transdermal patches: Design and current approaches to painless drug delivery. *Acta Pharmaceutica*, 69(2):197–215, 2019.

[112] K. S. Ryatt, M. Mobayen, J. M. Stevenson, H. I. Maibach, and R. H. Guy. Methodology to measure the transient effect of occlusion on skin penetration and stratum corneum hydration in vivo. *British Journal of Dermatology*, 119(3):307–312, 9 1988.

[113] N M Price, L G Schmitt, J McGuire, J E Shaw, and G Trobough. Transdermal scopolamine in the prevention of motion sickness at sea. *Clinical Pharmacology and Therapeutics*, 29(3):414–419, 3 1981.

[114] Zohar Nachum, Avi Shupak, and Carlos R. Gordon. Transdermal scopolamine for prevention of motion sickness: Clinical pharmacokinetics and therapeutic applications. *Clinical Pharmacokinetics*, 45(6):543–566, 2006.

[115] G. Buchkremer, H Bents, M Horstmann, K Opitz, and R. Tölle. Combination of behavioral smoking cessation with transdermal nicotine substitution. *Addictive Behaviors*, 14(2):229–238, 1 1989.

[116] William R. Good, Marilou S. Powers, Patricia Campbell, and Lotte Schenkel. A new transdermal delivery system for estradiol. *Journal of Controlled Release*, 2:89–97, 11 1985.

[117] Priyanka Arora and Biswajit Mukherjee. Design, development, physicochemical, and in vitro and in vivo evaluation of transdermal patches containing diclofenac diethylammonium salt. *Journal of Pharmaceutical Sciences*, 91(9):2076–2089, 9 2002.

[118] D. J.R. Duthie, D. J. Rowbotham, R. Wyld, P. D. Henderson, and W. S. Nimmo. Plasma fentanyl concentrations during transdermal delivery of fentanyl to surgical patients. *British Journal of Anaesthesia*, 60(6):614–618, 1988.

[119] Werner H. Poewe, Olivier Rascol, Niall Quinn, Eduardo Tolosa, Wolfgang H. Oertel, Emilia Martignoni, Markus Rupp, and Babak Boroojerdi. Efficacy of pramipexole and transdermal rotigotine in advanced Parkinson's disease: a double-blind, double-dummy, randomised controlled trial. *Lancet Neurology*, 6(6):513–520, 2007.

[120] Bengt Winblad, Jeffrey Cummings, Niels Andreasen, Georg Grossberg, Marco Onofrj, Carl Sadowsky, Stefanie Zechner, Jennifer Nagel, and Roger Lane. A six-month double-blind, randomized, placebo-controlled study of a transdermal patch in Alzheimer's disease - Rivastigmine patch versus capsule. *International Journal of Geriatric Psychiatry*, 22(5):456–467, 2007.

[121] Majella E. Lane. The transdermal delivery of fentanyl. *European Journal of Pharmaceutics and Biopharmaceutics*, 84(3):449–455, 8 2013.

[122] J. F.G.M. Hurkmans, H. E. Bodde, L. M.J. Van Driel, H. Van Doorne, and H. E. Junginger. Skin irritation caused by transdermal drug delivery systems during long-term (5 days) application. *British Journal of Dermatology*, 112(4):461–467, 1985.

[123] Raza Aly, Charlene Shirley, Bob Cunico, and Howard I. Maibach. Effect of prolonged occlusion on the microbial flora, pH, carbon dioxide and transepidermal water loss on human skin. *Journal of Investigative Dermatology*, 71(6):378–381, 1978.

[124] J Faergemann, R Aly, D R Wilson, and H I Maibach. Skin occlusion: Effect on Pityrosporum orbiculare, skin P_CO2, pH, transepidermal water loss, and water content. *Archives of Dermatological Research*, 275(6):383–387, 11 1983.

[125] Kyung Won Kim, Kwang-Sung Kim, Hyeongmun Kim, Sang Hun Lee, Jae-Hak Park, Ju-Hee Han, Seung-Hyeok Seok, Jisuk Park, YoonSeok Choi, Young Il Kim, Joon Koo Han, and Joo-Hiuk Son. Terahertz dynamic imaging of skin drug absorption. *Optics Express*, 20(9):9476, 2012.

[126] Gyuseok Lee, Ho Namkung, Youngwoong Do, Soonsung Lee, Hyeona Kang, Jin Woo Kim, and Haewook Han. Quantitative label-free terahertz sensing of transdermal nicotine delivered to human skin. *Current Optics and Photonics*, 4(4):368–372, 2020.

[127] Victor Carrer, Cristina Alonso, Mercè Pont, Miriam Zanuy, Mònica Córdoba, Sonia Espinosa, Clara Barba, Marc A. Oliver, Meritxell Martí, and Luisa Coderch. Effect of propylene glycol on the skin penetration of drugs. *Archives of Dermatological Research*, 312(5):337–352, 2020.

[128] Emma L. Tombs, Vasiliki Nikolaou, Gabit Nurumbetov, and David M. Haddleton. Transdermal Delivery of Ibuprofen Utilizing a Novel Solvent-Free Pressure-sensitive Adhesive (PSA): TEPI® Technology. *Journal of Pharmaceutical Innovation*, 13(1):48–57, 3 2018.

[129] David M. Haddleton, Gabit Nurumbetov, Andrew Ross, and Vasiliki Nikolaou. Patch. *World Intellectual Property Organization*, page WO2020016582A1, 2020.

[130] John W. Tukey. Comparing Individual Means in the Analysis of Variance. *Biometrics*, 5(2):99, 6 1949.

[131] L. Bartosova and J. Bajgar. Transdermal Drug Delivery In Vitro Using Diffusion Cells. *Current Medicinal Chemistry*, 19(27):4671–4677, 10 2012.

[132] Stéphane Diridollou, Jean de Rigal, Bernard Querleux, Frédéric Leroy, and Victoria Holloway Barbosa. Comparative study of the hydration of the stratum corneum between four ethnic groups: influence of age. *International Journal of Dermatology*, 46(s1):11–14, 10 2007.

[133] Raja K Sivamani, Gabriel C Wu, Norm V Gitis, and Howard I Maibach. Tribological testing of skin products: gender, age, and ethnicity on the volar forearm. *Skin Research and Technology*, 9(4):299–305, 11 2003.

[134] Roshan Gunathilake, Nanna Y. Schurer, Brenda A. Shoo, Anna Celli, Jean Pierre Hachem, Debra Crumrine, Ganga Sirimanna, Kenneth R. Feingold, Theodora M. Mauro, and Peter M. Elias. PH-Regulated mechanisms account for pigment-type differences in epidermal barrier function. *Journal of Investigative Dermatology*, 129(7):1719–1729, 2009.

[135] Corinne Fotoh, Ahmed Elkhyat, Sophie Mac, Jean Marie Sainthillier, and Philippe Humbert. Cutaneous differences between Black, African or Caribbean

Mixed-race and Caucasian women: biometrological approach of the hydrolipidic film. *Skin Research and Technology*, 14(3):327–335, 8 2008.

[136] Jeffrey T. Reed. Skin Type, but Neither Race nor Gender, Influence Epidermal Permeability Barrier Function. *Archives of Dermatology*, 131(10):1134, 10 1995.

[137] Pearl Grimes, Brenda L. Edison, Barbara A. Green, and Richard H. Wildnauer. Evaluation of inherent differences between African American and white skin surface properties using subjective and objective measures. *Cutis*, 73(6):392–396, 2004.

[138] Monica M Young, Anja Franken, and Johan L du Plessis. Transepidermal water loss, stratum corneum hydration, and skin surface pH of female African and Caucasian nursing students. *Skin Research and Technology*, 25(1):88–95, 1 2019.

[139] K. Lammintausta, H. I. Maibach, and D. Wilson. Irritant reactivity in males and females. *Contact Dermatitis*, 17(5):276–280, 11 1987.

[140] H. Hadi, A. I. Awadh, N. M. Hanif, N. F.A. Md Sidik, M. R.N. Mohd Rani, and M. S.M. Suhaimi. The investigation of the skin biophysical measurements focusing on daily activities, Skin care habits, And gender differences. *Skin Research and Technology*, 22(2):247–254, 2016.

[141] Xomalin G. Peralta, Dawn Lipscomb, Gerald J. Wilmink, and Ibtissam Echchgadda. Terahertz spectroscopy of human skin tissue models with different melanin content. *Biomedical Optics Express*, 10(6):2942, 6 2019.

[142] Rayko Ivanov Stantchev, Xiao Yu, Thierry Blu, and Emma Pickwell-MacPherson. Real-time terahertz imaging with a single-pixel detector. *Nature Communications*, 11(2353):1–8, 2020.

[143] Ke Su, Robert K. May, Ian S. Gregory, Philip F. Taday, Y. C. Shen, and J. Axel Zeitler. Terahertz sensor for non-contact thickness measurement of car paints. *International Conference on Infrared, Millimeter, and Terahertz Waves, IRMMW-THz*, pages 22–23, 2013.